NPS ARCHIVE
2000.06
KRUSE, D.

DUDLEY KNOX LIBRARY
NAVAL POSTGRADUATE SCHOOL
MONTEREY CA 93943-5101

NAVAL POSTGRADUATE SCHOOL
Monterey, California

THESIS

LARGE EDDY SIMULATION OF INTERACTIONS BETWEEN FREE CONVECTION, WIND DRIVEN CURRENTS, AND BAROCLINICITY IN LABRADOR SEA DEEP MIXED LAYERS

by

Denise M. Kruse

June 2000

Thesis Co-Advisors: Peter Guest
Ramsey Harcourt

Approved for public release; distribution is unlimited.

DUDLEY KNOX LIBRARY
NAVAL POSTGRADUATE SCHOOL
MONTEREY CA 93943-5101

REPORT DOCUMENTATION PAGE		Form Approved OMB No. 0704-0188

Public reporting burden for this collection of information is estimated to average 1 hour per response, including the time for reviewing instruction, searching existing data sources, gathering and maintaining the data needed, and completing and reviewing the collection of information. Send comments regarding this burden estimate or any other aspect of this collection of information, including suggestions for reducing this burden, to Washington headquarters Services, Directorate for Information Operations and Reports, 1215 Jefferson Davis Highway, Suite 1204, Arlington, VA 22202-4302, and to the Office of Management and Budget, Paperwork Reduction Project (0704-0188) Washington DC 20503.

1. AGENCY USE ONLY *(Leave blank)*	2. REPORT DATE June 2000	3. REPORT TYPE AND DATES COVERED Master's Thesis
TITLE AND SUBTITLE : Large Eddy Simulation of Interactions Between Free Convection, Wind Driven Currents, and Baroclinicity in Labrador Sea Deep Mixed Layers.		5. FUNDING NUMBERS
6. AUTHOR(S) Kruse, Denise M.		
7. PERFORMING ORGANIZATION NAME(S) AND ADDRESS(ES) Naval Postgraduate School Monterey, CA 93943-5000		8. PERFORMING ORGANIZATION REPORT NUMBER
9. SPONSORING / MONITORING AGENCY NAME(S) AND ADDRESS(ES) N/A		10. SPONSORING / MONITORING AGENCY REPORT NUMBER

11. SUPPLEMENTARY NOTES The views expressed in this thesis are those of the author and do not reflect the official policy or position of the Department of Defense or the U.S. Government.

12a. DISTRIBUTION / AVAILABILITY STATEMENT Approved for public release; distribution is unlimited.	12b. DISTRIBUTION CODE

ABSTRACT *(maximum 200 words)* Understanding the dynamics of deep convection leading to the formation of deep water is important not only for studying the small-scale generation regions, but also for studying the large-scale thermohaline circulation. Large Eddy Simulation (LES) is used to model deep convection with an imposed mean horizontal density gradient of two different strengths and wind forcing from various directions, with strong surface cooling representative of the Labrador Sea. Results from these different cases are compared and analyzed to understand the effects of horizontal density gradients and wind direction on turbulence statistics for deep convection. Both the strength of horizontal density gradients and wind direction relative to the gradient affect mixed layer scalar variances, turbulent vertical fluxes, Vertical Turbulent Kinetic Energy (VTKE), and stability during deep convection.

Wind direction dominates over gradient strength in determining vertical flux magnitude with larger variation in strong gradient cases. Levels of VTKE are more dependent on gradient strength, with weaker gradients producing higher values of VTKE than stronger gradients regardless of wind direction. Wind direction does alter VTKE levels in the same manner as it alters vertical flux levels. The presence of a horizontal gradient is a stabilizing factor in areas of strong surface cooling.

14. SUBJECT TERMS Large Eddy Simulation, Labrador Sea, Deep Convection, Baroclinicity	15. NUMBER OF PAGES 102
	16. PRICE CODE

17. SECURITY CLASSIFICATION OF REPORT	18. SECURITY CLASSIFICATION OF THIS PAGE	19. SECURITY CLASSIFICATION OF ABSTRACT	20. LIMITATION OF ABSTRACT
Unclassified	Unclassified	Unclassified	UL

NSN 7540-01-280-5500 Standard Form 298 (Rev 2-89) Prescribed by ANSI Std. 239-18

THIS PAGE INTENTIONALLY LEFT BLANK

Approved for public release; distribution is unlimited

LARGE EDDY SIMULATION OF INTERACTIONS BETWEEN FREE CONVECTION, WIND DRIVEN CURRENTS, AND BAROCLINICITY IN LABRADOR SEA DEEP MIXED LAYERS

Denise M. Kruse
Lieutenant Commander, United States Navy
B.S., The George Washington University, 1989

Submitted in partial fulfillment of the
requirements for the degree of

MASTER OF SCIENCE IN METEOROLOGY AND PHYSICAL OCEANOGRAPHY

from the

NAVAL POSTGRADUATE SCHOOL
June 2000

NPS ARCHIVE
2000.06
KRUSE, D.

Thesis
K8455
c.1

THIS PAGE INTENTIONALLY LEFT BLANK

DUDLEY KNOX LIBRARY
NAVAL POSTGRADUATE SCHOOL
MONTEREY CA 93943-5101

ABSTRACT

Understanding the dynamics of deep convection leading to the formation of deep water is important not only for studying the small-scale generation regions, but also for studying the global-scale thermohaline circulation. Large Eddy Simulation (LES) is used to model deep convection with an imposed mean horizontal density gradient of two different strengths and wind forcing from various directions, with strong surface cooling representative of the Labrador Sea. Results from these different cases are compared and analyzed to understand the effects of horizontal density gradients and wind direction on turbulence statistics for deep convection. Both the strength of horizontal density gradients and wind direction relative to the gradient affect mixed layer scalar variances, turbulent vertical fluxes, Vertical Turbulent Kinetic Energy (VTKE), and stability during deep convection.

Wind direction dominates over gradient strength in determining vertical flux magnitude with larger variation in strong gradient cases. Levels of VTKE are more dependent on gradient strength, with weaker gradients producing higher values of VTKE than stronger gradients regardless of wind direction. Wind direction does alter VTKE levels in the same manner as it alters vertical flux levels. The presence of a horizontal gradient is a stabilizing factor in areas of strong surface cooling.

THIS PAGE INTENTIONALLY LEFT BLANK

TABLE OF CONTENTS

I. INTRODUCTION 1

A. STATEMENT OF THE PROBLEM 1

B. OVERVIEW 2

II. BACKGROUND 3

A. LABRADOR SEA 4

1. Current Structure 5

2. Water Types and Characteristics 6

3. Meteorology 7

B. DEEP CONVECTION 8

C. GEOSTROPHIC AND NONGEOSTROPHIC FLOW 10

D. LARGE EDDY SIMULATION MODEL 13

III. MODEL FOR LARGE EDDY SIMULATION 17

IV. PROCEDURE 21

A. CASE DIFFERENTIATION 21

B. PARAMETER DESCRIPTION 22

C. COMPARISON 23

V. RESULTS 31

A. BOX MODE EFFECTS 31

B. COMPARISON OF PARAMETERS OVER TIME AT VARIOUS DEPTHS 32

1. Horizontal Velocities 33

2. Mean Salinity and Temperature 35

3. Turbulent Fluxes and VTKE 37

C. BULK AVERAGES OVER SPACE AND TIME 42

1. Salinity Gradients, Temperature Gradients, and Stability 42

2. Salinity Advection, Temperature Advection, and VTKE Relationship 43

D. BUOYANCY FLUX TKE RELASHIONSHIP 46

1. Gradient, Cooling, and Wind Effect on VTKE 46

2. Components of Buoyancy Flux and the Conversion to VTKE 48

E. STABILITY COMPARISONS 50

F. COOLING EFFECTS ON THE EKMAN DEPTH 52

IV. CONCLUSIONS AND RECOMMENDATIONS 87

A. CONCLUSIONS 87

B. RECOMMENDATIONS 88

LIST OF REFERENCES 91

INITIAL DISTRIBUTION LIST 93

I. INTRODUCTION

A. STATEMENT OF THE PROBLEM

Deep convection resulting in the formation of deep and bottom waters, which extend across the world's oceans, occurs in a limited number of areas. Understanding the dynamics of this process and conditions altering the resulting depth and characteristics of the deep water is important not only for studying the limited generation regions, but also for studying the global-scale thermohaline circulation. Since the waters formed in the few deep convection areas spread across all of the oceans, they have an impact reaching much further than the regions of formation.

Most of the deep convection regions are located in polar and subpolar regions, which are difficult areas to collect observations. There was a large and highly successful collection effort during the winters of 1997 and 1998 in the Labrador Sea Deep Convection Experiment. Observations of convection leading to deepening of the mixed layer to over 1200 meters were recorded and are being analyzed. Because occasions of such data collection are rare and expensive, and nature does not provide controlled experiments, computer simulations of the processes are also required to further research. With the combination of measurements and model output, comparisons can be made to check and improve the model's results, and the two together allow a more complete understanding of the dynamics.

Models are often simplified to study one parameter at a time and to reduce required computer time and power. Simplification of a problem is useful in isolating the effects. However, the conditions and motions of the ocean tend to be nonlinear, with

energy transfer occurring at many levels due to different forcing mechanisms. One simplification often applied to a model is the assumption of horizontal homogeneity of temperature and salinity. This greatly simplifies the problem, but it rarely occurs in nature due to uneven heating, cooling, evaporation, salt influx, precipitation, and advection of various water types. Another common simplification is the neglect of wind forcing. Wind forcing is significant over the Labrador Sea is, so inclusion of this forcing provides a more realistic representation.

B. OVERVIEW

Large Eddy Simulation (LES) is used to model deep convection with an imposed mean horizontal density gradient having two different strengths and wind forcing from various directions with strong surface cooling, representative of the Labrador Sea. Results from different cases are compared and analyzed to understand the effects of horizontal density gradients and wind direction on turbulence statistics of deep convection. Chapter II provides background information about regions of oceanic deep convection, the meteorology and oceanography of the Labrador Sea, air-sea interaction dynamics, and the LES model. Chapter III provides further details on the development and the equations and assumptions for the LES model. Chapter IV outlines the various cases studied and the procedures taken. Chapter V presents model results and compares differences in temperature and salinity stratification and variances, vertical scalar fluxes, Vertical Turbulent Kinetic Energy (VTKE), and stability. Chapter VI summarizes the results and provides some conclusions and recommendations for further study.

II. BACKGROUND

Three-dimensional global-scale thermohaline circulation distributes and renews ocean properties such as temperature, salinity, carbon dioxide, dissolved oxygen, and other dissolved nutrients and gases. The atmosphere and interaction between the air and the sea play a large role in this complex system. The world's oceans receive uneven heating, with the water near the lower latitudes receiving more direct energy and warming on a continual basis from the atmosphere than the oceans at the higher latitudes. Due to the strong stratification of the thermocline existing in much of the ocean, this heat cannot usually be mixed deeper than about a hundred meters. Instead, a large portion of the heat is advected zonally to colder areas at high latitudes. This water motion allows the lower latitude ocean to absorb even more heat. The heat in the ocean must be released back into the atmosphere at some point to maintain a thermal balance.

At the higher latitudes, the atmosphere can become very dry and much colder than the ocean for extended periods of time allowing excess heat to transfer back to the atmosphere. This creates vertical motion as the surface water becomes colder and therefore denser than the underlying water. Vertical motion allows the colder water to sink to its equilibrium depth, mixing with the warmer water below. Mixing also helps bring more energy in the form of heat to the surface to allow even further cooling of the water. Cooling and downward mixing occurs when the air temperature is colder than the water temperature. However, there are conditions in just a few areas of the world that optimize the process and enable the creation of very dense water. This water sinks to great depths, becoming the deep waters and bottom waters of the world's oceans. These deep waters must generally flow toward the equator to compensate for the volume of low

latitude warmer water that flowed toward the poles. On the large scale, uneven heating of the world's oceans is largely responsible for the circulation that maintains the balance of properties.

While vertical circulation is driven by global gradients in surface heat flux, the release of heat to the atmosphere and the creation of deep water take place on several scales extending from basin-wide circulation to scales down to 1km or less. There are two types of deep convection. One type of deep convection occurs along continental shelves when seawater becomes very dense due to cooling from the atmosphere and brine rejection due to ice formation. This water sinks along the shelf slope to great depths. The other type of deep convection is in the open ocean. This is the type of deep convection that occurs in the Labrador Sea, which is the area of interest in this study. Open ocean deep convection is known to occur in the Gulf of Lyon in the Mediterranean Sea, the seas around Antarctica, the Greenland Sea, and the Labrador Sea. There is also some evidence of open ocean deep convection in the Adriatic Sea, the Ligurian Sea, Baffin Bay, the Dead Sea, and the boundary between the Weddel Sea and the Drake Passage (Killworth, 1983).

Recent research suggests the existence of three phases in the phenomenon. These include preconditioning, overturning, and restratification (Clark and Gascard, 1983; Killworth, 1983; Denbo and Skyllingstad, 1996; Marshall and Schott, 1999). More details of these three phases will be covered later.

A. LABRADOR SEA

With its weak stratification, harsh winters, cold, dry air accompanying the west-northwest average wind direction, and its general circulation, water composition, and

topography, some of the deepest convection in the world occurs in the Labrador Sea. Lazier (1980) presents temperature, salinity, and density data collected at Ocean Weather Ship Bravo located near the middle of the Labrador Sea at 56° 30' North 51° 00' West (Fig 2.1). His data was collected continuously from 1964 to 1974 enabling a description of Labrador Sea conditions and changes over the years. Every winter the stratification of the Labrador Sea is broken down and mixing occurs from 200 to 2000 meters depth depending on the forcing both from above and below (Lab Sea Group, 1998).

1. Current Structure

The Labrador Sea is the body of water between the east coast of Labrador, Canada, and the west coast of Greenland south of Davis Strait. A combination of several currents concentrated along the coast form a cyclonic flow around the Labrador Sea (Fig 2.1). These currents include the West Greenland Current flowing northward along the Greenland west coast, splitting south of Davis Strait with a branch continuing northward along the coast and a branch flowing westward. The westward flowing branch constitutes the northern boundary of the encircling cyclonic flow. Just off the Labrador coast, the westward flowing branch of the West Greenland Current joins with the Baffin Current flowing southward on the west side of Davis Strait. Along Baffin Island, this becomes the Labrador Current after passing through Hudson Strait and flowing southward over the Labrador slope and continental shelf. The Labrador Current meets up with the eastward flowing North Atlantic Current off Newfoundland. The North Atlantic Current branches to the North in the Irminger Sea forming the northward flowing Irminger Current. The Irminger Current merges with the Southward flowing East Greenland Current, becoming the West Greenland Current as it rounds the southern point

of Greenland (Clark and Gascard, 1983). This complex system of currents and multiple water types provide the necessary preconditioning for deep convection in the Labrador Sea.

2. Water Types and Characteristics

The currents carry different types of water into, around, and out of the Labrador Sea. The West Greenland Current carries cold, fresh surface water mixed with warmer, saltier Irminger Sea water from below. The subsurface Irminger Sea water, which exists at depths between approximately 200 and 700 meters, allows the Labrador Sea to remain ice free seaward of the continental shelf by warming it from below (Lab Sea Group, 1998). Cold, fresh water also enters at the surface from Canadian continental runoff, Arctic flow through the Davis Strait, and melting sea ice. These sources of water create Labrador Sea Water. In the central part of the Labrador Sea lies the 500km by 600km by 2.3km deep Labrador Sea Water produced during previous winters. The high-salinity dense North Atlantic Deep Water (NADW) lies beneath the Labrador Sea Water, starting at approximately 2500 meters. Strong stratification between the NADW and the Labrador Sea water prevents convection from penetrating further than 2500 meters (Lilly et al., 1999). Each water type has its own distinct temperature and salinity signature, which has varied somewhat over the years. From records extending from 1908 to present, the range of temperature and salinity values for Labrador Sea Water is 2.7 to 3.6° C and 34.83 to 34.9 psu. At 2.7° C and 34.83 psu, today's Labrador Sea Water is the coldest, freshest and densest ever observed (Lilly et al., 1999).

3. Meteorology

The atmospheric conditions and the air-sea interaction over the ocean provide the final ingredients for the occurrence of deep convection and deepwater production. As seen in studies of the Mediterranean, Greenland Sea, and the Labrador Sea, strong atmospheric forcing of cold, dry air blowing from land over the relatively warmer water is required. This phenomenon induces the large heat and moisture fluxes required to release the oceanic heat into the atmosphere (Lab Sea Group, 1998). During the winter, the atmosphere above the Labrador Sea is influenced by the combination of the Azores High and the Icelandic Low. These features produce general cyclonic circulation over the North Atlantic, which will produce predominantly northwest to west-northwest winds over the Labrador Sea. Wind from this direction brings the cold, dry air from Canada over the warmer Labrador Sea.

The relative strengths of the two atmospheric features are indicated by the North Atlantic Oscillation (NAO) index, the sea level air pressure difference between the Azores High and the Icelandic Low. The NAO determines the strength and direction of the prevailing winds. It will also influence the number of extratropical cyclones moving over the area. It has been determined that the air-sea interaction is modulated by the number of extratropical cyclones that pass over the area and that heat loss is enhanced by west or northwesterly winds over the Labrador Sea (Lab Sea Group, 1998). When the NAO is low, the jet stream shifts southward preventing storms from traversing the Labrador Sea. It is proposed that the NAO plays a major role in deep convection variability, with a weak NAO contributing to the lack of convection in the Labrador Sea in the early 1970's and a strong NAO contributing to the strong convection in the early

and mid 1990's (Marshall and Schott, 1999). Studies have shown that variations in salinity, which are also a result of atmospheric forcing, also play a role in the variability of deep convection in the Labrador Sea from year to year.

Heat loss from the water is the most important effect of the atmospheric forcing relevant to deep convection. The average winter heat loss from the ocean to the atmosphere in the central Labrador Sea is greater than 300 Wm^{-2}, and atmospheric models indicate that the highest heat loss occurs in an elliptical region about 150 km wide just off the ice edge (Lab Sea Group, 1998). Prior to the Labrador Sea Convection Experiment, which took place from the summer of 1996 through 1998, there were no direct measurements of heat, moisture, and momentum fluxes between the Labrador air and sea boundary. Briefly looking at some of the results from the data collection, a blocking high over the area from December 1996 through mid January 1997 prevented cyclones from passing over the area resulting in low, 150 Wm^{-2} average total heat flux at site Bravo. This began a period of west-northwesterly winds and constituted a cold outbreak regime (Lab Sea Group, 1998). With more cyclonic circulation during the following six weeks, higher average heat fluxes of greater than 420 Wm^{-2} resulted, with peaks greater than 1000 Wm^{-2}.

B. DEEP CONVECTION

The study of how deep waters are formed is a relatively new area of research. Much has been discovered recently, but there is much more yet to be learned. Through field observations, which are difficult and costly due to the harsh conditions present in areas of deep water convection, laboratory experiments, and numerical simulations, more details of the process will be studied and understood in the future.

There was an understanding that deep convection occurred in the Labrador Sea early in the 20th century, however it was unclear as to how and to what depth the convection extended. Research throughout the 20th century has brought oceanographers to a better understanding of what conditions are required for deep convection, what areas of the world possess these conditions, and what types of motions and forcing are involved.

A brief summary of these necessary conditions and the basic phases and dynamics will be discussed. Further details and in depth discussions may be found (Killworth, 1983; Clark and Gascard, 1983; Gascard and Clark, 1983; Marshall and Schott 1999; Lazier 1980; The Lab Sea Group, 1998; Lilly et.al. 1999). Three distinguishable phases of open ocean deep are identified: the preconditioning, deep convection, and lateral exchange phases (MEDOC Group 1969) (Fig 2.2).

Preconditioning requires the presence of several elements. There must be mean cyclonic circulation. Isopycnals dome upward within the cyclonic circulation resulting in weak static stability. There also must be different water masses. Warmer more saline water, such as the Irminger Sea water below colder fresher water, provides salt to the surface water being cooled, resulting in potentially deeper convection than without this source of salt. The last element required for preconditioning is cold winds blowing over the area to force sufficient heat loss resulting in vertical convection.

When enough cooling has occurred to break through the weak stratification, deep convection takes place. Deep convection is widespread over hundreds of kilometers, but consists of numerous individual plumes of scale approximately 1km with vertical velocities of up to 10 cm/s. Once the cooling event stops, the vertical transfer of heat

stops and heat is only transferred horizontally. A deep mixed patch is formed and spreads laterally during the final stage of lateral exchange and spreading.

C. GEOSTROPHIC AND NONGEOSTROPHIC FLOW

Geostrophic and nongeostrophic forcing influences horizontal velocities in all areas of the ocean, including regions of deep convection. Horizontal velocity is caused by both the wind and by temperature and salinity gradients. Under nonturbulent conditions, the equations of motion can be simplified and scaled, resulting in linear equations that can then be readily solved. The total horizontal velocity can be separated into its u and v components and further into its geostrophic components resulting from the pressure gradient and its Ekman velocity component (ageostrophic) associated with the vertical friction from the wind forcing in the horizontal equations of motion.

Simplified horizontal equations of motion applied to stable ocean areas include friction parameterized by a constant vertical eddy viscosity A_z.

$$\frac{du}{dt} = fv - \frac{1}{\rho}\frac{\partial p}{\partial x} + A_z \frac{\partial^2 u}{\partial z^2} \tag{2.1}$$

$$\frac{dv}{dt} = -fu - \frac{1}{\rho}\frac{\partial p}{\partial y} + A_z \frac{\partial^2 v}{\partial z^2} \tag{2.2}$$

Here, u is the eastward velocity component, v is the northward velocity component, ρ is the water density, f is the coriolis parameter, p is the pressure, and $A_z\, \partial^2 u/\partial z^2$ and $A_z\, \partial^2 v/\partial z^2$ are the horizontal forces per unit mass in x and y respectively due to vertical gradients in shear stress.

If a steady state with constant wind is assumed, $\partial u/\partial t = \partial v/\partial t = 0$, and Equation (2.1) and Equation (2.2) can be simplified.

$$fv - \frac{1}{\rho}\frac{\partial p}{\partial x} + A_z \frac{\partial^2 u}{\partial z^2} = 0 \tag{2.3}$$

$$-fu - \frac{1}{\rho}\frac{\partial p}{\partial y} + A_z \frac{\partial^2 v}{\partial z^2} = 0 \tag{2.4}$$

The u and v components of velocity can be separated into the geostrophic and Ekman (ageostrophic) components associated with the density and wind forcing respectively, $u = u_g + u_e$ and $v = v_g + v_e$. These can then be placed into the horizontal equations of motion, Equation (2.3) and Equation (2.4).

$$fv_g + fv_e = \frac{1}{\rho}\frac{\partial p}{\partial x} - A_z \frac{\partial^2 u_g}{\partial z^2} - A_z \frac{\partial^2 u_e}{\partial z^2} \tag{2.5}$$

$$-fu_g - fu_e = \frac{1}{\rho}\frac{\partial p}{\partial y} - A_z \frac{\partial^2 v_g}{\partial z^2} - A_z \frac{\partial^2 v_e}{\partial z^2} \tag{2.6}$$

Usually the vertical gradients of the geostrophic velocity are very small, $A_z\, \partial^2 u_g / \partial z^2 \leq 10^{-3}\, 1/\rho\, \partial p/\partial x$, so these terms are dropped. Due to the linearity of these equations, it is possible to separate Equation (2.5) and equation (2.6) into geostrophic balance equations (2.7) and the Ekman equations (2.8).

$$-fu_g = \frac{1}{\rho}\frac{\partial p}{\partial y}, \quad fv_g = \frac{1}{\rho}\frac{\partial p}{\partial x} \tag{2.7}$$

$$fu_e = A_z \frac{\partial^2 v_e}{\partial z^2} \quad fv_e = -A_z \frac{\partial^2 u_e}{\partial z^2} \tag{2.8}$$

Equations (2.8) are the Ekman layer equations with the Coriolis force acting on the ageostrophic flow. These equations can be solved fairly easily.

In unstable and turbulent areas of the ocean, such as the Labrador Sea, the equations of motion must remain nonlinear with horizontal and vertical velocities

interacting with each other and exchanging energy. The geostrophic balance and Ekman equations cannot be simplified to Equations (2.8 and 2.9) in the Labrador Sea because the eddy viscosity, A_Z, is not a constant and depends on depth. With depth dependence, the stress term, $\partial/\partial z\, A_z\, \partial u/\partial z$, will not reduce to $A_z\, \partial^2 u/\partial z^2$. This produces a term in the geostrophic equations too large to be neglected and results in Ekman equations that are not straight forward. Separation of the horizontal velocities into geostrophic and ageostrophic elements is difficult due to the additional influence of the strong vertical forcing. Lateral variations in the Labrador Sea exist because of uneven heating or cooling, precipitation, evaporation, and brine rejection. These variations do have an effect on the resulting horizontal velocities, which in turn have an effect on the vertical motions, physics and processes involved in deep convection.

Mathematical challenges in separating the components of horizontal velocity in an unstable area due to the nonlinearity of the equations make studying these relationships and understanding the interactions difficult. Hence, the effect of horizontal gradients in the Labrador Sea has not been well understood. A numerical simulation of the area with an imposed gradient is a viable and useful way to study this effect on deep convection. Because of the small radius of deformation in the high latitude oceans and the small scale processes involved in deep convection, a large eddy simulation (LES) model must be employed. LES can represent small scale turbulence well as long as the domain spacial is small enough to enable small grid spacing. LES models use the fully non-linear equations of motion.

D. LARGE EDDY SIMULATION MODEL

Large Eddy Simulation (LES) is a modeling technique able to resolve eddies containing energy at and below the integral scale of motion. Turbulent Kinetic Energy (TKE) is resolved down to the inertial subrange, the – 5/3 log-slope inertial energy cascade. The parameterization of eddy viscosity for the subgrid scale is time and space dependent (Stone 1999).

The LES technique was first used in an atmospheric model by Smagorinsky (1963) and Lilly (1967) to parameterize the effect of unresolved turbulence. Deardorff (1972) applied an LES model to planetary boundary layer turbulence to determine nonlinear eddy viscosity. Moeng (1984) continued to develop the LES code by employing a Fast Fourier Transform (FFT) algorithm and increasing resolution, thus reducing phase error. Garwood et al. (1994) applied the LES code created by Moeng (1984) to the ocean for nonhydrostatic deep convection studies. Further improvements to the LES model have been made by Harcourt and Garwood (1994) using horizontally isotropic filtering methods to improve resolved spectra and by Harcourt (1999) by using an upwind numerical scheme for scalar advection near sharp boundaries to reduce errors. Stone (1999) applied a lateral temperature and salinity gradient in her study of the Greenland Sea, which was altered slightly and applied to the LES model in this study of the Labrador Sea.

Brown (1996) used an LES model of the atmosphere to study the effects of geostrophic wind varying with height in both convective and nonconvective environments of the atmosphere, which is similar in many ways to the study performed in this application to the ocean environment. There are, however, several differences

between the two studies. Brown (1996) specified constants for the variation of the geostrophic wind with height, $\partial U_G/\partial z$ and $\partial V_G/\partial z$. In this work, we specify the variation of the temperature and salinity horizontally and simulate the geostrophic velocity variation with depth in the model. In the calculation of $\partial\theta/\partial t$, Brown omits the temperature advection, $u\,\partial\theta/\partial x$. Brown claims to have observed no effect with its addition, and he neglected it for simplification. Possibly, Brown tested $U_G\,\partial T_G/\partial x$ or used small values of $\partial T_G/\partial x$. This term is included in the LES study discussed here. Originally the term was left out. However, when included, notable effects were seen. Also, the effects of the geostrophic flow induced by the horizontal gradient are investigated more thoroughly in this study than in Brown (1996).

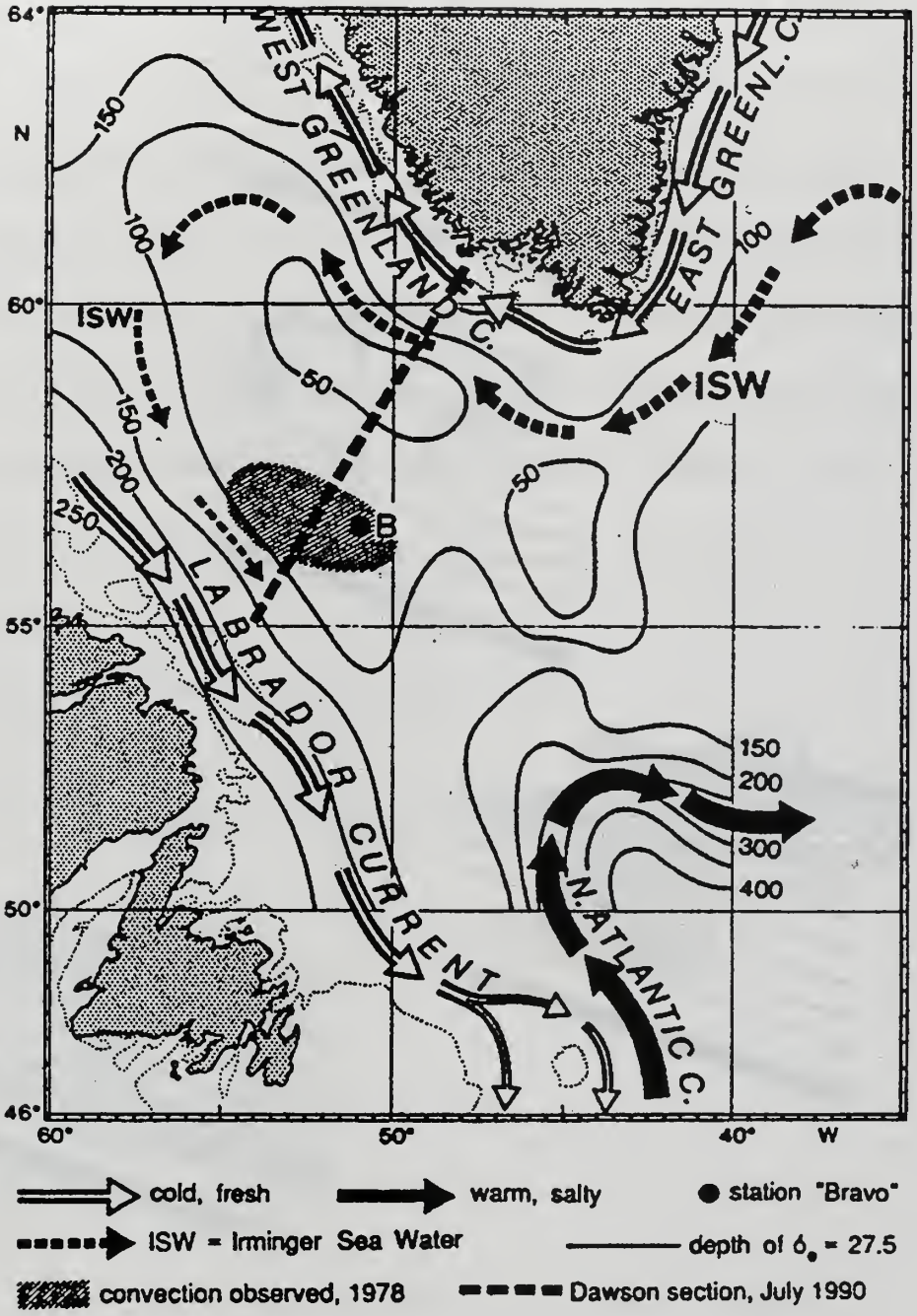

Figure 2.1. The Labrador Sea with current structure and station Bravo location identified (from Marshall and Schott 1998.)

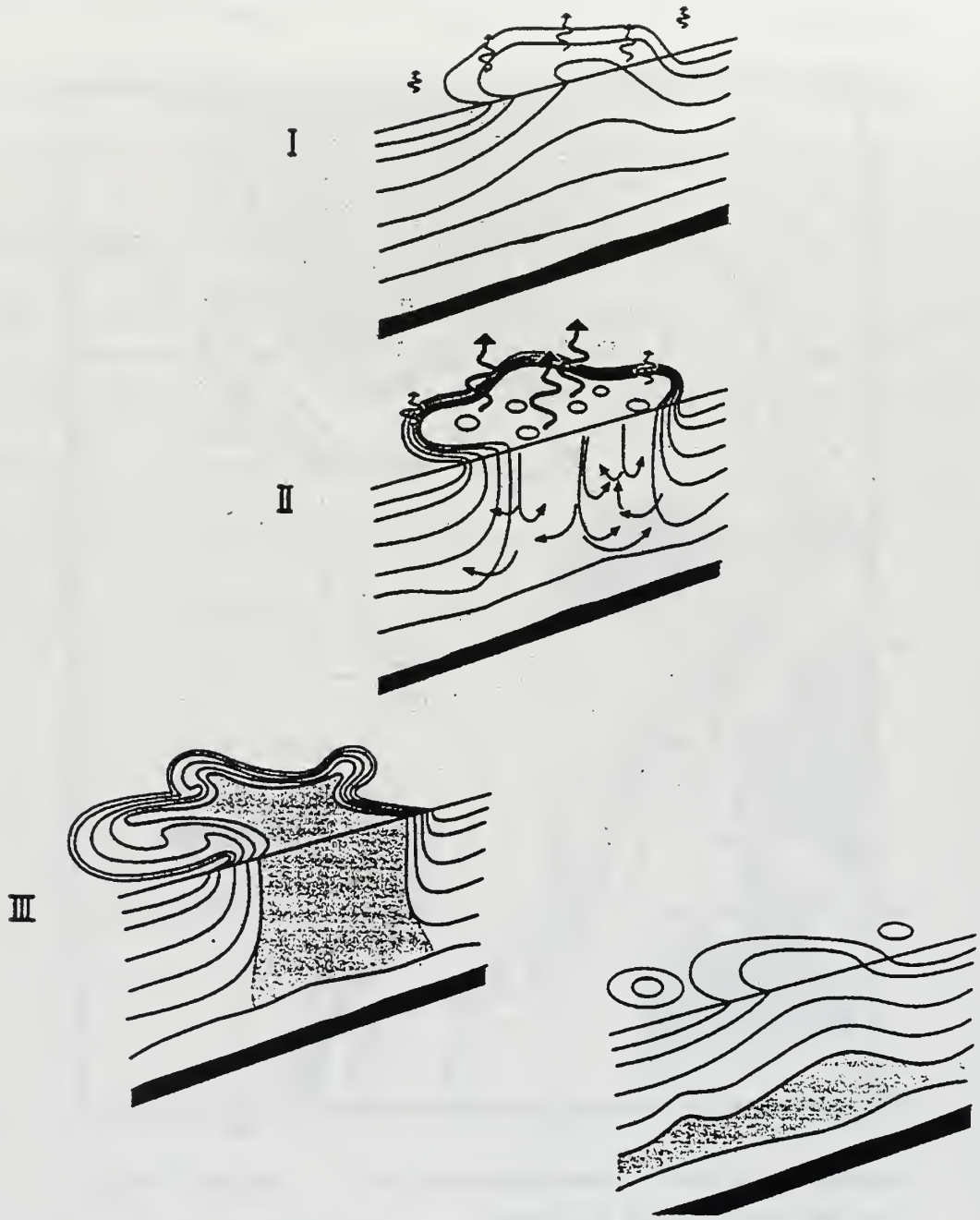

Figure 2.2. The three phases of open-ocean deep convection: (I) preconditioning, (II) deep convection, and (III) lateral exchange and spreading. (Marshall and Schott 1998)

III. MODEL FOR LARGE EDDY SIMULATION

The LES model employed in this study used a Boussinesq approximation applied to the vorticity forms of the Navier-Stokes equations (Equations 3.1, 3.2, 3.3), written in terms of vorticity components ζ_i ,the continuity equation (Equation 3.4), and heat and salinity budget equations (Equations 3.7,3.8) to calculate three dimensional, nonhydrostatic geophysical turbulences. A gradient of temperature and salinity in the east-west direction was also included, and its effect is added to the appropriate terms (Equations 3.5,3.6). The temperature and salinity gradient terms are added to the x derivative after it is calculated in the spectral domain and returned to the spatial domain.

$$\frac{\partial u}{\partial t} = v\zeta_z - w\zeta_y - \frac{\partial P^*}{\partial x} + \frac{\partial P_G}{\partial x}(iz) + f_z v - 2f_y w - \frac{\partial \tau_{xx}}{\partial x} - \frac{\partial \tau_{xy}}{\partial y} - \frac{\partial \tau_{xz}}{\partial z} \tag{3.1}$$

$$\frac{\partial v}{\partial t} = w\zeta_x - u\zeta_z - \frac{\partial P^*}{\partial y} + f_z u - \frac{\partial \tau_{xy}}{\partial x} - \frac{\partial \tau_{yy}}{\partial y} - \frac{\partial \tau_{yz}}{\partial z} \tag{3.2}$$

$$\frac{\partial w}{\partial t} = u\zeta_y - v\zeta_x - \frac{\partial P^*}{\partial z} + g[\alpha(\theta - \theta_0) - \beta(S - S_0)] + 2f_y u - \frac{\partial \tau_{xz}}{\partial x} - \frac{\partial \tau_{yz}}{\partial y} - \frac{\partial \tau_{zz}}{\partial z} \tag{3.3}$$

$$\frac{\partial u}{\partial x} + \frac{\partial v}{\partial y} + \frac{\partial w}{\partial z} = 0 \tag{3.4}$$

$$\frac{\partial \theta^*}{\partial x} = \frac{\partial \theta}{\partial x} + \frac{\partial \theta_G}{\partial x} \tag{3.5}$$

$$\frac{\partial S^*}{\partial x} = \frac{\partial S}{\partial x} + \frac{\partial S_G}{\partial z} \tag{3.6}$$

$$\frac{\partial \theta}{\partial t} = -u(\frac{\partial \theta^*}{\partial x}) - v\frac{\partial \theta}{\partial y} - w\frac{\partial \theta}{\partial z} + \frac{\partial}{\partial x}(K_\theta \frac{\partial \theta^*}{\partial x}) + \frac{\partial}{\partial y}(K_\theta \frac{\partial \theta}{\partial y}) + \frac{\partial}{\partial z}(K_\theta \frac{\partial \theta}{\partial z}) \tag{3.7}$$

$$\frac{\partial S}{\partial t} = -u(\frac{\partial S^*}{\partial x}) - v\frac{\partial S}{\partial y} - w\frac{\partial S}{\partial z} + \frac{\partial}{\partial x}(K_S \frac{\partial S^*}{\partial x}) + \frac{\partial}{\partial y}(K_S \frac{\partial S}{\partial y}) + \frac{\partial}{\partial z}(K_S \frac{\partial S}{\partial z}) \tag{3.8}$$

u and v are the easterly and northerly horizontal velocity components, w is the vertical velocity, f_z is the vertical coriolis parameter, f_y is the horizontal coriolis parameter, K_θ, K_S, and K_M, are the eddy mixing coefficients for temperature, salinity, and momentum, θ is the potential temperature, S is the salinity, α is the thermal expansion coefficient, β is the salinity coefficient, τ_{ij} is the shear stress, and $\partial\theta_G/\partial x$, $\partial S_G/\partial z$, and $\partial P_G/\partial x$ are the effects caused by the gradient imposition. The vertical coriolis parameter is set to zero for these equations.

The shear stresses are computed using Equation (3.9).

$$\tau_{ij} = -K_M\left(\frac{\partial u_i}{\partial x_j} + \frac{\partial u_j}{\partial x_i}\right) \tag{3.9}$$

The dynamic pressure is computed using Equation (3.10) and includes resolved and unresolved energy with e representing the unresolved energy.

$$P^* = \frac{p}{\rho_0} + \frac{2}{3}e + \frac{u_k u_k}{2} \tag{3.10}$$

The unresolved total kinetic energy is computed using Equation (3.11) with terms representing advection, shear production, buoyancy flux, turbulent transport, and dissipation (Stone, 1999).

$$\frac{\partial e}{\partial t} = -u\frac{\partial e}{\partial x_i} - \tau_{ij}\frac{\partial u_i}{\partial x_i} + gK_\theta\left(\alpha\frac{\partial\theta}{\partial z} - \beta\frac{\partial S}{\partial z}\right) + \frac{\partial}{\partial x_i}\left(2K_M\frac{\partial e}{\partial x_i}\right) - \varepsilon \tag{3.11}$$

The thermal expansion coefficient varies linearly with depth, and with $\alpha_1 = \partial\alpha/\partial z =$ constant, it is computed using Equation (3.12).

$$\alpha = \alpha_0 - \alpha_1 z \tag{3.12}$$

The pressure gradient term is calculated first at the bottom, assuming it to be a level of no motion, using Equation (3.13) and integrated upward using Equation (3.14).

$$\frac{\partial P_G}{\partial x}(nnz) = g(-\alpha \frac{\partial \theta_G}{\partial x}\frac{dz}{2} + \beta \frac{\partial S_G}{\partial x}\frac{dz}{2}) \tag{3.13}$$

$$\frac{\partial P_G}{\partial x}(iz) = \frac{\partial P_G}{\partial x}(iz+1) + g(-\alpha \frac{\partial \theta_G}{\partial x} * dz + \beta \frac{\partial S_G}{\partial x} * dz) \tag{3.14}$$

Bottom boundary conditions are slip with respect to the mean flow and no-slip with respect to mean flow perturbations, and boundary conditions are doubly periodic in x and y. The equations involved in the model are solved using second order centered finite differencing in the vertical, a spectral method in the horizontal, and time advancement with an Adams-Bashforth scheme. At the grid scale and smaller, turbulence is assumed to be isotropic, and subgrid scale fluxes of momentum, salinity, and temperature are determined using second order turbulence closure. (Stone, 1999) For further details on the LES model and its equations and parameters see Moeng (1984), Garwood et al. (1994), Harcourt (1999), and Stone (1999).

THIS PAGE INTENTIONALLY LEFT BLANK

IV. PROCEDURE

A. CASE DIFFERENTIATION

Sixteen LES model runs were performed and analyzed for this study imposing various parameters (Table 4.1). To avoid confusion, meteorological references to wind direction will be followed throughout this paper. Northerly wind will refer to a wind from the north, 360 degrees, easterly wind will be from the east, 90 degrees, and southerly wind will refer to a wind from the south, 180 degrees, etc.

Case	$\partial\theta_G/\partial x$ (°C/km)	$\partial S_G/\partial x$ (psu/km)	Q_0 (W/m)	U_{15} (m/s)	ϕ_u (Degrees)	ΔT (Days)
GB	0.02	0.0016	400	00	N/A	15.6
G	0.02	0.0016	400	00	N/A	16.70
B	0.0	0.0	400	00	N/A	16.70
GW225	0.02	0.0016	400	12	From 225	10.80
GBW180	0.02	0.0016	400	12	From 180	18.44
GBW292	0.02	0.0016	400	12	From 292	13.58
GBW360	0.02	0.0016	400	12	From 000	13.92
GBW045	0.02	0.0016	400	12	From 045	19.48
GBW112	0.02	0.0016	400	12	From 112	13.92
GBW225	0.02	0.0016	400	12	From 225	13.23
gB	0.005	0.0004	400	00	N/A	16.70
gW225	0.005	0.0004	400	12	From 225	19.48
gBW045	0.005	0.0004	400	12	From 045	28.50
gBW225	0.005	0.0004	400	12	From 225	28.85
gBW360	0.005	0.0004	400	12	From 000	20.87
gBW180	0.005	0.0004	400	12	From 180	24.69

Table 4.1. LES Model Runs Completed

The gradient imposed is an east to west gradient in temperature and salinity with temperature and salinity both decreasing to the east. The gradients used in the strong gradient cases, $\partial\theta_G/\partial x$ =0.02° C/km and $\partial S_G/\partial x$ =0.0016 psu/km, are probably stronger than those found in the central Labrador Sea. Due to some early programming problems,

small temperature and salinity gradients were not being properly advected. Because anticipated effects were not observed they were increased to the strong gradient values. Once the programming problem was detected and corrected, this strong a gradient proved to be too large, so a weaker gradient, ¼ of the magnitude, was used. The results shown here are free from the earlier programming problem. In images of the model data created using VIS5D, the differences in horizontal gradient strength and the resulting dynamics are easily seen (Figs. 4.1, 4.2, and 4.3). Case B produces small scale plumes evenly spread across the box domain (Fig. 4.1). Case gB produces plume scales larger than the no gradient case, however, still well within the box parameters (Fig. 4.2). Case GB produces much larger scale plumes and horizontal features larger than the box domain (Fig. 4.3).

The stronger gradients resulted in a significant box mode effect, producing large fluctuations in the data throughout the time series. This made analysis of some data difficult because it was hard to separate and identify the effect of the box mode on the results. Due to the limitations in the size of area being modeled imposed by the dimensions of the box, energy of wavelengths longer than the box dimensions cannot be represented. This causes a build up of energy in the longest wavelength representable, which is the box mode. If the wavelengths were not limited by the size of the box, there would be signals at the longer wavelengths and the box mode would not have any effect on the model results.

B. PARAMETER DESCRIPTION

All of the LES model cases were done over a domain 6.4 km x 6.4 km x 949.37 m deep on a grid having 20 vertical levels, 128x128x50 grid points, and 50x50x19 meter

grid spacing, and a time step of 30 seconds. An LES model previously used for study of the Labrador Sea was altered adding gradient terms as done by Stone (1999) in her study of the Greenland Sea. This model was spun up initially with no wind to reach a steady state representative of the Labrador Sea. Constant parameters were chosen for the best representation of the Labrador Sea (Table 4.2). The values of α_1, α_0, and β are values appropriate for a water temperature of 3° Celsius and salinity of 34.85 psu.

α_0	α_1	β	f_{horiz}
8.7848e-5	2.4964e-8	7.7733e-4	1.4e-5

Table 4.2. Values of LES Constants

In all runs, if wind forcing was applied, the wind forcing was of a constant speed of 12 m/s and constant direction the entire time. If cooling was applied, there was constant cooling of 400 W/m^2.

C. COMPARISON

The main purpose of this study was to determine, through numerical model application, the effect gradients of temperature and salinity combined with different directions of wind forcing have on the dynamics of an area of deep convection. Weak and strong gradients were applied, surface wind stress was applied in varying directions, cooling was applied to most cases, and also several cases included no cooling to determine its role on certain dynamics. There were cases with no wind forcing and with no gradient, which were used to compare the results of the other cases in order to better understand the effects of the wind and the gradient.

What is expected is a combination of geostrophic flow resulting from the imposed gradients combining with the nongeostrophic flow resulting from the wind stress and interactions between convection and the geostrophic wind (Figs. 4.4 and 4.5). The expectations from the model can be predicted with knowledge of what surface velocities should result from the various wind forcing directions and the imposed horizontal gradient. Due to the complexity of the motions in an area of deep convection and the non-linearity of the horizontal and vertical velocities, the relationships are not as straight forward as in a stable and strongly stratified area of the ocean. The wind and gradients will have an effect on the currents, which in turn will affect the temperature, and salinity distribution, which will affect the turbulence over the area. The model results will indicate the strength of the effect of the various gradients and wind forcing directions compared to each other and to the strength of the cooling effects. They will also indicate relationships and the combinations of the effects of the gradients, wind, and cooling involved.

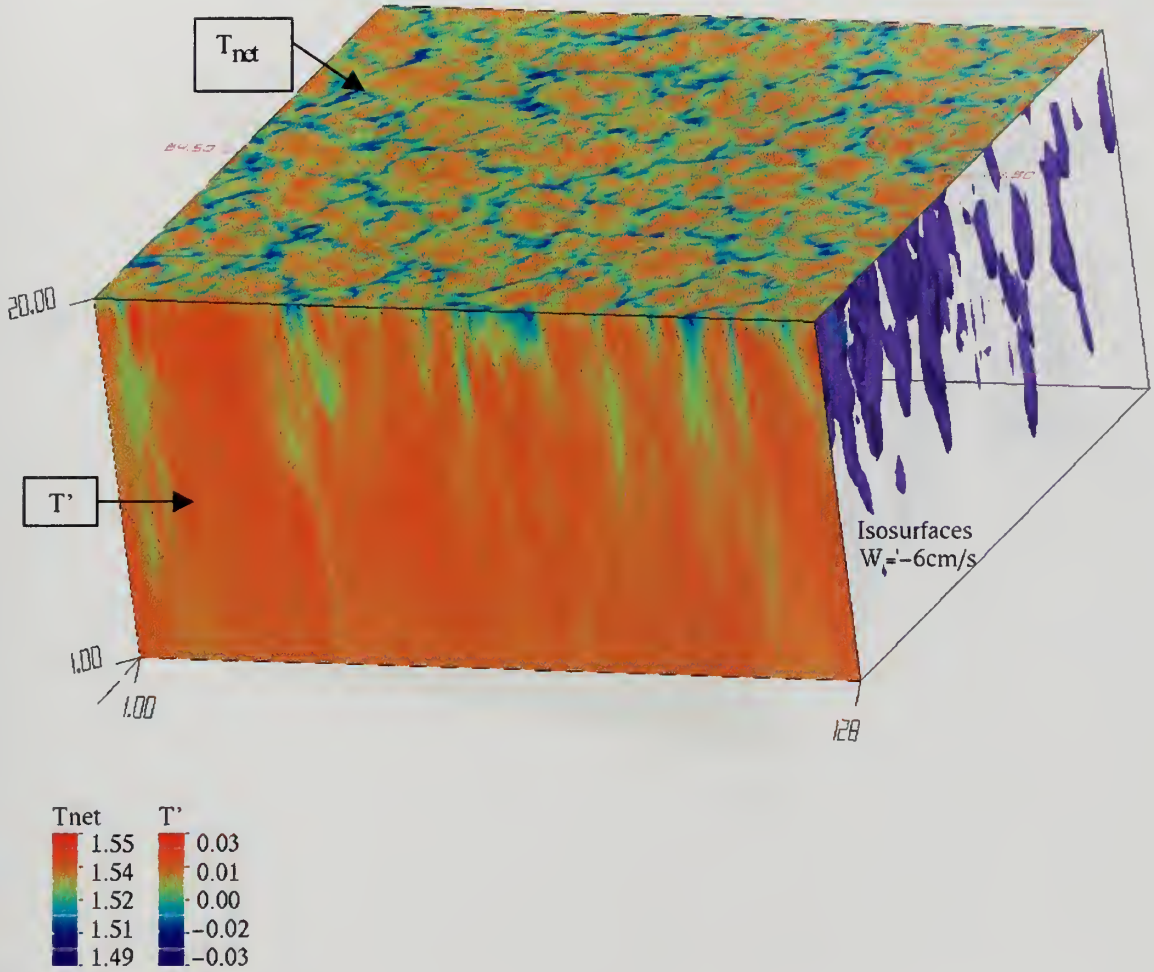

T

Figure 4.1. LES temperature at the surface, T_{net}, and relative temperature fluctuations, T', with depth in °C from a no gradient case with cooling and no wind, case B. The blue plumes represent the areas of downward vertical velocity equal to or greater than 6 cm/s.

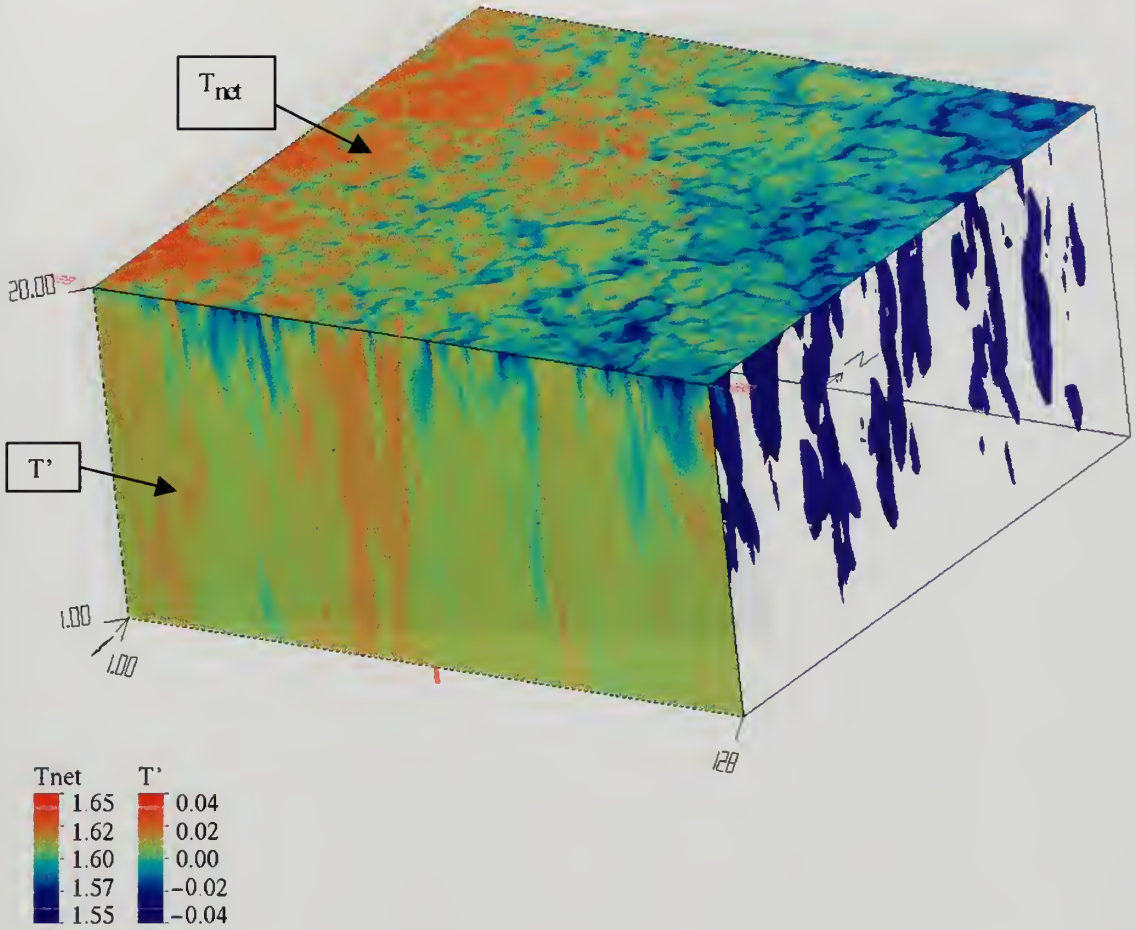

Figure 4.2. LES temperature at the surface, T_{net}, and relative temperature fluctuations, T', with depth in °C from the weak gradient case with cooling and no wind, case gB. The blue plumes represent the areas of downward vertical velocity equal to or greater than 5cm/s.

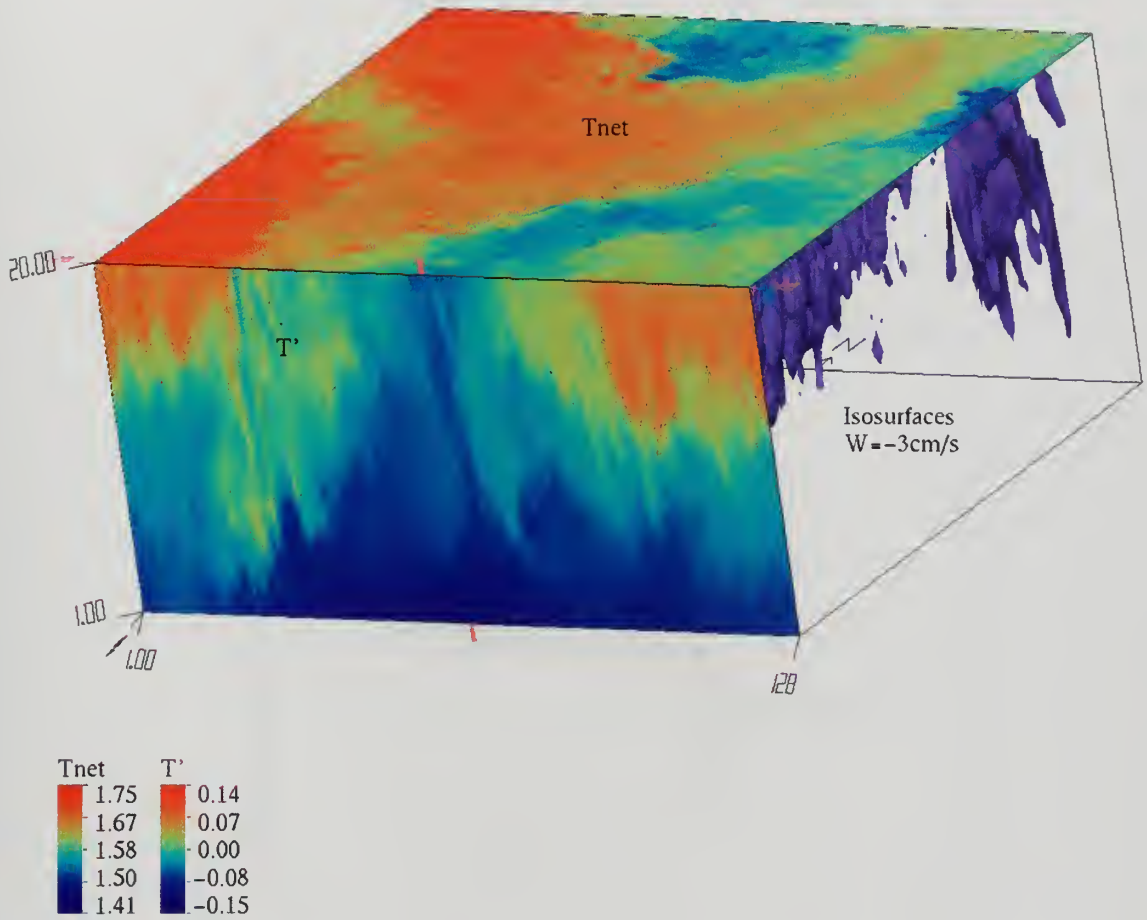

Figure 4.3. LES temperature at the surface, T_{net}, and relative temperature fluctuations, T', with depth in °C from the strong gradient case with cooling and no wind, case GB. The blue plumes represent the areas of downward vertical velocity equal to or greater than 3cm/s.

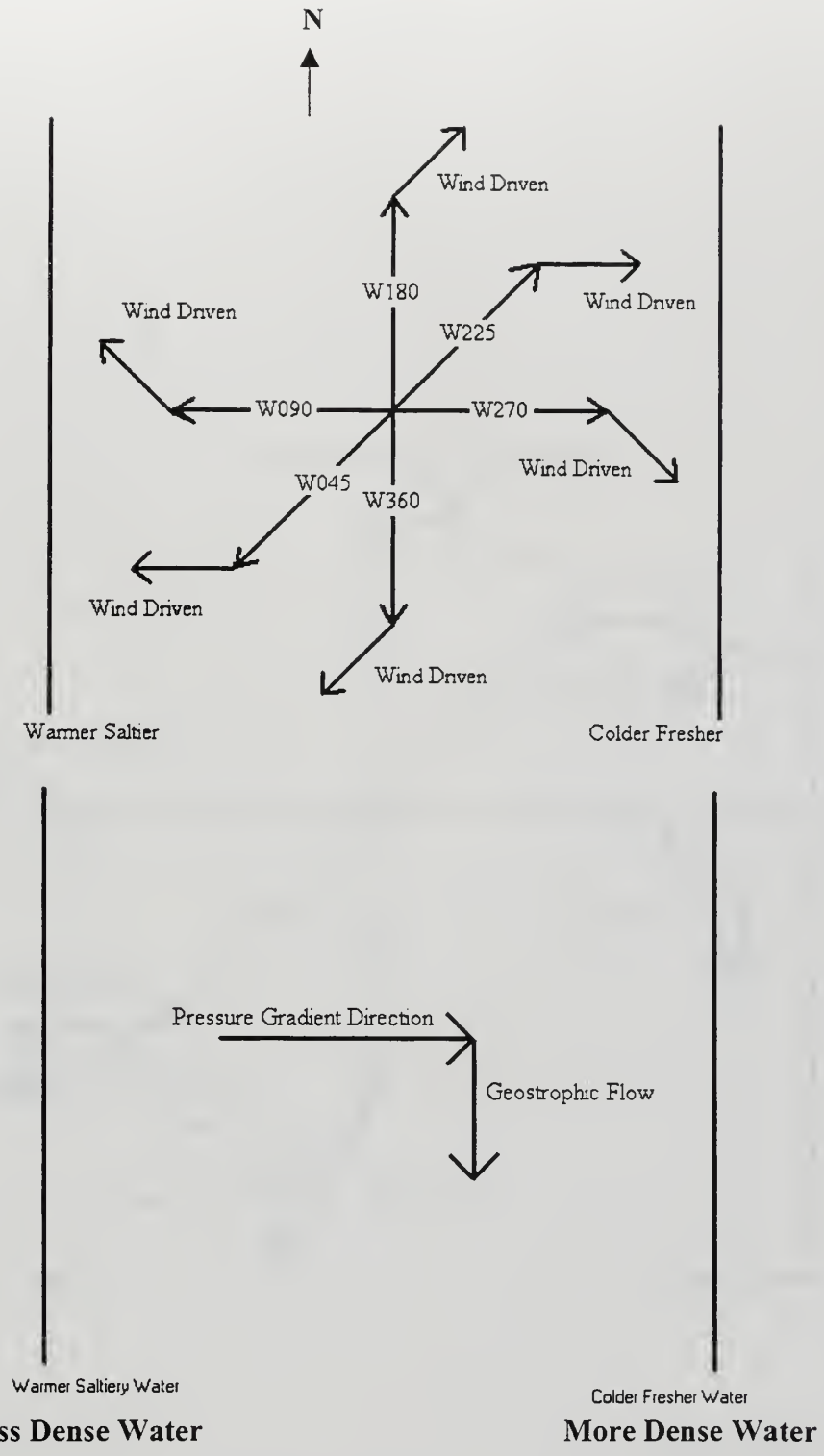

Figure 4.4. Surface current induced by wind (top panel) and gradient (bottom panel). Wind direction, indicated on the arrows, produces the wind driven surface current 45° to the right (top). Warmer saltier water to the west and colder fresher water to the east produces an eastward gradient direction resulting in a southward geostrophic surface flow (bottom).

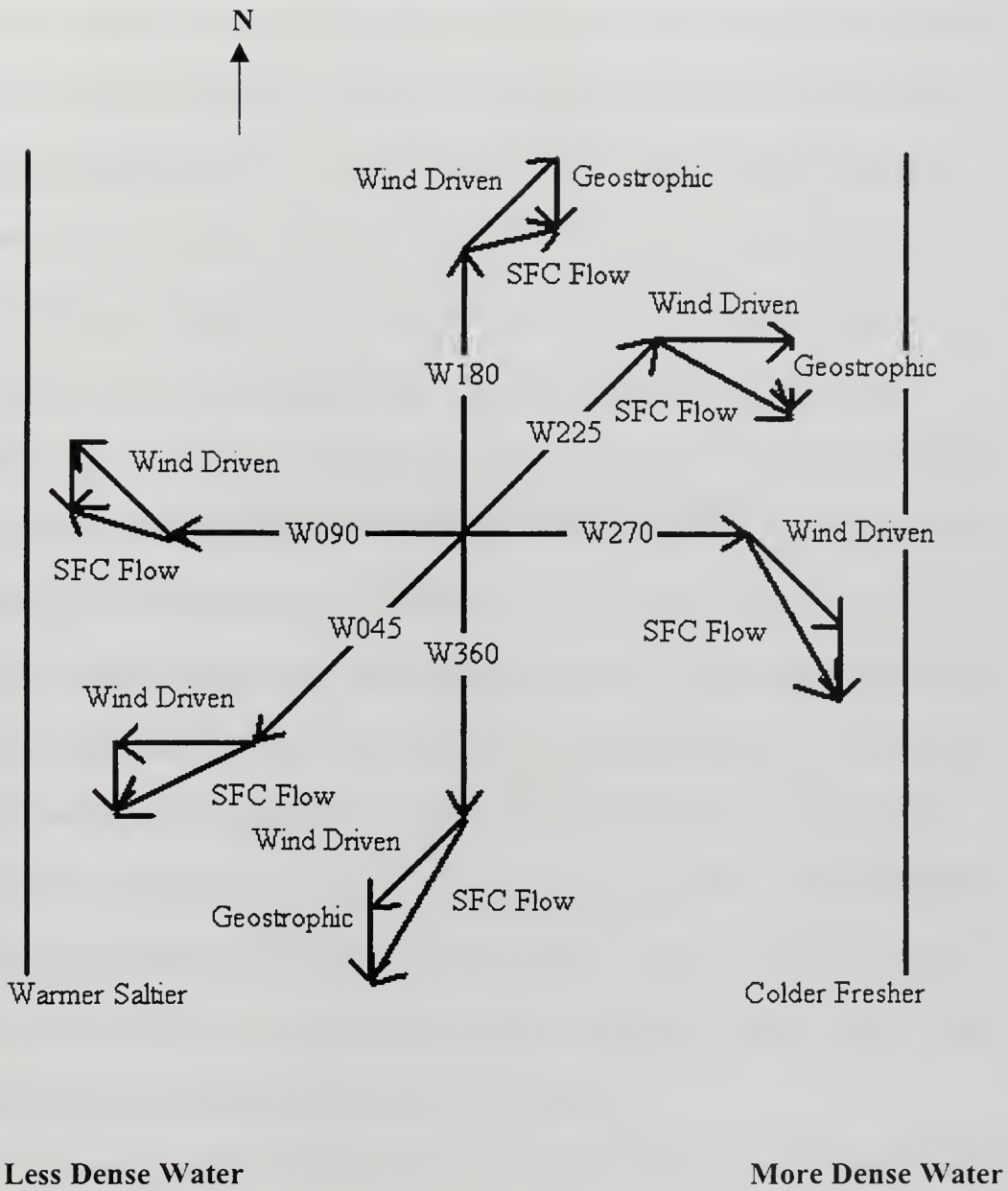

Figure 4.5. Total surface flow (SFC Flow) combining wind driven and geostrophic flow resulting from wind forcing and the east-west gradient of temperature and salinity.

THIS PAGE INTENTIONALLY LEFT BLANK

V. RESULTS

A. BOX MODE EFFECTS

Differences between the strong and weak gradient cases are clearly evident in the time series of the different cases (Figs 5.1-5.4). Large fluctuations, particularly in the temperature variance time series of strong gradient cases, dictate the occurrence of a box mode effect, with more significant effects in the northerly wind cases. This effect is not seen in the weak gradient cases. Also, notable differences inlayer-averaged, scalar variances and vertical fluxes, and in levels of Vertical Turbulent Kinetic Energy ($VTKE = \overline{w^2}$) are evident in cases having different horizontal gradient strengths.

Time series plots of the some of the strong gradient cases show the large fluctuations created by the concentration of scalar and velocity fluctuations in the lowest available horizontal wave number, the box mode (Figs 5.1 and 5.2). All of the cases have multiple spikes because the build up of energy in the lowest wave number is not averaged over several integral length scales. The amplitudes of the spikes from case GBW360 are noticeably larger, and those from case GBW180 are noticeably smaller. The larger low frequency build up in the northerly wind case indicates there is more energy being created than can properly be represented. The spikes alter the results that would truly be occurring, raising the levels of energy in the box mode. The strong box mode effect also shows that if allowed to grow outside the constrains of the model's box, there would be more energy at the frequencies too low to be represented.

Time series plots of weak gradient cases indicate no poorly resolved spikes due to box modes (Figs 5.3 and 5.4). All of the weak gradient cases were initialized from the last time step of the strong gradient run with wind blowing in the same direction. Large

oscillations in horizontal velocities are stabilized by the reduction in gradients after approximately 200 time steps, or about 3.5 days. A sharp drop in horizontal momentum flux and temperature advection occurs when the smaller gradient is applied. Increases in the vertical component of Turbulent Kinetic Energy (TKE), turbulent heat flux, and vertical momentum flux occur when a weaker gradient replaces the stronger gradient.

For all cases, the first 200 time steps were removed before averaging the data for the depth plot charts. In most runs, this eliminates the transient non-equilibrium solution and variability occurring due to model spin up.

B. COMPARISON OF PARAMETERS OVER TIME AT VARIOUS DEPTHS

Time series of the U and V components of current velocities, mean temperature and salinity, turbulent heat and salinity flux, and VTKE at the first level, representing the surface, the seventh level, at approximately 300 meters, and the fourteenth level, at approximately 650 meters, of the various LES model cases show the effects of cooling, large and small gradients, and wind forcing on different levels over time (Figs 5.5-5.16). There are differences between different depths for both large and small gradient cases, with larger variations between the large gradient cases. However, cooling appears to be the dominant factor in thermal changes and VTKE production. The gradient and the degree of wind forcing against the gradient increase or decrease these effects in a non-linear way depending on the wind direction and the gradient strength. The discussion of current velocities will be kept brief and emphasis will be placed on explaining the effects of cooling, horizontal gradients, and wind forcing on VTKE and on TKE production.

1. Horizontal Velocities

Because the horizontal density gradient imposed as far-field forcing is from east to west, the effects of this gradient dominate the meridional component of velocity, V. Temperature and salinity decrease from west to east, which produces a southerly flow (Fig 5.5). This geostrophic current exists for both the strong and the weak gradient cases with larger flow velocities in the strong gradient cases. The effects of surface wind stress are more dominant and easily seen in the U component of velocity; however, the gradient does promote a small component of westerly flow (Fig 5.5). Cooling reduces southerly and westerly flow, and its effect is larger for weak gradients.

Cases with wind producing no surface flow in the north-south direction, $\varphi = 45°$ and 225°, have meridional surface velocity, V, similar to cases with no wind (Figs 5.6 and 5.7). There are some differences below the surface where the current rotates with depth above about 300 meters, but these are small compared to V. Wind stress producing a north-south component to the surface flow alters the southerly surface flow, increasing it for northerly and decreasing it for southerly wind. However, this effect decreases with depth. The surface wind stress effects are more easily visible deeper in the weak gradient cases vice the strong gradient cases because of the relative magnitude of the meridional velocity due to the gradient strength. For the weak gradient cases, the effects extend below 300 meters depth. Below 600 meters wind driven effects are not evident in any cases. The only case producing flow with a northerly component at the surface is gBW180 (Fig 5.8). This is the only case in which the wind driven current exceeded the geostrophic current at the surface. A case with wind out of the southeast would probably have an even stronger effect.

Adding to or removing cooling from a strong gradient case does not alter the mean magnitude of meridional velocity component V, at the surface or at depth. This shows the strong gradient controls the meridional velocity. This is not the case for the weak gradient. Adding cooling to a weak gradient case reduces V at the surface to approximately 50% of its value without cooling. Values of surface V for gW225 are twice the values for gBW225 and at all levels half as big as values for GW225 and GBW225 (Figs 5.6 and 5.7).

The zonal component of velocity, U, is controlled much more by the wind direction than by any other factors. With cooling and no gradient, case B, the U component of velocity oscillates about zero. A strong gradient alone, case G, produces a very small westerly flow at the surface and mid levels, advecting cold fresh water into the area at all levels. Adding cooling reduces this westerly flow and results in a similar pattern to when only cooling is present

The weaker gradient with cooling, case gB, oscillates similarly to the cooling only case. However, the surface velocity remains mostly easterly. This produces slight advection at the surface of warm, salty water from the west. Cooling tends to make flow more easterly. The U velocity follows what is expected on the surface resulting from wind forcing. It has strongest easterly values with a southwesterly wind and strongest westerly values with a northeasterly wind. This produces surface advection of warm salty water and cold fresh water respectively. Northerly winds produce weaker westerly flow, and southerly winds produce weaker easterly flow than do the northeasterly and southwesterly winds respectively. This flow rotates and decreases in strength with depth.

The easterly and westerly flow of water across the gradient transports water of different characteristics so as to increase or decrease stability depending on the direction of flow. Easterly flow at the surface will push warmer more saline water over colder fresher water. This promotes stability, and competes with hydrostatic instability driven by surface cooling. Surface cooling then produces saltier cold plumes that sink and mix with the fresher water. Westerly flow at the surface will put colder fresher water over warmer saltier water. This produces instability as cooling occurs, resulting in the formation of more dense plumes. Thermobaricity further affects the intensity of deep convection, making the colder plumes more dense at depth than saltier plumes with the same potential density. The advection resulting from wind forcing across a gradient will alter the amount of temperature and salinity present in the water column and the resulting turbulent fluxes and VTKE.

2. Mean Salinity and Temperature

The time series plots of mean salinity and of temperature for various levels show the importance of surface cooling and wind direction on their rates of change and stability (Figs 5.5-5.10). All cases are decreasing in temperature at about 650 meters depth and all cases with cooling are also decreasing in temperature at the surface. The salinity values increase and decrease more depending on the orientation of the wind forcing with respect to the imposed gradient. The cooling rates depend more strongly on whether or not there is surface heat loss, and only small changes result from varying wind direction.

Case B shows steady cooling at all levels with a minimum temperature at the surface. Below the surface, the temperature is nearly homogeneous, contributing to the low stability for this case. The mean salinity fluctuates about a constant at all levels.

This produces a low vertical gradient of salinity. In the gradient only case, case G, temperature and salinity increase at the surface, and decrease below 600 meters (Fig 5.5). This decrease in temperature and salinity at depth is due to a westerly component of flow induced by pressure gradients that are unbalanced by friction or Coriolis forces when surface cooling is absent. The temperatures warm at the top because of this flow and because there is no cooling. The result is a more stable situation with the vertical gradient of salinity and temperature increasing over time, restratifying the water column.

Combining a strong gradient with cooling in the absence of wind stress, case GB, produces temperature decreases at all levels. However, the surface remains warmer than lower level temperatures due to the horizontal advection in the presence of the mean gradient. The salinity fluctuates slightly about a constant mean at the surface and decreases slightly at the lower levels. This makes case GB more stable than the cooling case, B, but less stable than the gradient-only case, G. The gB case shows a greater effect from cooling. The fluctuations are of smaller magnitude, and the surface temperature becomes the coldest over time. The salinity at lower levels does not decrease with time, and the vertical gradients of salinity and temperature are smaller. This produces stability more similar to the cooling only case.

Adding wind forcing does not notably change the results for the temperature, but the effects are seen in the salinity values. Cooling increases slightly for winds advecting colder fresher water and decreases when warmer saltier water is advected. The tendencies in the strong gradient cases are less evident than in the weak gradient cases. However, weak gradient cases show a steady increase of salinity at all levels with time. This results from easterly induced flow and a steady decrease from westerly induced flow

(Figs 5.9 and 5.10). For northeasterly and southwesterly induced flow there is a steady but smaller increase and decrease respectively in salinity than for cases inducing easterly and southerly flow

3. Turbulent Fluxes and VTKE

The turbulent heat flux $(\overline{w'\theta'})$ either buoyantly produces or consumes TKE depending on its sign. Release of warmer temperatures upward to areas of colder temperatures results in $\overline{w'\theta'} > 0$, so TKE and VTKE increase together. If water from above warms the water below, $\overline{w'\theta'} < 0$, energy is consumed, and TKE production decreases. The opposite is true for turbulent salinity flux $(\overline{w's'})$. Salinity moving upward, $\overline{w's'} > 0$, requires energy, so TKE production and VTKE decrease. Salinity moving downward, $\overline{w's'} < 0$, creates turbulence and increases VTKE. These two turbulent fluxes combine to produce the buoyancy flux. Although the buoyancy flux determines the buoyant production of TKE, the level of VTKE depends as well on redistribution between horizontal and vertical components, dissipation, turbulent transport, and shear production.

Vertical TKE is very important in determining entrainment rates for deeply convecting mixed layers. Because the purpose of this study is to determine the effects horizontal gradients and wind on the deep convection process, TKE production and its effects on VTKE will be examined closely.

Cooling, horizontal gradients and wind forcing all affect the turbulent fluxes in various ways (Figs 5.11-5.17). Cooling acts to increase $\overline{w'\theta'}$ and a gradient acts to decrease $\overline{w'\theta'}$. Wind forcing affects both $\overline{w'\theta'}$ and $\overline{w's'}$ either to increase or decrease

them depending on the direction relative to the horizontal gradients. It also works to mix the upper level waters. Because the cooling effect dominates $\overline{w'\theta'}$ production, effects of surface wind stress are more easily seen in $\overline{w's'}$. The resulting buoyant TKE production, $\overline{w'b'}$, however, indicates the effects of wind on $\overline{w'\theta'}$ dominate over $\overline{w's'}$.

Case B, with surface cooling only, produces positive $\overline{w'\theta'}$ which decreases linearly with depth. Salinity flux is approximately zero at all levels. This results in stronger VTKE at lower levels as cooling parcels accelerate with depth. With the warming surface due to restratification in case G, $\overline{w'\theta'}$ at the surface becomes slightly negative (Fig 5.11). The midlevels remain positive indicating continued buoyant production of TKE in the layer interior after the surface heat loss is turned off. The pattern of vertical salinity flux is similar, and will act in opposition to $\overline{w'\theta'}$ in the net buoyancy flux resulting in TKE production or consumption. The resulting VTKE is increasing in time both near the surface and at mid-depths, but with values much lower than the cooling cases. Fluctuating VTKE near the surface appear correlated to fluctuation of $\overline{w's'}$ about zero. Fluctuations of VTKE in the interior appear correlated to variations in both $\overline{w'\theta'}$ and $\overline{w's'}$. The lower values of VTKE for case G, with no cooling, are expected given the lower values of $\overline{w'\theta'}$.

Both cases GB and gB have positive $\overline{w'\theta'}$ at the surface to mid-level depths with $\overline{w's'}$ fluctuating about zero (Figs 5.12 and 5.13). The weak gradient case, gB, has heat flux values only slightly lower than case B, indicating the stronger effect of cooling. The resulting VTKE of case gB is close to but less than the VTKE of case B. The turbulent heat flux values for case GB are lower than those for cases gB and B showing the effect

the strong gradient has on reducing $\overline{w'\theta'}$ and thus reducing VTKE. Mixing across the thermal wind of the strong gradient tends to increase surface temperatures and cooling decreases them. Combining the two effects produces a flux of heat upward, but at a slower rate than without a strong gradient. Turbulent salinity flux is reduced from case G and fluctuates about zero at all depths in both cases GB and B, which will produce larger buoyancy flux and VTKE values, although production of VTKE by turbulent heat flux will be much larger than the effect of the turbulent salinity flux. Combining a strong gradient and cooling reduces VTKE at all levels from those for the cooling only case and increases VTKE relative to the gradient only case (Figs 5.11 and 5.12). These changes in VTKE correspond to changes in $\overline{w'\theta'}$ values, being lower for case GB than case B and higher than case G.

Adding wind from the southwest, which advects warmer, saltier water, to a case with a gradient and no cooling, cases gW225 and GW225, makes $\overline{w'\theta'}$ and $\overline{w's'}$ more negative with depth and decreases the positive values of subsurface $\overline{w'\theta'}$ and $\overline{w's'}$. This results in lower production of VTKE by turbulent heat flux and higher VTKE production by turbulent salinity flux. The weaker gradient case, gW225, produces a steady surface level VTKE with lower value than case GW225, and lower subsurface values. Wind increases the production of VTKE near the surface with VTKE values larger for case GW225 than case G at the first level. Salinity flux and shear production from surface wind stress must dominate TKE production near the surface and heat flux must dominate below the surface resulting in lower VTKE levels in the lower levels for case GW225 than case G.

Cases with both strong and weak gradients including cooling and wind forcing, independent of wind direction, have positive vertical heat flux at the surface, with interior values above or close to zero. There is a small decrease in $\overline{w'\theta'}$ with wind stress producing an easterly flow advecting warmer, saltier water, cases GBW180, GBW225, gBW180, and GBW225, and an increase with the wind stress producing westerly advection of colder, fresher water, cases GBW360, GBW045, gBW360, gBW045. However, the effect of the wind forcing and the resulting advection is much more evident in the vertical salinity flux (Figs 5.11-5.14). Wind producing surface westerly flow, advecting colder fresher water, has positive surface $\overline{w's'}$ and mostly positive subsurface $\overline{w's'}$. This decreases buoyancy flux and decrease VTKE countering the effect of the increase produced by $\overline{w'\theta'}$ increases. Surface wind stress producing easterly flow has negative surface $\overline{w's'}$ and mostly negative subsurface $\overline{w's'}$. This has an opposing effect on buoyancy flux and VTKE as forcing in the opposite direction and counters the decreases in $\overline{w'\theta'}$ in cases with wind from 225 and 180 degrees. Buoyancy flux, $\overline{w'b'}$, is higher for northerly winds in both strong and weak gradient cases showing the dominance of the temperature effects. Comparing similar wind stress directions, the strong and weak gradients have similar surface buoyancy flux near the surface. However, the strong gradient cases contain higher subsurface levels of buoyancy flux.

Adding cooling to cases GW225 and gW225 increases the levels of both near-surface and subsurface VTKE. Interior VTKE for both cases, GBW225 and gBW225, is increased much more than the near-surface VTKE, resulting in case gBW225 having sub-surface VTKE greater than near-surface VTKE (Fig 5.15). The near-surface VTKE for gB is slightly less than the surface VTKE for gBW225 resulting from the higher salinity

flux in case gBW225 due to the advection resulting from the wind and the wind mixing (Figs 5.13 and 5.15). Case GBW225 has lower values of VTKE than gBW225, and higher surface but lower subsurface values than GB (Figs 5.12, 5.14, and 5.15). The surface values for all of the strong gradient cases with wind forcing, no matter what the direction, produce comparable surface VTKE values. Similarly, all of the weak gradient cases with wind forcing produce comparable surface VTKE values. The level of VTKE for weak gradient cases is larger at all depths than that for the strong gradient cases. This was also seen in the comparison of cases B and GB.

Wind forcing with a northerly component as in cases GBW360, gBW360, GBW045, and gBW045 produces sub-surface VTKE values greater than those produced when wind forcing has a southerly component (Figs 5.14-5.17). The northerly component cases advect colder, fresher water. The temperature component is the controlling factor in this difference. The northerly component cases have positive $\overline{w's'}$, and the southerly component cases have negative $\overline{w's'}$. Heat flux is greater for the northerly component cases, overcoming the positive $\overline{w's'}$ values, which act to reduce VTKE.

The wind directions and gradient strength clearly have an impact on the characteristics of temperature and salinity and energy throughout the entire water column. Depending on wind direction, horizontal currents stabilize the water column by pushing lighter fluid over heavier fluid, or destabilize it by forcing heavy fluid over lighter fluid. The magnitude and tendencies change from case to case requiring close examination of the forcing, the resulting conditions, and the consequences on vertical motion and stability.

C. BULK AVERAGES OVER SPACE AND TIME

The data for each case was averaged over 3-D space and time to give a bulk mean representation of the magnitudes of various turbulent statistics (Figs 5.18- 5.20). Even though this averaging removes details regarding changes with depth and time, it does provide a way to make overall comparisons among cases with different wind direction, gradient strength, and surface heat loss. Layer averaged turbulence statistics are plotted as a function of the angle of the wind, φ (Figs 5.18-5.20). Cases with no wind forcing are plotted at $\varphi = 0°$, while northerly winds are plotted as $\varphi = 360°$. Going left to right across each plot, the wind is veering from northeasterly to southerly to southwesterly to northerly at the far right. There are two extra cases for the strong gradient that were not run for the weak gradient. Both the strong and weak gradient cases show a similar shape and change of magnitude with wind direction. However, sensitivity to surface wind direction depends upon the degree of baroclinicity. These differences will now be examined more closely.

1. Salinity Gradients, Temperature Gradients, and Stability

The vertical gradients of temperature and salinity provide a good picture of the stability (Figs 5.18). In all cases, the mean temperature and salinity gradients change in the same manner for various wind forcings. There is very little change in vertical gradient for the weak gradient cases with all cases close to zero except near the surface where cases with cooling are unstable. Temperature and salinity gradients are both negative for cases gBW180 and gBW045 indicating lower stability for those wind forcing directions.

The strong gradient cases have much greater variability of vertical temperature and salinity gradient between cases with different various wind forcing. Case GBW180 results in the lowest mean gradient with GBW045 having the second lowest. Although the sensitivity to wind stress and direction is much larger for the strong gradient cases, the pattern of response correlates well with the effect of wind direction in the low gradient cases. Case GBW360 produces the strongest vertical gradients for the interior, resulting in the most stable case with cooling.

The resulting stability follows closely the tendencies of the vertical gradients of temperature and salinity. Analysis of the overall stability of the various cases shows the effect of a weak gradient imposed in an area of cooling with or without wind is to increase the stability slightly (Fig 5.18). The average remains unstable, however, for all weak gradient cases with surface cooling because of the large near-surface instability. A strong gradient, with or without wind, increases the overall stability. The smallest increase is seen with no wind present followed by southerly winds. The largest increase in stability is present with forcing by northerly winds. Northerly winds advect colder, fresher water over warmer, saltier water. One would expect this to produce a more unstable environment.

2. Salinity Variance, Temperature Variance, and VTKE Relationship

There is greater overall variance of salinity and temperature for a strong gradient case vice a weak gradient case, resulting in larger corresponding variances (Fig 5.19). For both strong and weak gradient cases, there is a larger amount of temperature and salinity variance for northeasterly and northerly winds producing westerly flow than for southwesterly and southerly winds producing easterly flow at the surface. Similarly there

is more positive turbulent heat and salinity flux in the cases where westerly surface flow advects colder, fresher water than in cases where easterly flow advects warmer, saltier water (Figs 5.19). Increasing the turbulent heat flux increases VTKE production. Increases in turbulent salinity flux decrease VTKE. Decreasing both has the opposite effect. The negative turbulent salinity flux produced by the large gradients with southerly wind forcing will consume rather than produce VTKE. These two elements largely counteract each other in the buoyant TKE production $(\overline{w'b'})$.

The mean buoyancy flux (Fig 5.20) takes into account both resolved and unresolved heat and salinity fluxes.

$$\overline{w'b'}+\tau_{3b} = g(\alpha_0 + \alpha_1 z)(\overline{w'\theta'} + \tau_{3\theta}) - g\beta(\overline{w's'} + \tau_{3s}) \tag{5.1}$$

In equation (5.1) α_0, and α_1 are the thermal and thermobaric expansion coefficients, β is the expansion coefficient for salinity, g is the acceleration due to gravity, and τ_{3b}, $\tau_{3\theta}$, and τ_{3s} are the subgrid vertical fluxes of buoyancy, b, θ, and s, in the LES subgrid parameterization.

The effects of turbulent heat and salinity flux tend to cancel, making the buoyancy flux much less variable (Fig 5.20). Heat flux, $\overline{w'\theta'}$, appears to dominate in the production of buoyancy flux, $\overline{w'b'}$, producing lower values for southerly winds and higher values for northerly winds corresponding to the lower and higher values of $\overline{w'\theta'}$ and the VTKE producing and consuming values of salinity flux, $\overline{w's'}$. There is more variation in vertical fluxes among strong gradient cases than among weak gradient ones. Strong gradients have lower $\overline{w'b'}$ values than weak gradients for southerly winds and higher values for northerly winds.

The pattern of response in layer averaged VTKE is similar to the pattern of buoyant VTKE production in mean $\overline{w'b'}$ (Fig 5.20). There are higher amounts of VTKE in the northerly wind cases than the southerly wind cases. Also, there is significantly more VTKE produced in the weak gradient cases. These differences between strong and weak gradient levels of VTKE must be due to either differences in net VTKE production, redistribution to horizontal TKE, or different rates of dissipation.

The difference in the strong and weak gradient cases could have to do with different scaling relations between vertical and horizontal motions and buoyancy flux depending on the limitations felt by the two different situations. Marshall and Schott (1998) discuss two such scalings. One is not limited by depth and is affected by the Earth's rotation, Equation (5.2). The other is limited by depth and independent of rotation, Equation (5.3).

$$w \approx \left(\frac{B_0}{f}\right)^{\frac{1}{2}} \tag{5.2}$$

$$w \approx (B_0 h)^{\frac{1}{3}} \tag{5.3}$$

The relation limited by depth produces a larger vertical velocity from a similar buoyancy flux value than does the relation affected by rotation. The stronger gradient cases may follow one relation and the weak gradient cases may follow the other. This could explain differences in buoyancy flux to VTKE conversion. There is no obvious difference between the relationships for the two gradient strengths (Fig 5.21). They both appear to more closely follow the relation limited by depth. The differences in magnitude for buoyancy flux and resulting VTKE production for small and large gradient cases can possibly be explained by a difference in shear production, redistribution, or dissipation.

These quantities are also involved in the production of VTKE as discussed in Chapter III, Equation (3.11).

D. BUOYANCY FLUX VTKE RELATIONSHIP

1. Gradient, Cooling, and Wind Direction Effect on VTKE

The presence or absence of surface cooling and the associated buoyant production of VTKE has the largest effect on the level of VTKE (Fig 5.22). The most significant factor after cooling is the strength of the horizontal buoyancy gradient and the thermal wind shear. With cooling, a strong gradient results in less vertical TKE and a weak gradient or no gradient results in more VTKE. This is reversed in cases without cooling where the stronger gradients yield larger values of VTKE because of stronger shear production.

The next factor to consider in VTKE levels is the wind stress and direction. The weak gradient cases with westerly wind-driven surface flow produce higher VTKE values than does the case without wind and do the weak gradient cases with easterly wind-driven surface flow. This indicates that surface wind stress can lower or raise the level of VTKE depending on the orientation of the surface wind with respect to the horizontal density gradient. The strong gradient cases with cooling all have smaller VTKE values than the weak gradient cases with cooling. The strong gradient cases also differ in value depending on wind forcing direction. With constant cooling and a gradient, strong or weak, wind with a northerly component or no wind will produce more VTKE than wind with a southerly component. Near the surface, above about 150 meters depth, the presence of wind forcing becomes very important in the production of VTKE with higher values generated through shear production when wind forcing is applied no

matter what the direction. Vertical TKE decreases toward the surface for all cases with cooling. In cases with no wind forcing, near surface VTKE is lower than in cases with wind forcing. All cases with cooling and wind forcing approach similar VTKE near the surface. Cases with no cooling have increased VTKE near the surface, and cases forced by wind increase even more.

An understanding of the mean profile of VTKE as a function of depth (Fig 5.22) for all of the cases is important. Two thirds of the subgrid kinetic energy is added to the VTKE to account for the subgrid kinetic energy that is parameterized by the LES model. By plotting all of the results in one figure, it is easy to see what conditions reduce or increase VTKE amounts, and definite, distinct groupings are evident. The build up of VTKE at the bottom boundary, especially evident in the strong gradient cases, is due to the closed bottom boundary of the LES model. This has no physical meaning relevant to entraining boundary layers.

The smallest values of VTKE occur in the cases with no cooling. Below 150 meters, the VTKE in case G, with no wind and no cooling, is larger than the cases with a southwesterly wind. Although closer to the surface, VTKE increases for cases with wind stress. Comparison of cases G, GW225, and gW225 shows that when no cooling is involved, a horizontal gradient increases the values of VTKE, with a stronger gradient resulting in a greater increase. This pattern is not replicated in cases with surface cooling. All of the strong gradient cases with cooling produce lower values of VTKE than do the weak gradient cases. Both weak and strong gradient cases with wind stress have larger VTKE levels near the surface where the shear production is largest.

Profiles of VTKE for cases with cooling are all similar in shape except the weak and no gradient cases peak at a lower depth, and they all converge near the surface. Different cases fall into distinct groups according to cooling, gradient strength and wind direction. Cases with weak or no gradient have the largest VTKE values and are all fairly similar in value. Within each grouping, cases with a northerly wind component have elevated levels of VTKE. Those with no wind, including the case with no gradient, have intermediate levels of VTKE, and cases with a southerly wind component have reduced VTKE. The shapes of all these profiles are very similar except at the surface where the VTKE of the cases with no wind, gB and B decrease substantially.

The next highest values of VTKE are obtained in strong gradient cases with either no wind or when the wind has a northerly component. Again, the VTKE in case GB, with no wind forcing, decreases near the surface resembling more cases gB and B. Similarly, cases with wind and a strong gradient are closer in value near the surface to the small gradient cases with wind. The greatest reduction of VTKE due to surface wind stress in cases with cooling is found for GBW225 and GBW180. These are the strong gradient cases with a southerly winds. Again, near the surface, these cases approach values of the other cases with cooling and wind.

2. Components of Buoyancy Flux and the Conversion to VTKE

Taking one example case from each of the distinct VTKE groupings, variations in the levels of VTKE are compared to variations in buoyant TKE production (Figs 5.23 and 5.24). Comparisons using different cases show similar results and relationships. A different relationship is found for the weak gradient cases between buoyancy flux and VTKE production than exists for the strong gradient cases. There appears to be a direct

relation within the same gradient regime. However, there are obvious differences in the production process between the two gradient strength cases.

The comparisons show that large changes in turbulent heat flux, $\overline{w'\theta'}$, and salinity flux, $\overline{w's'}$, are not fully compensating in buoyancy flux, $\overline{w'b'}$ (Figs 5.24 and 5.25). For case G, the comparable positive values of $\overline{w'\theta'}$ producing VTKE combine with the high positive values of $\overline{w's'}$ consuming VTKE. This results in substantially lower $\overline{w'b'}$ values and ultimately lower levels of VTKE. The effects on $\overline{w'b'}$ by the large variations of $\overline{w'\theta'}$ for the cases with cooling are reduced by the large variations of $\overline{w's'}$. The high positive values of $\overline{w's'}$ for case GBW360 resulting from the advection of lower salinity water over higher salinity water combine with the large $\overline{w'\theta'}$ values reducing the buoyancy flux that would result from the $\overline{w'\theta'}$ values alone. The $\overline{w's'}$ values close to zero for case gBW360 with positive values in the upper half and negative values in the lower half, act to reduce $\overline{w'b'}$ in the lower half and increase $\overline{w'b'}$ in the upper half increasing the slope of $\overline{w'b'}$, but causing little overall variation in magnitude. The large negative values of $\overline{w's'}$ for case GBW180 with the advection of saltier water over fresher water combine with the positive but relatively low values of $\overline{w'\theta'}$ to increase $\overline{w'b'}$.

It is clear that there is no direct relation between the $\overline{w'b'}$ magnitude and the resulting VTKE amounts. The weak gradient case, gBW360, with values of $\overline{w'b'}$ between those in GBW180 and GBW360, produces greater VTKE than either case. A possible explanation for these results, suggested above, is the requirement for the strong and weak gradient cases with cooling to follow different scaling relations between buoyancy flux and VTKE. The buoyancy flux is more sensitive to the combination of

gradient strength than it is to wind direction alone. However, the amount of VTKE, though also affected by the wind direction, is more determined by the strength of the gradient.

The decrease of the VTKE near the surface of the various cases is associated with a decrease in the buoyancy flux as well (Fig 5.23). For all cases there is a distinctive bend in the $\overline{w'b'}$ curves near the surface. This bend is a small error arising from the difference between the linearly interpolated values of $\overline{w'b'}$ and the interpolation by the upstream advection scheme.

E. STABILITY COMPARISONS

An analysis of the *rms* temperature fluctuation, $\theta_{rms} = \sqrt{\overline{\theta'\theta'}}$, occurring in the various cases shows again the effects of strong and weak gradients and wind direction. Stronger horizontal gradients and northerly winds produce more stable conditions, while weaker gradients and southerly winds produce less stable environments. The variations in *rms* temperature fluctuations correlate well with those of vertical temperature and salinity gradients and hence also with stability (Fig 5.25).

There is a clear distinction between the strong and weak gradient cases. All of the strong gradient cases have vertical, salinity and temperature values that are higher than the weak gradient cases at all depths. The strong gradient cases all produce a similar shape of θ_{rms} and of salinity and temperature stratification resulting in similar changes in stability values. Values of $\partial\theta/\partial z$ and $\partial s/\partial z$ peak at about 150 meters, decreasing to a minimum at about 500 meters with another larger and more distinct peak at about 800 meters. A northerly wind produces higher values of all three parameters resulting in

greater stability. The southerly wind cases produce lower values, similar to the values of case GB.

The weak gradient cases have more uniform profiles. For all of the weak gradient cases, there is a slight increase near the surface in temperature variance, θ_{rms}^2, which drops off with depth. All cases decrease gradually with depth except gBW360. This case has elevated temperature variance between 600 meters and the bottom, a trend otherwise found only for strong gradient cases. The northerly wind, which increases temperature variance, combines with the weak gradient to create the largest effect for the weak gradient, resembling the strong gradient cases.

Vertical gradients of temperature and salinity for weak gradient cases are all similar in shape, increasing slightly with depth except for the large negative temperature gradient in the upper layer due to cooling. Mean profiles of vertical temperature and salinity gradients are close to zero below about 150 meters with the upper half slightly negative and the lower half slightly positive. This creates an unstable water column in the upper half and a neutral to slightly stable environment in the lower half.

The resulting strength of temperature variance and vertical gradients for the weak gradient cases, like the strong gradient cases, depend upon wind direction. The northerly wind cases produce larger temperature variance and more positive vertical gradients of temperature and salinity than do the southerly wind cases. This results in more stability in the northerly wind cases. Unlike the strong gradient cases where GB values are similar to the southerly wind forced cases, gB is closer to the northerly wind force cases. The case with cooling and no gradient, case B, produces the lowest values of temperature variance and vertical gradients showing that even the small gradient has substantial

effects. A weak gradient alone increases temperature variance and stability in an area of cooling. Southerly winds will decrease this effect. If a strong gradient is imposed, there will be an even larger stabilizing effect and northerly winds will further increase this effect.

The effect of cooling is dominant above about 100 meters with unstable situations present for all cases with cooling. Also evident is the added effect of wind. Cooling cases including wind are more unstable near the surface than cooling cases with no wind. Below this level, the gradient strength modified by the wind direction determines the amount of temperature advection and stability present (Fig 5.26). The noncooling cases are all stable from the surface down to the bottom with the strong gradient cases becoming very stable near the surface and remaining more stable than case gW225 at all depths (Fig 5.27).

F. COOLING EFFECTS ON THE EKMAN DEPTH

An estimate of the depth to which the wind has an influence for the various cases was examined to see the changes resulting from cooling or the angle between horizontal gradients and wind direction. The Ekman depth is defined as the depth at which the flow is opposite in direction to that at the surface and the speed is approximately 4% of the surface speed. This should hold true for a horizontally homogeneous environments where vertical mixing can be represented by a constant eddy viscosity. As explained in chapter 2, due to the nonlinear interactions involved in a horizontally inhomogeneous area with cooling, this simple definition is not applicable. To estimate the Ekman depth from the model results the magnitudes of the U and V components of velocity were plotted. The corresponding gradient case without wind, GB, gB, G was subtracted to

remove the thermal wind, and the reference frame was rotated to direct the surface wind stress 45° to the left of the positive y axis (Figs 5.28-5.32). This results in a surface velocity in the direction of the positive y axis represented by the V component of model velocity. Because of nonlinear interactions and because the first level is not exactly the surface, but rather an average of the upper 50 meters, this is not precise. There is still some surface influence on the U component of velocity. Even with these considerations, for our purposes, the Ekman depth of the wind-driven current can be determined as the depth of the most negative V velocity. The level corresponding to the most negative wind-driven velocity in the rotated y-direction should be the level at which the flow is most opposite to a surface velocity rotated 45° to the right of the wind. The component profile is similar to that expected in a barotropic environment, with wind effects decreasing exponentially with depth in the upper layer (Fig 5.28).

Comparing the case with cooling to the case without cooling, GBW225 and GW225, there is a noticeable increase in the Ekman depth with cooling (Fig 5.28). Case GW225 has its minimum V velocity at approximately 180 meters and case GBW225 has a minimum at approximately 300 meters. All of the cases with cooling have similar depths of 300 meters for the minimum V velocities corresponding to the effective depth of the wind. This shows the wind direction does not have a notable effect on the depth. This depth of 300 meters is much greater than expected in stable areas. At the high latitudes of the Labrador Sea, the expected Ekman depth with winds of 12 meters per second is approximately 53 meters (Pond and Pickard, 1983). The cooling seems to have the effect of increasing the depth to which the wind has an effect through

the added mixing. The model results from a case with no cooling has a deeper than expected Ekman depth also due to the nonlinear relations involved.

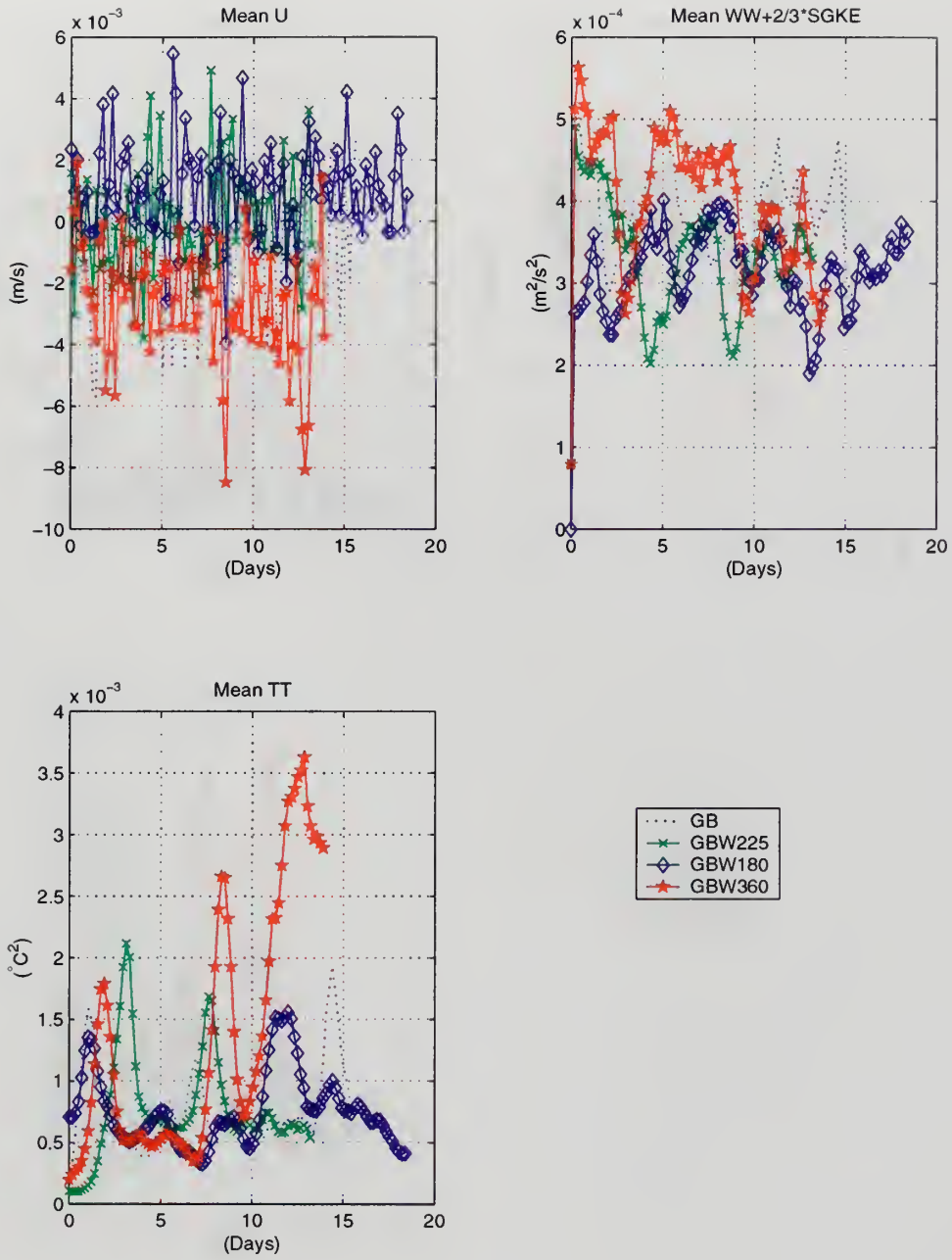

Figure 5.1. Examples of time series plots of layer-averaged zonal velocity, U (top left), TKE (top right), and temperature variance (bottom left) for several strong gradient cases.

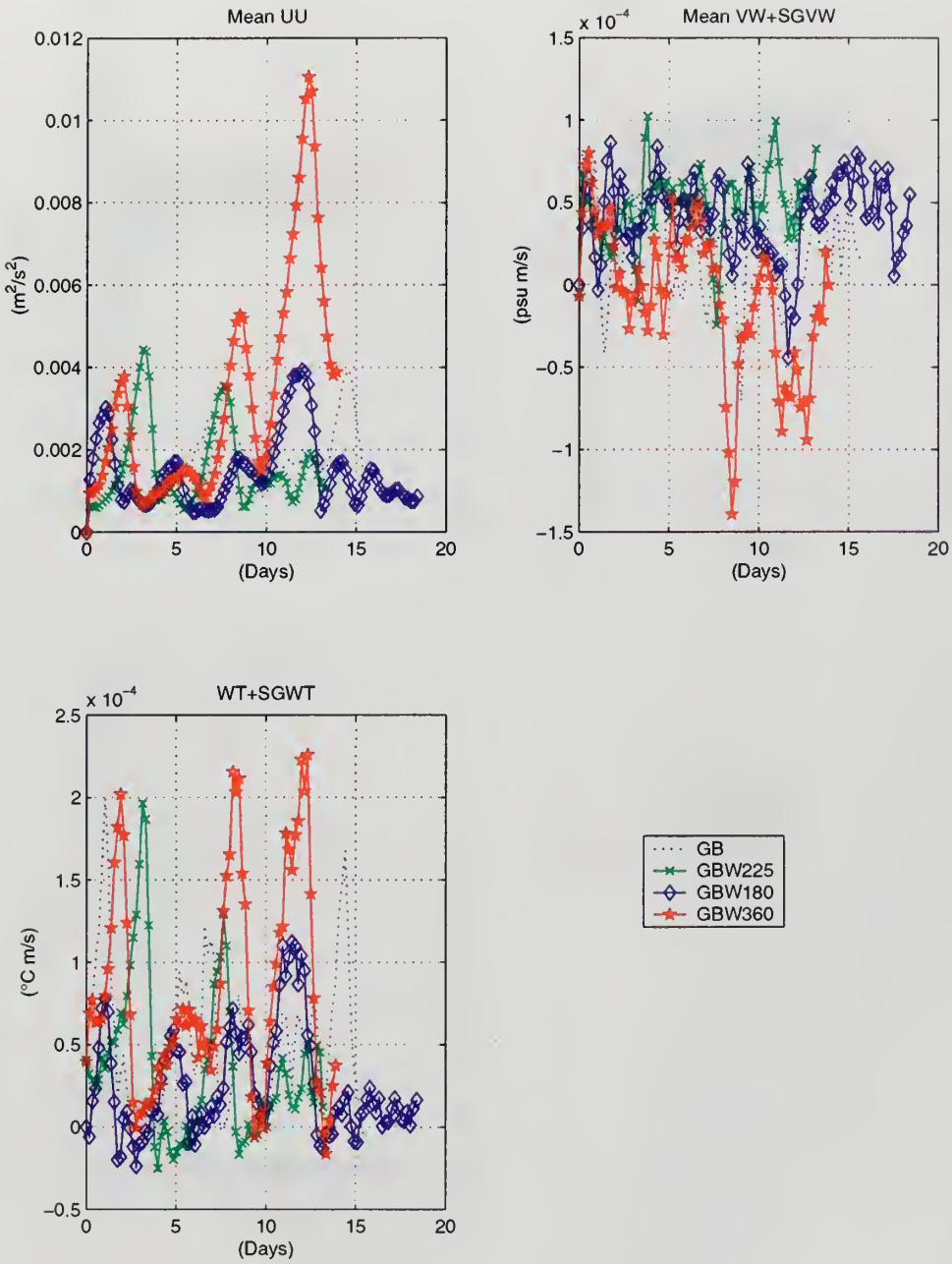

Figure 5.2. Examples of time series plots of layer-averaged zonal momentum variance (top left), the vertical flux of V (top right) and vertical heat flux (bottom left) for several strong gradient cases.

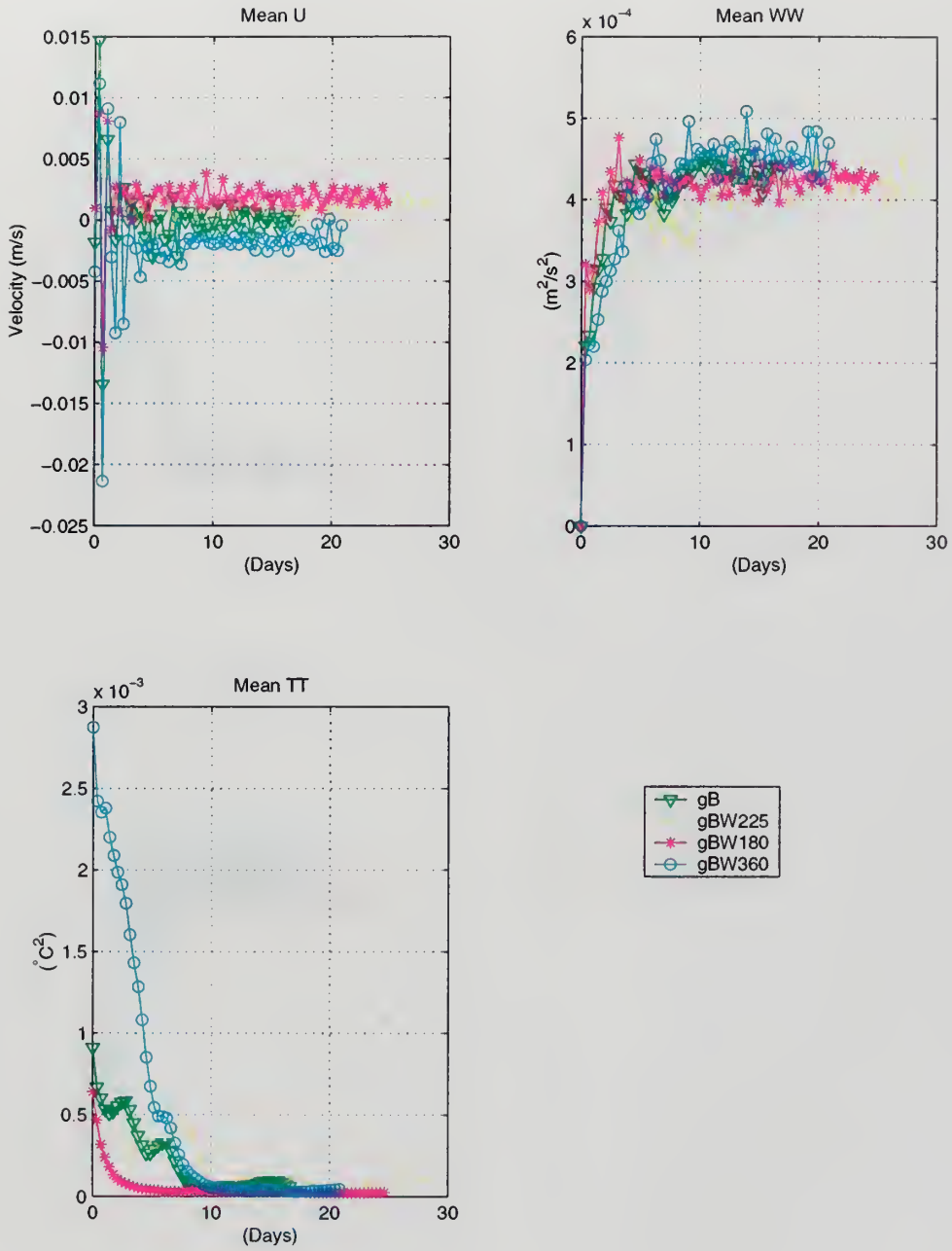

Figure 5.3. Examples of time series plots of layer-averaged zonal velocity, U (top left), TKE (top right), and temperature variance (bottom left) for several weak gradient cases.

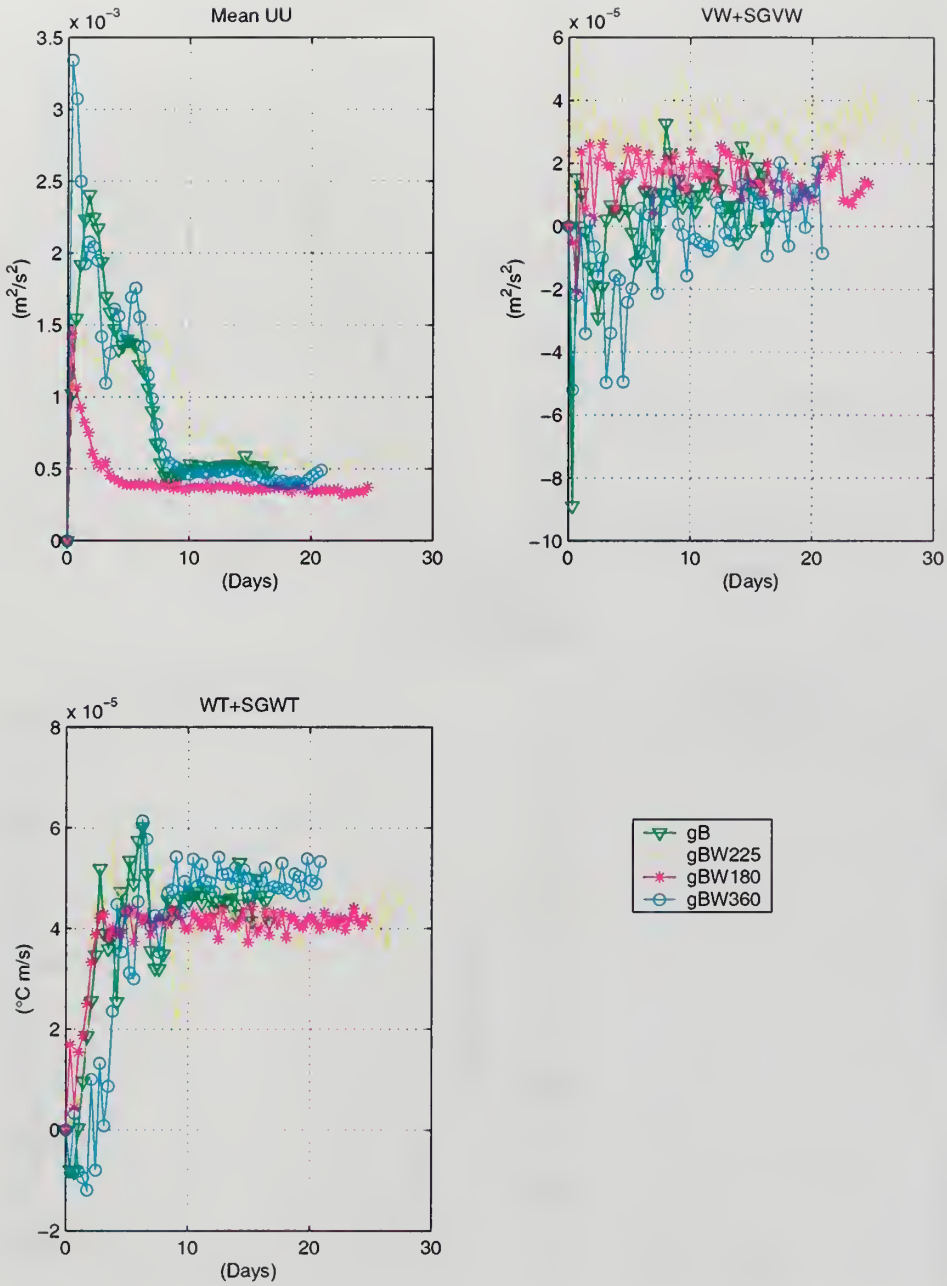

Figure 5.4. Examples of time series plots for layer-averaged zonal momentum variance (top left), net flux of V (top right) and net vertical heat flux (bottom left)for several weak gradient cases.

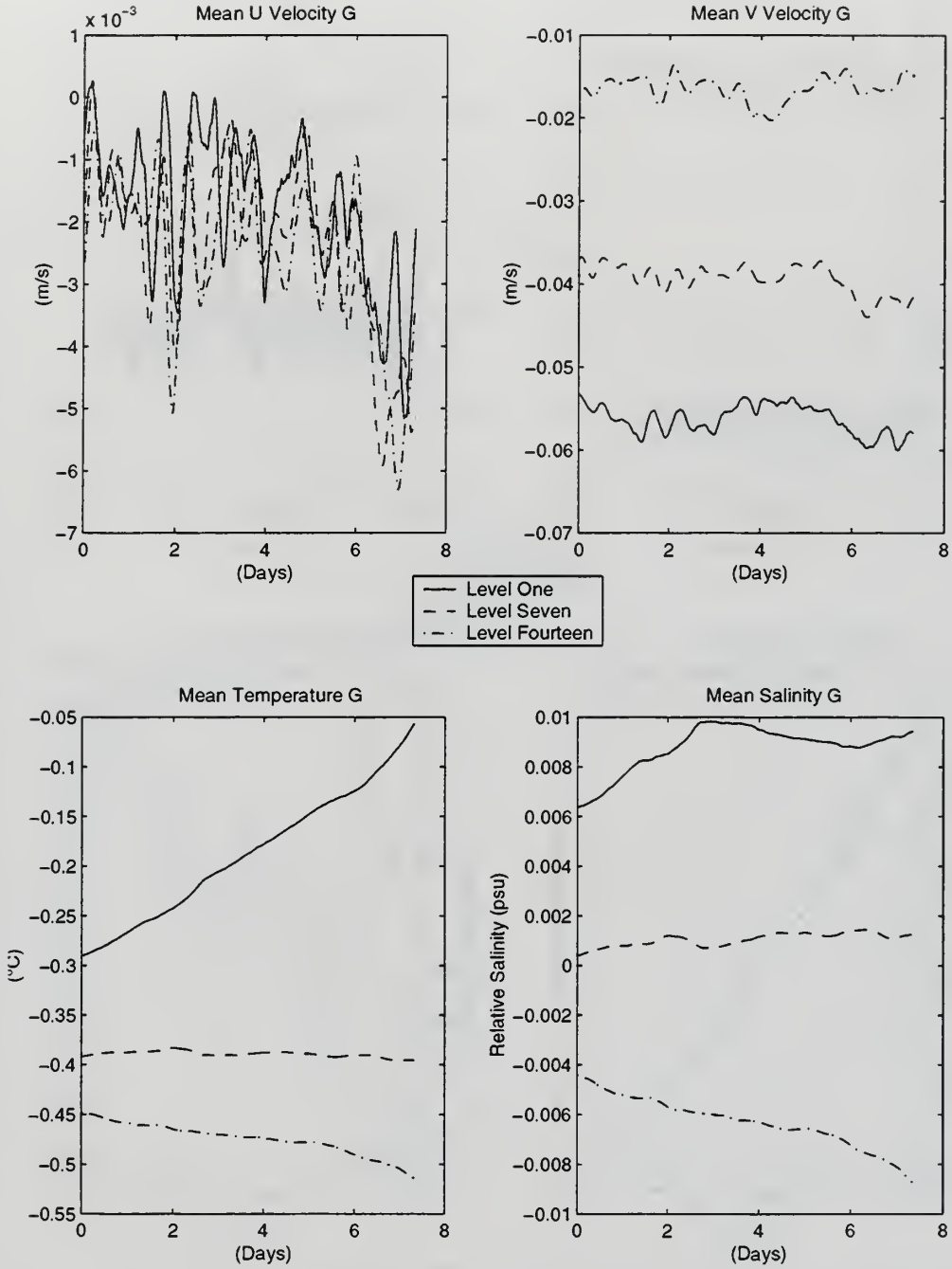

Figure 5.5. Time series of zonal (top left) and meridional (top right) horizontal velocities and mean potential temperature (bottom left) and mean salinity (bottom right) for LES case G at the surface (level 1), at 315 meters depth (level 7), and at 630 meters depth (level 14).

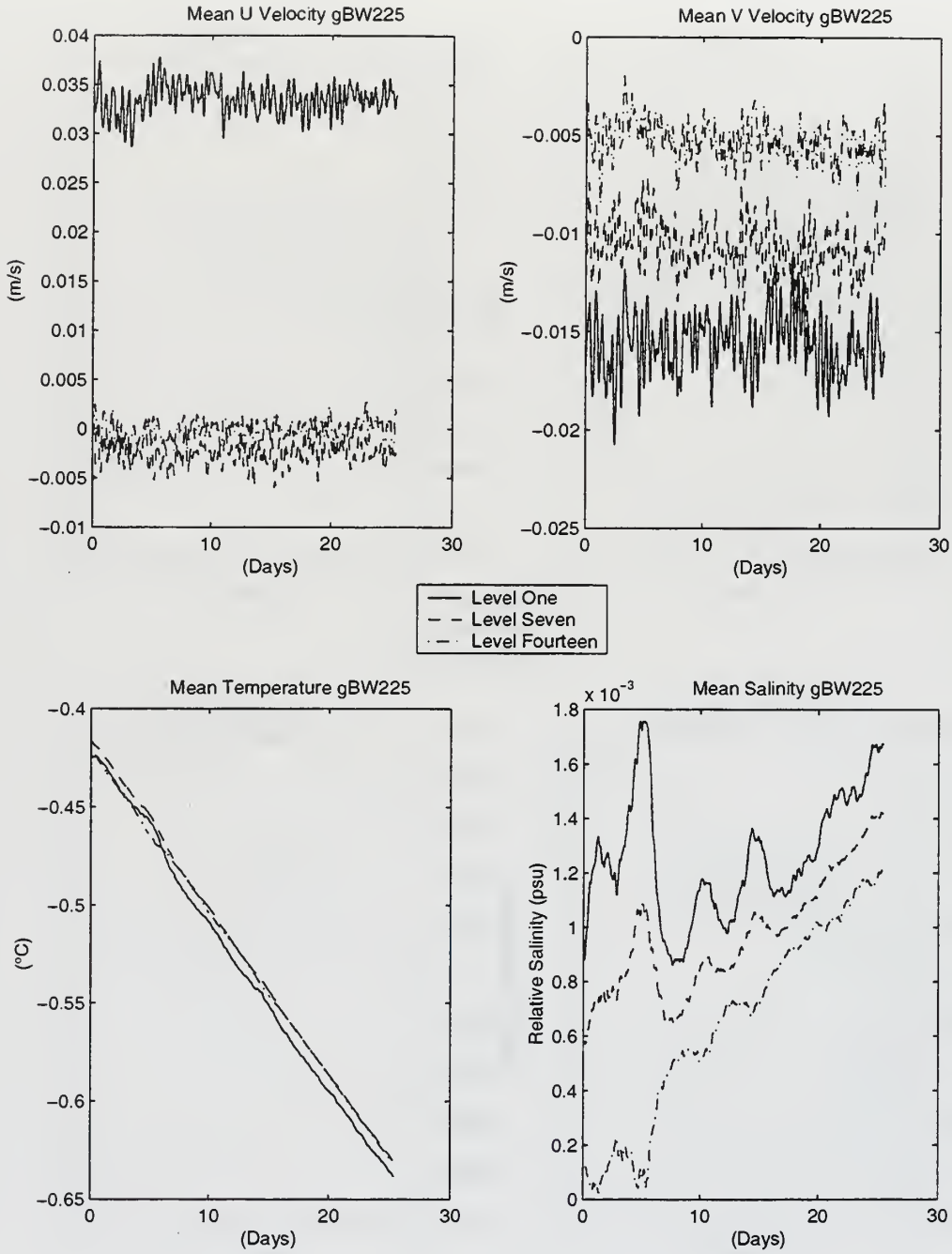

Figure 5.6. Time series of zonal (top left) and meridional (top right) horizontal velocities and mean potential temperature (bottom left) and mean salinity (bottom right) for LES case gBW225 at the surface (level 1), at 315 meters depth (level 7), and at 630 meters depth (level 14).

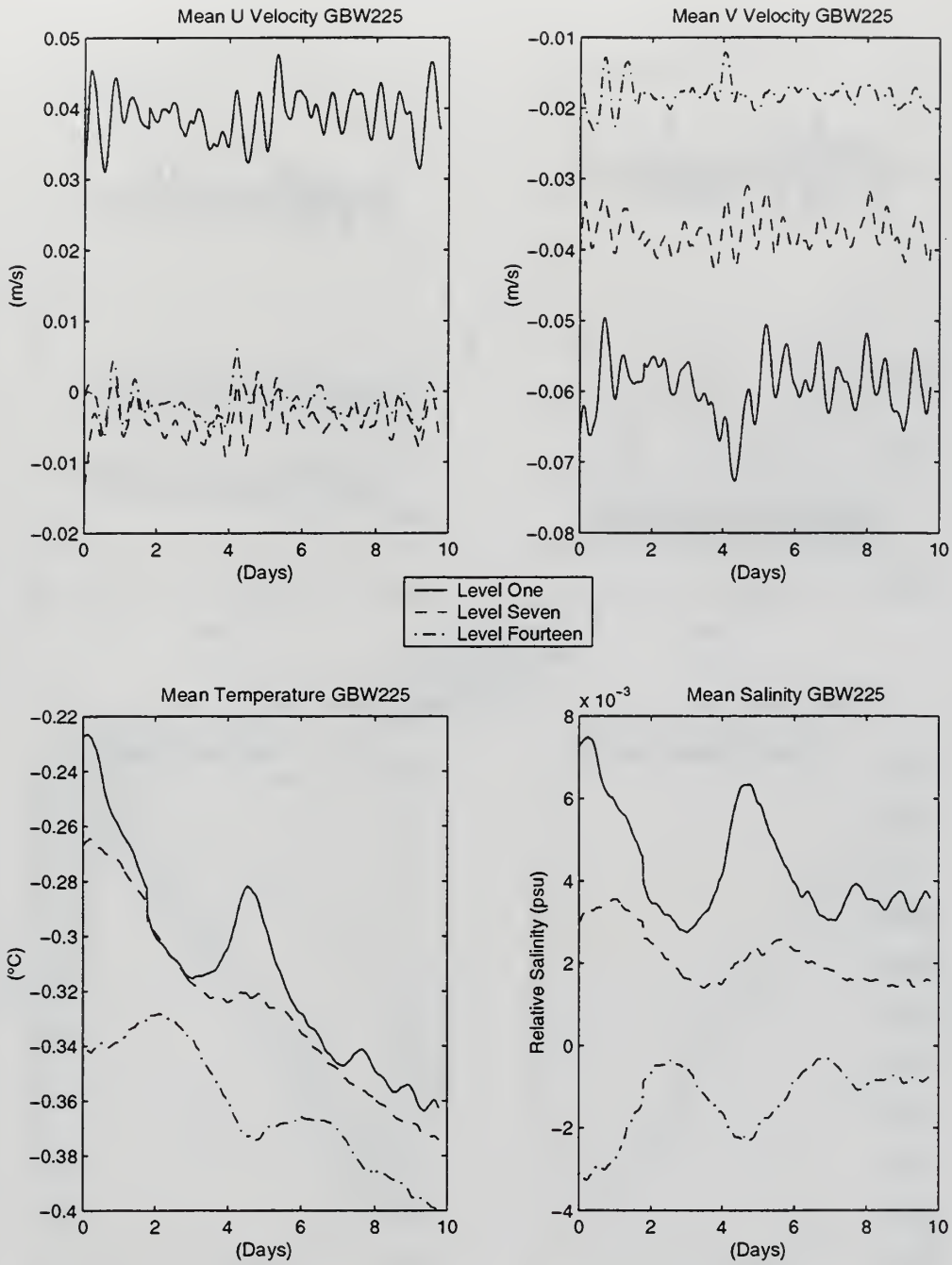

Figure 5.7. Time series of zonal (top left) and meridional (top right) horizontal velocities and mean potential temperature (bottom left) and mean salinity (bottom right) for LES case GBW225 at the surface (level 1), at 315 meters depth (level 7), and at 630 meters depth (level 14).

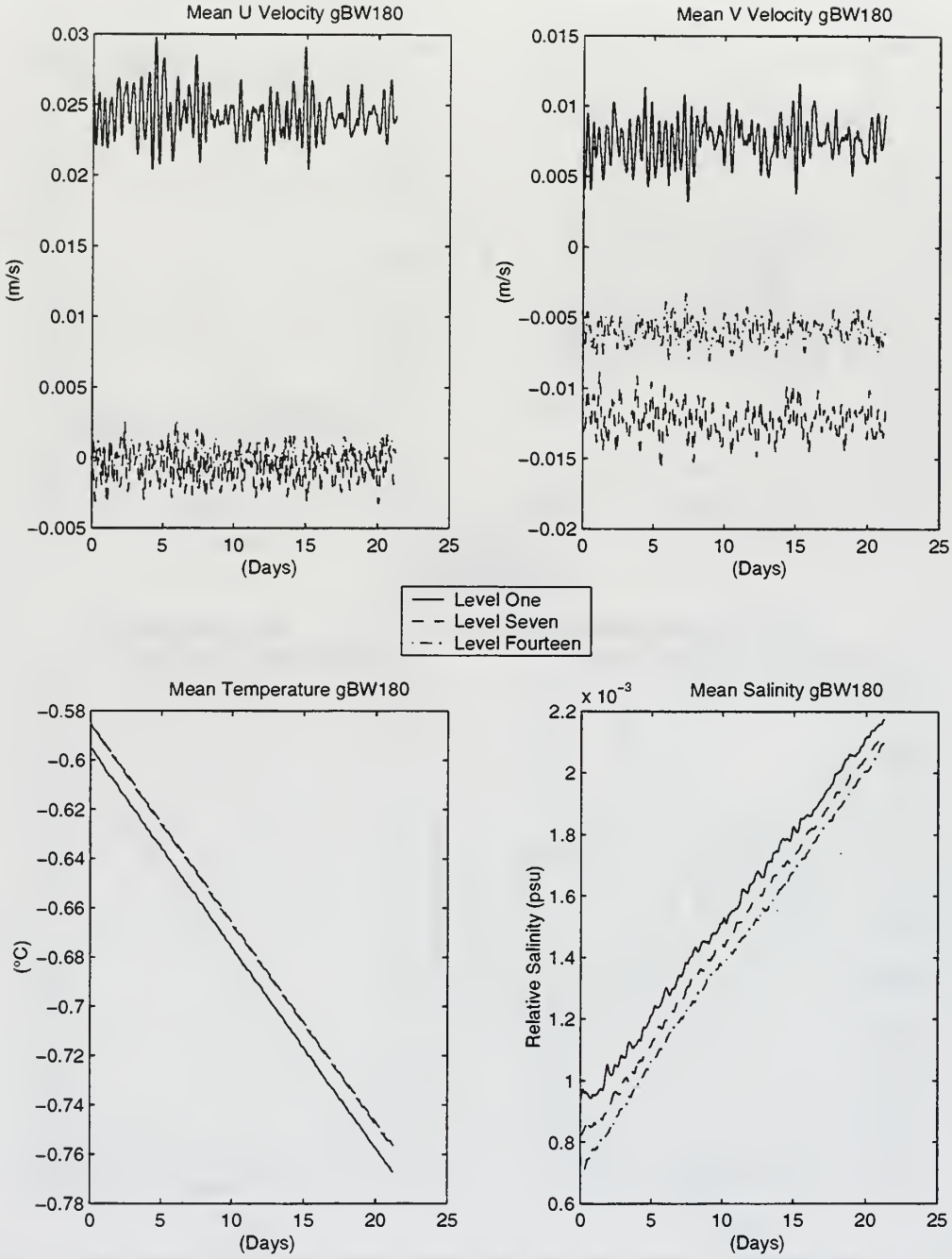

Figure 5.8. Time series of zonal (top left) and meridional (top right) horizontal velocities and mean potential temperature (bottom left) and mean salinity (bottom right) for LES case gBW180 at the surface (level 1), at 315 meters depth (level 7), and at 630 meters depth (level 14).

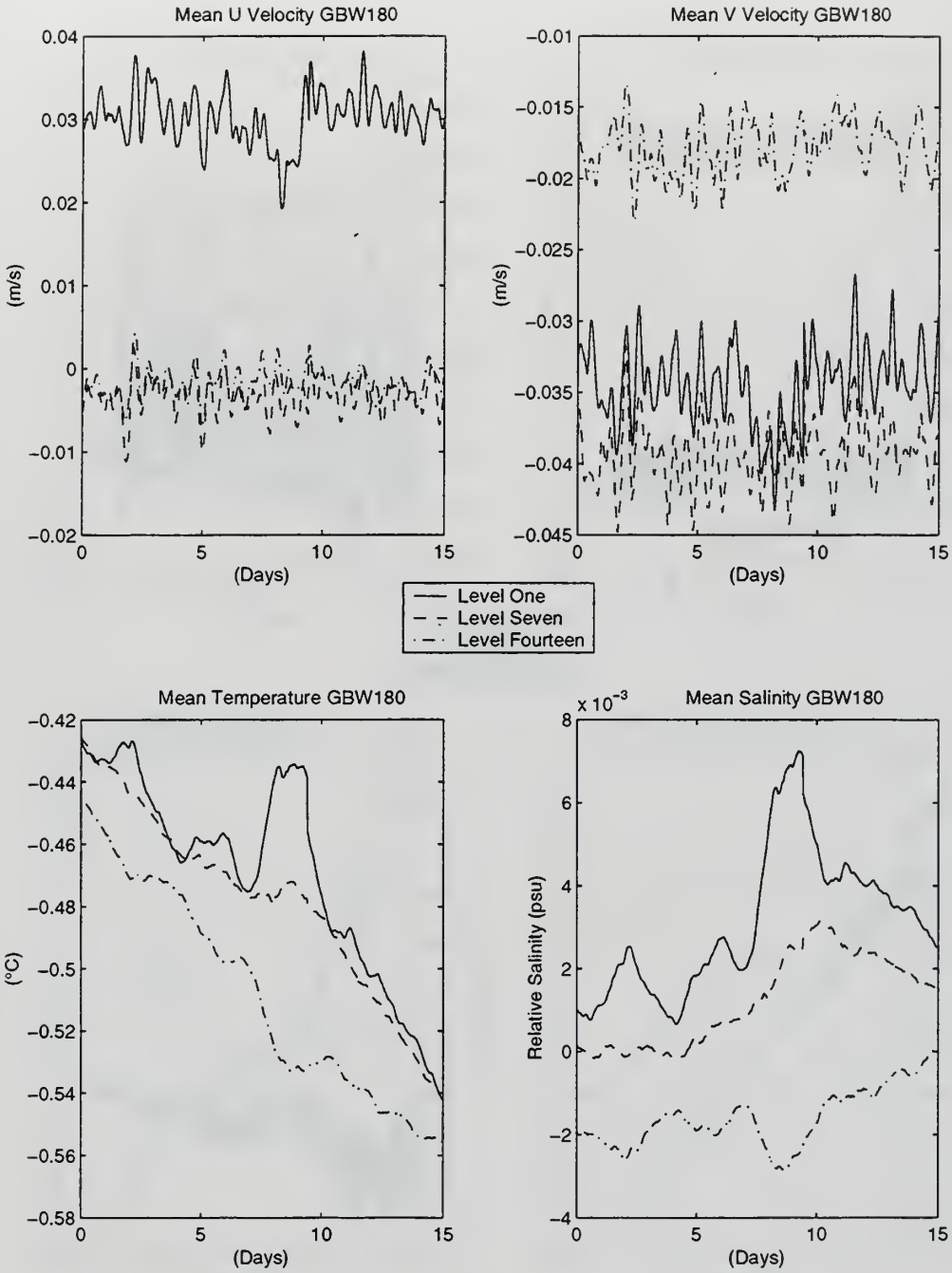

Figure 5.9. Time series of zonal (top left) and meridional (top right) horizontal velocities and mean potential temperature (bottom left) and mean salinity (bottom right) for LES case GBW180 at the surface (level 1), at 315 meters depth (level 7), and at 630 meters depth (level 14).

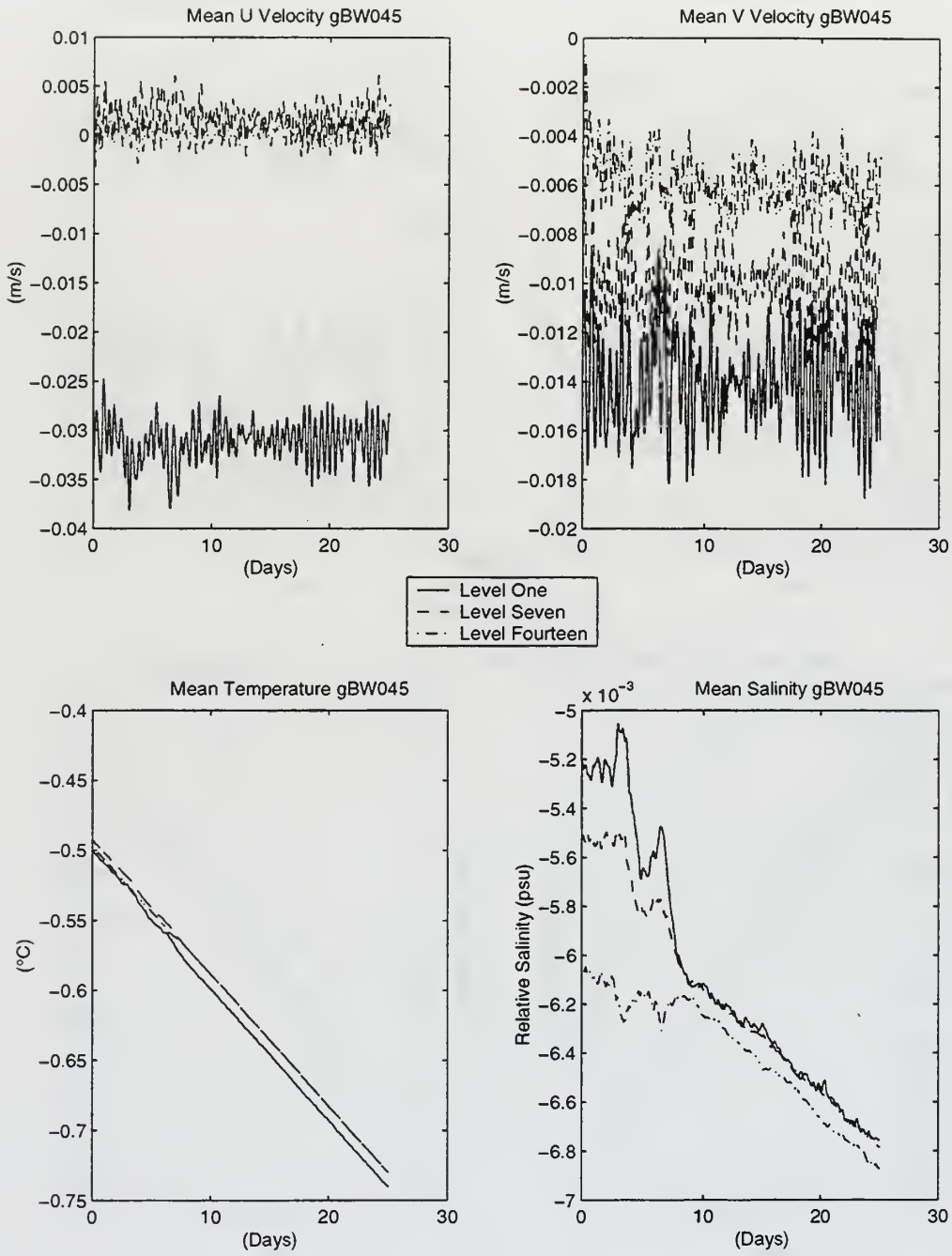

Figure 5.10. Time series of zonal (top left) and meridional (top right) horizontal velocities and mean potential temperature (bottom left) and mean salinity (bottom right) for LES case gBW045 at the surface (level 1), at 315 meters depth (level 7), and at 630 meters depth (level 14).

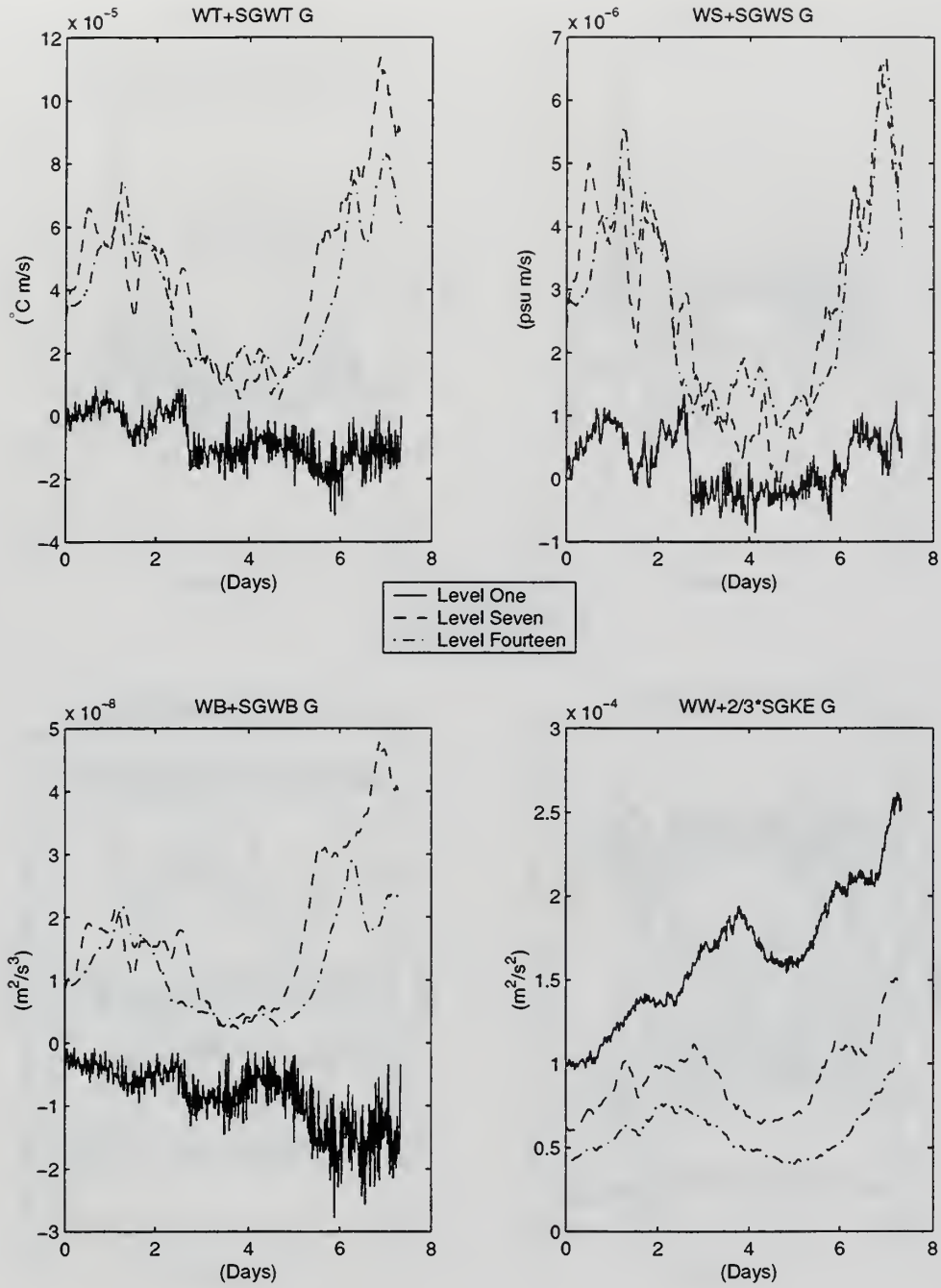

Figure 5.11. Time series of net turbulent heat flux (top left) turbulent salinity flux (top right) buoyancy flux (bottom left) and net VTKE (bottom right) for LES case G at the surface (level 1), at 315 meters depth (level 7), and at 630 meters depth (level 14).

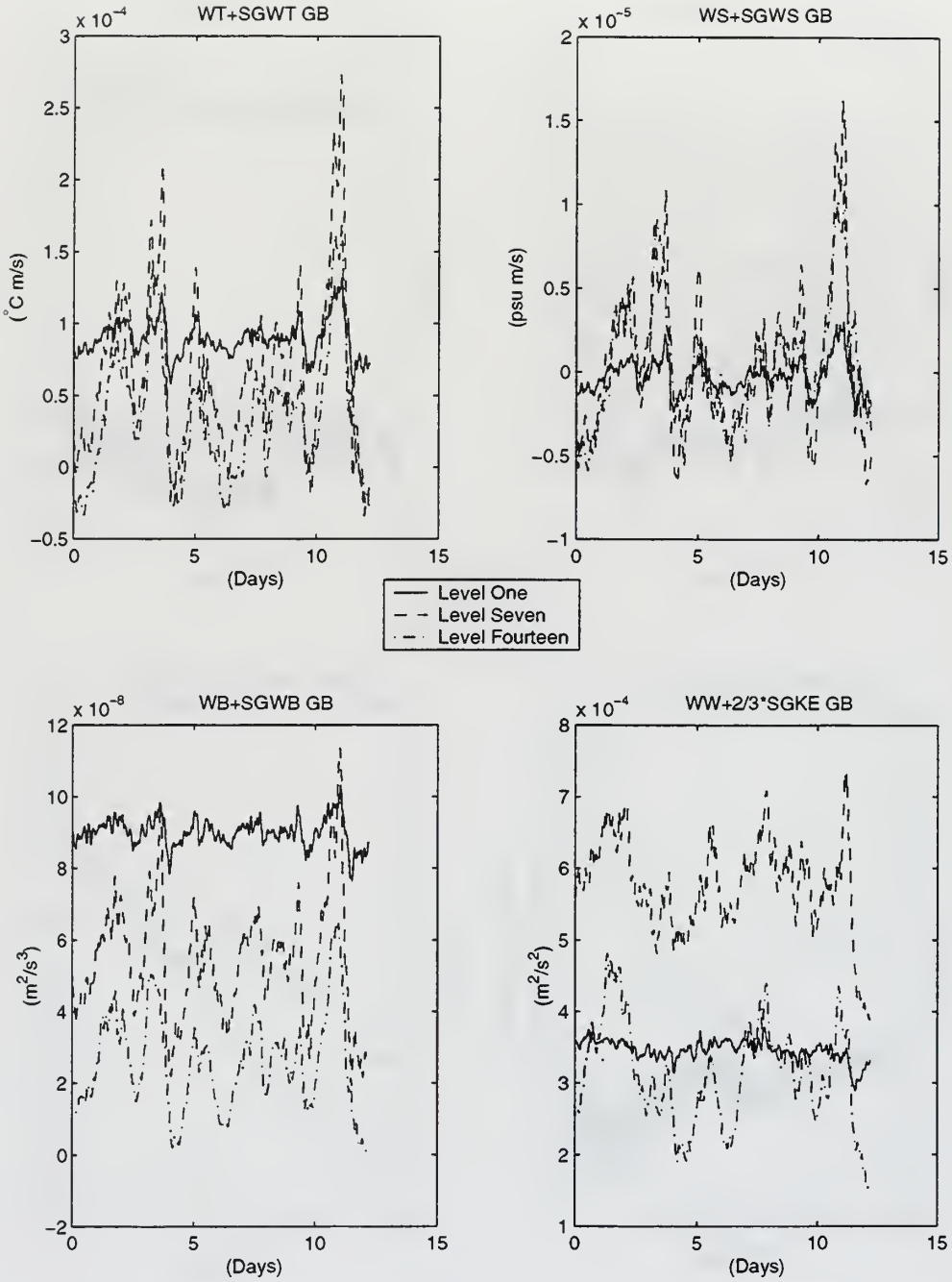

Figure 5.12. Time series of net turbulent heat flux (top left) turbulent salinity flux (top right) buoyancy flux (bottom left) and net VTKE (bottom right) for LES case GB at the surface (level 1), at 315 meters depth (level 7), and at 630 meters depth (level 14).

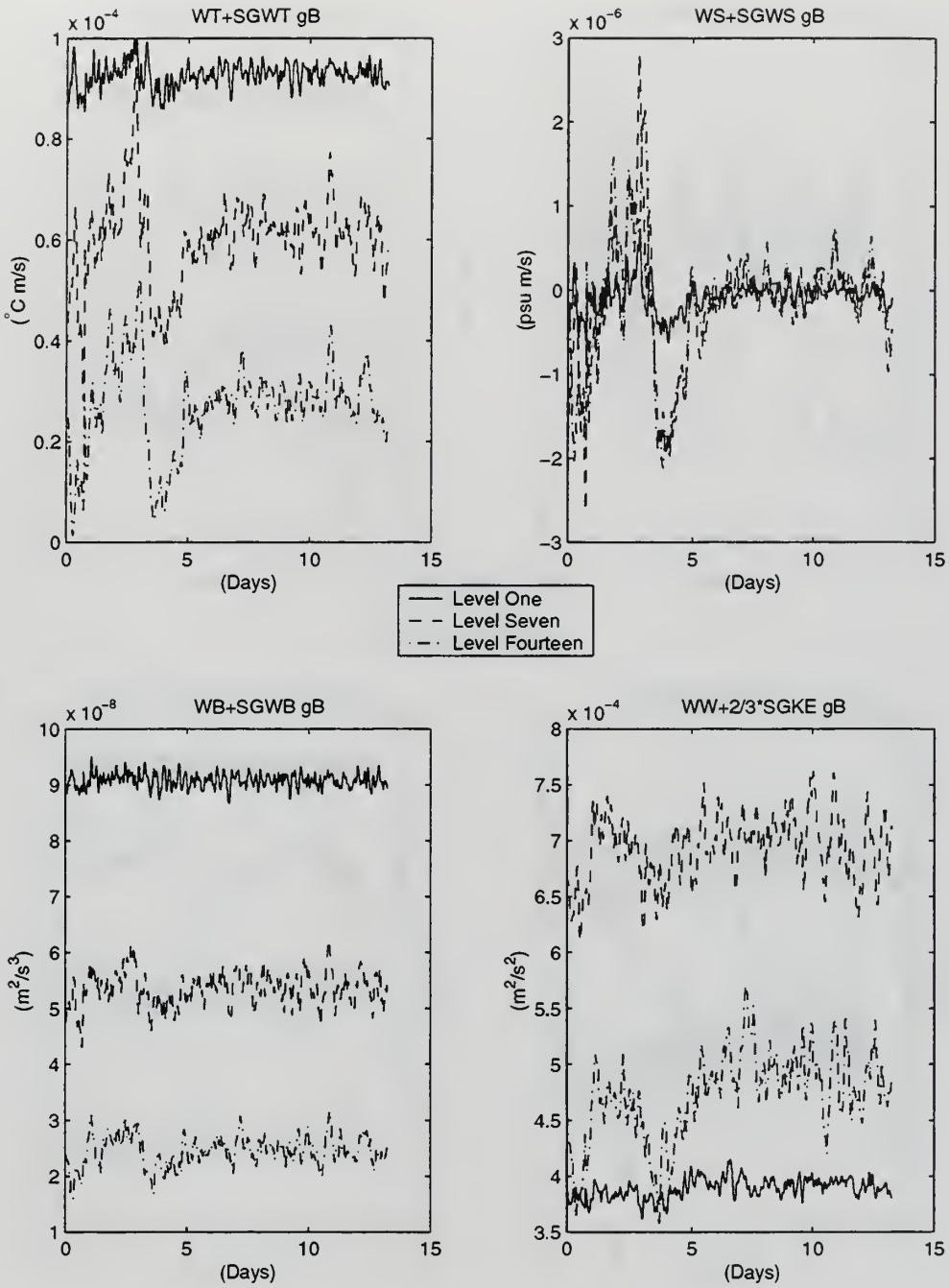

Figure 5.13. Time series of net turbulent heat flux (top left) turbulent salinity flux (top right) buoyancy flux (bottom left) and net VTKE (bottom right) for LES case gB at the surface (level 1), at 315 meters depth (level 7), and at 630 meters depth (level 14).

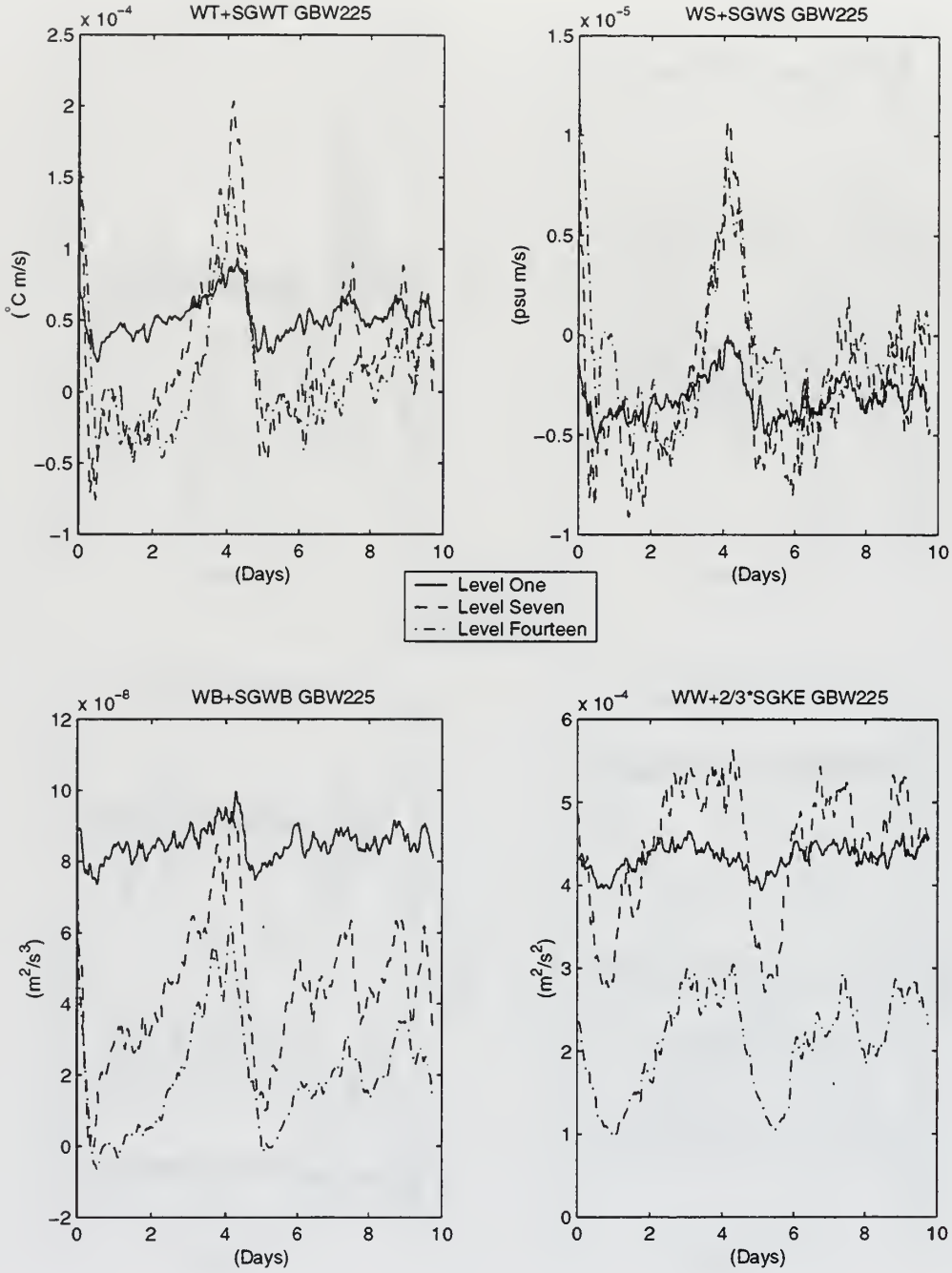

Figure 5.14. Time series of net turbulent heat flux (top left) turbulent salinity flux (top right) buoyancy flux (bottom left) and net VTKE (bottom right) for LES case GBW225 at the surface (level 1), at 315 meters depth (level 7), and at 630 meters depth (level 14

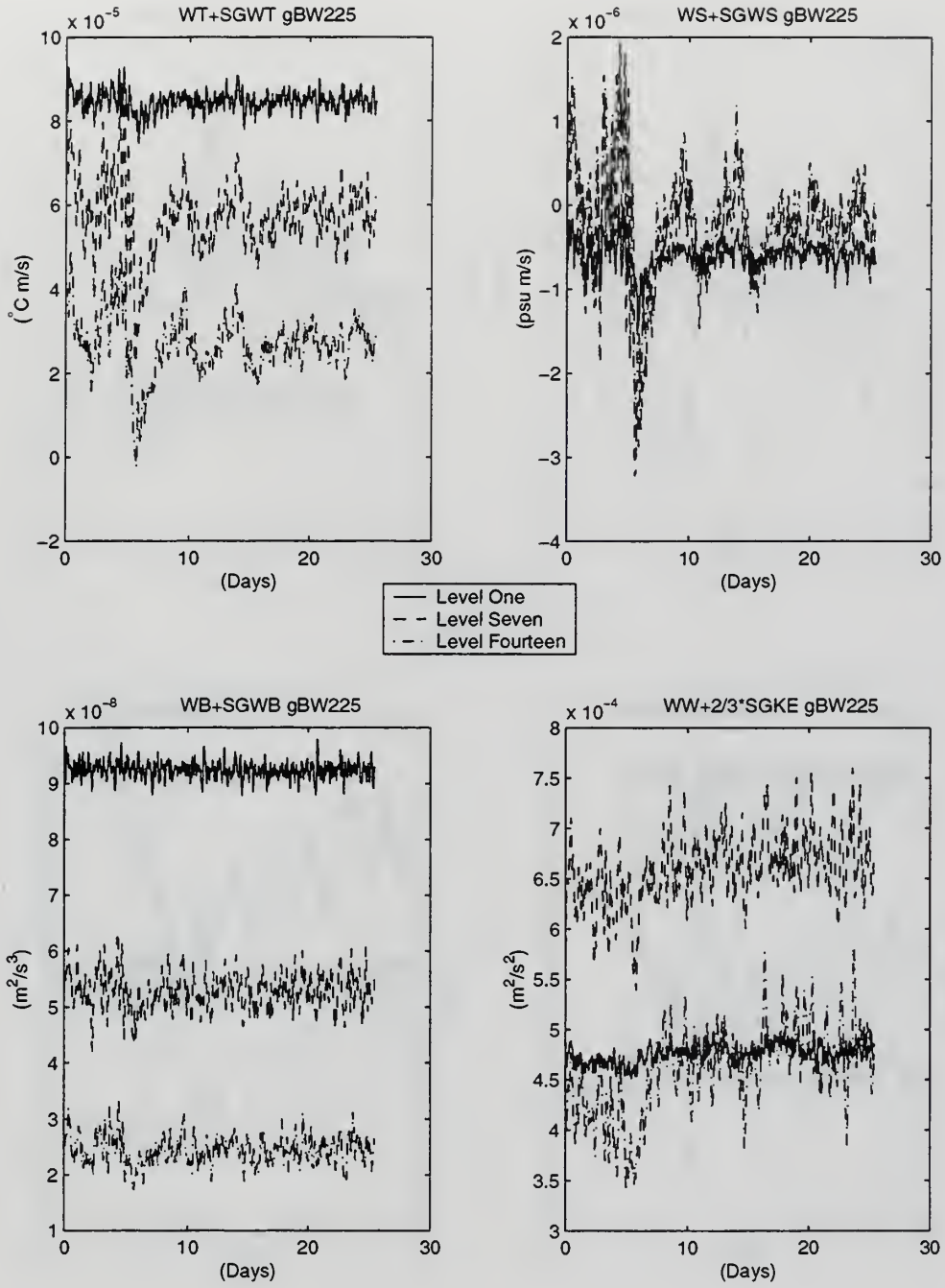

Figure 5.15. Time series of net turbulent heat flux (top left) turbulent salinity flux (top right) buoyancy flux (bottom left) and net VTKE (bottom right) for LES case gBW225 at the surface (level 1), at 315 meters depth (level 7), and at 630 meters depth (level 14).

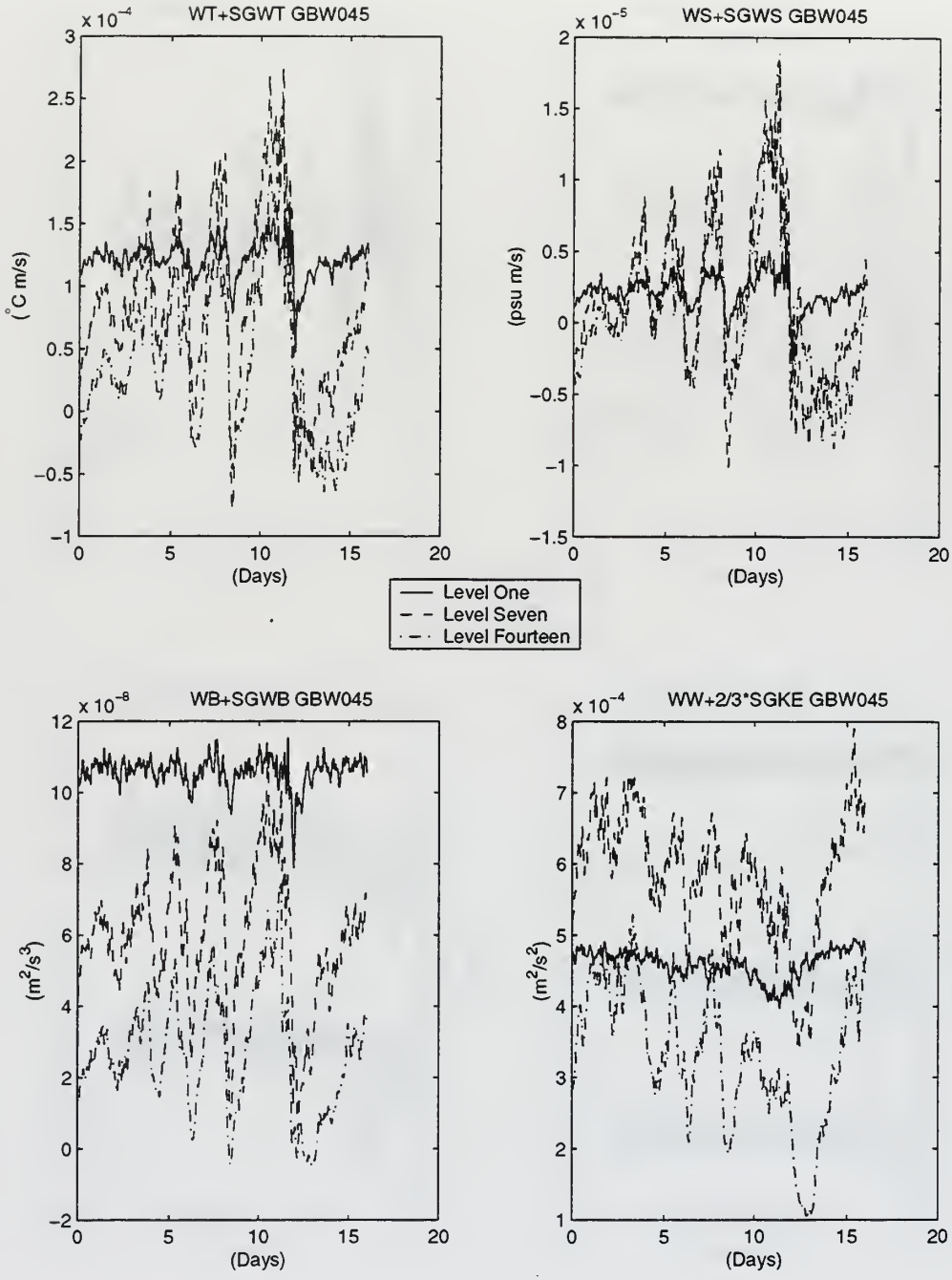

Figure 5.16. Time series of net turbulent heat flux (top left) turbulent salinity flux (top right) buoyancy flux (bottom left) and net VTKE (bottom right) for LES case GBW045 at the surface (level 1), at 315 meters depth (level 7), and at 630 meters depth (level 14).

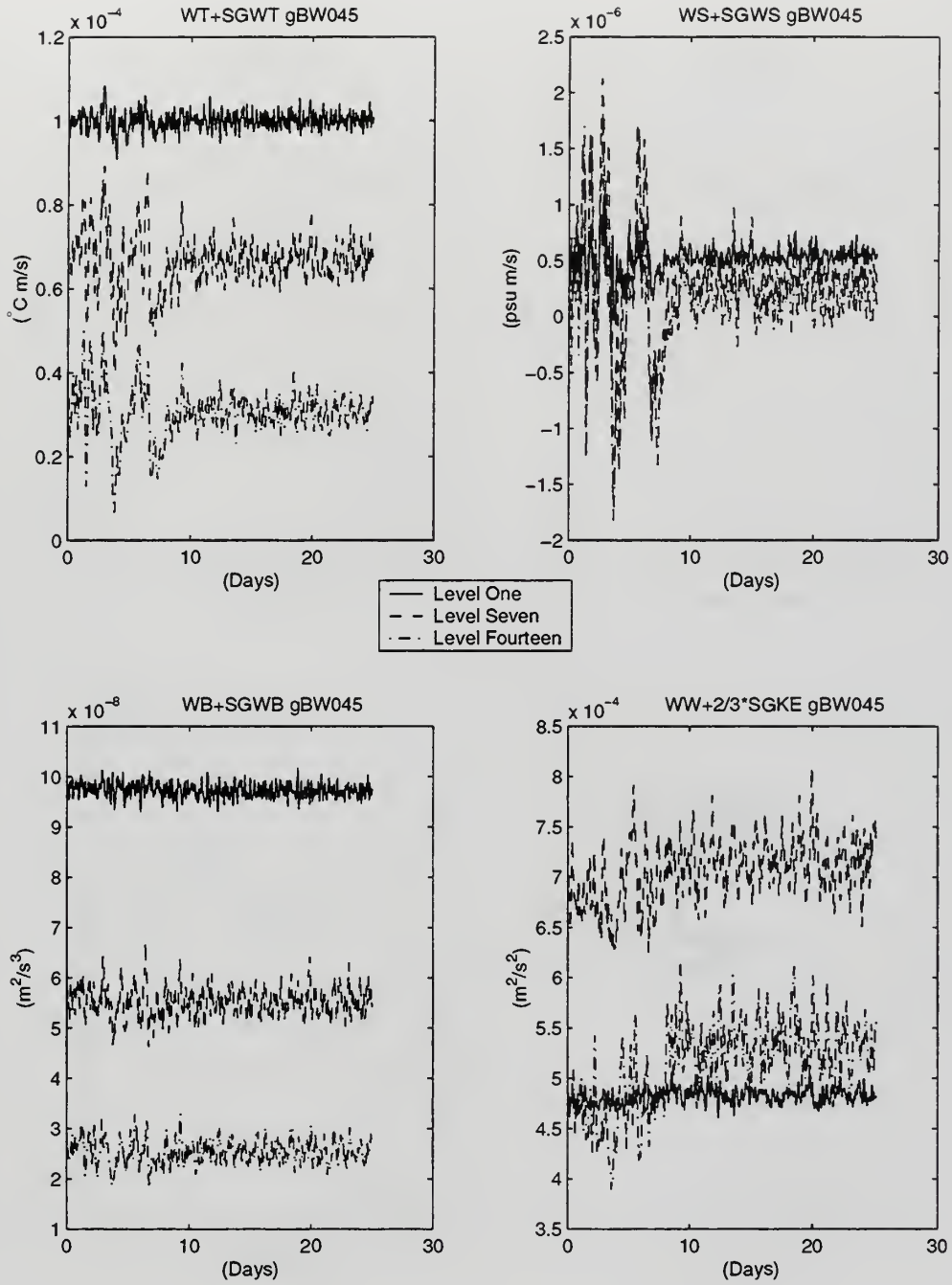

Figure 5.17. Time series of net turbulent heat flux (top left) turbulent salinity flux (top right) buoyancy flux (bottom left) and net VTKE (bottom right) for LES case gBW045 at the surface (level 1), at 315 meters depth (level 7), and at 630 meters depth (level 14).

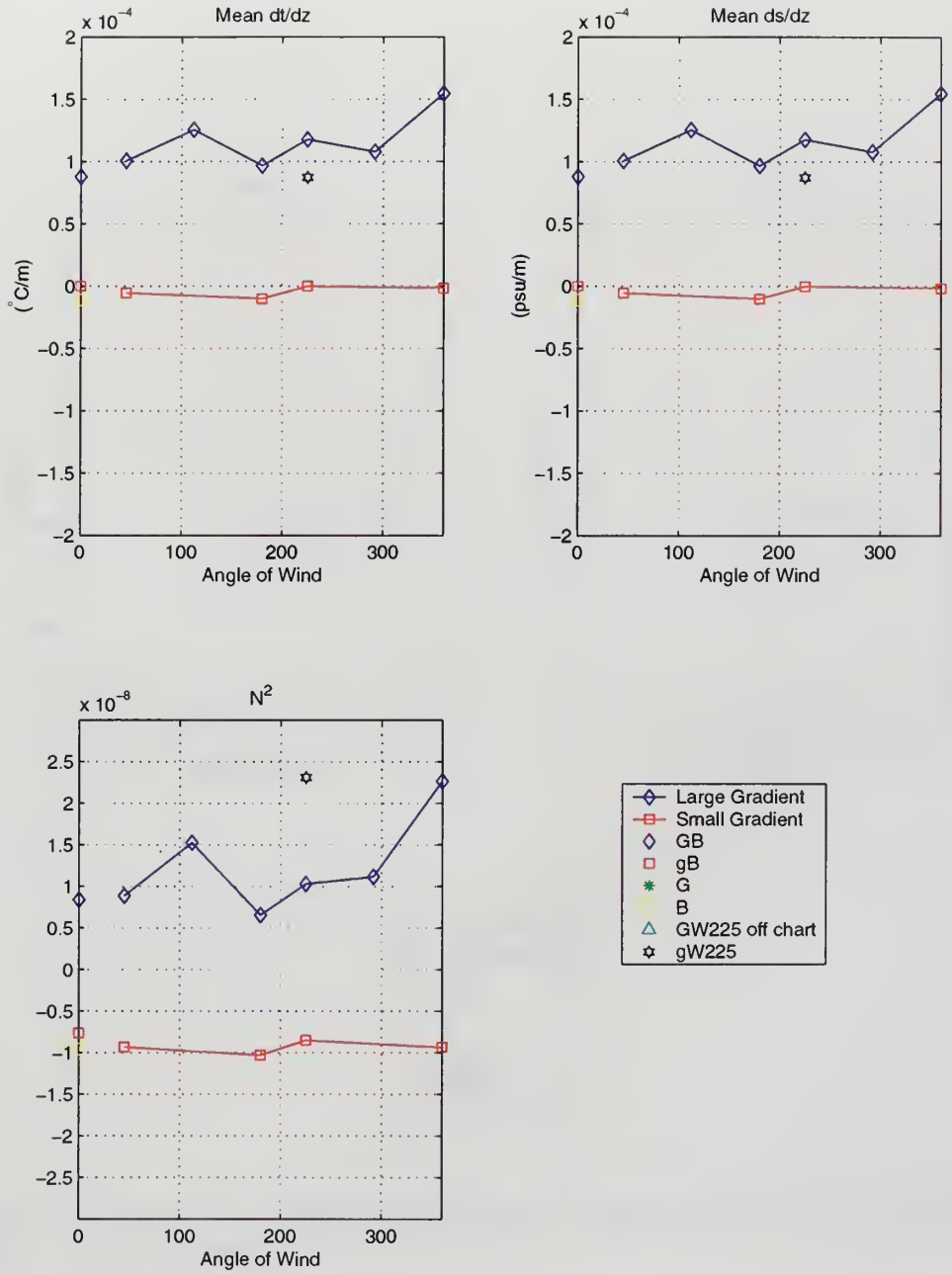

Figure 5.18. Bulk mean values of temperature gradient (top left), salinity gradient (top right), and Buoyancy frequency (bottom left) for all LES cases with cooling.

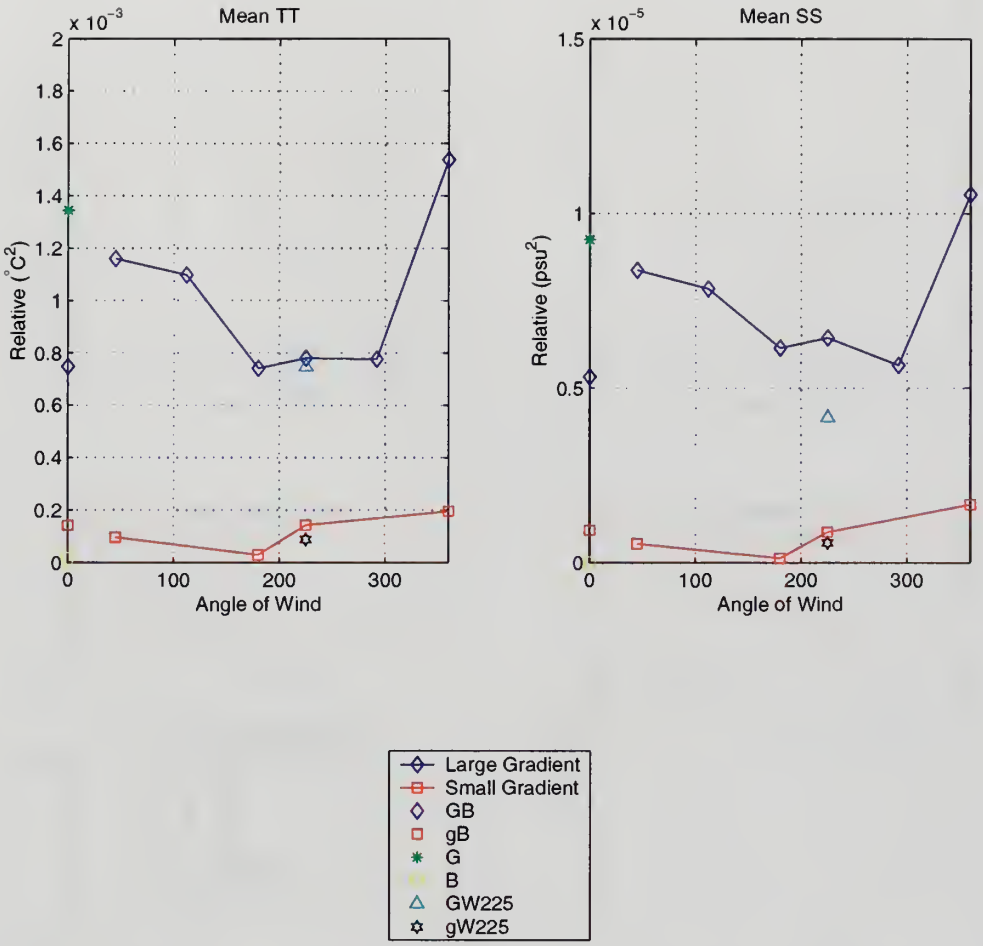

Figure 5.19. Bulk mean values of temperature variance (left), and salinity variance (right), for all LES cases.

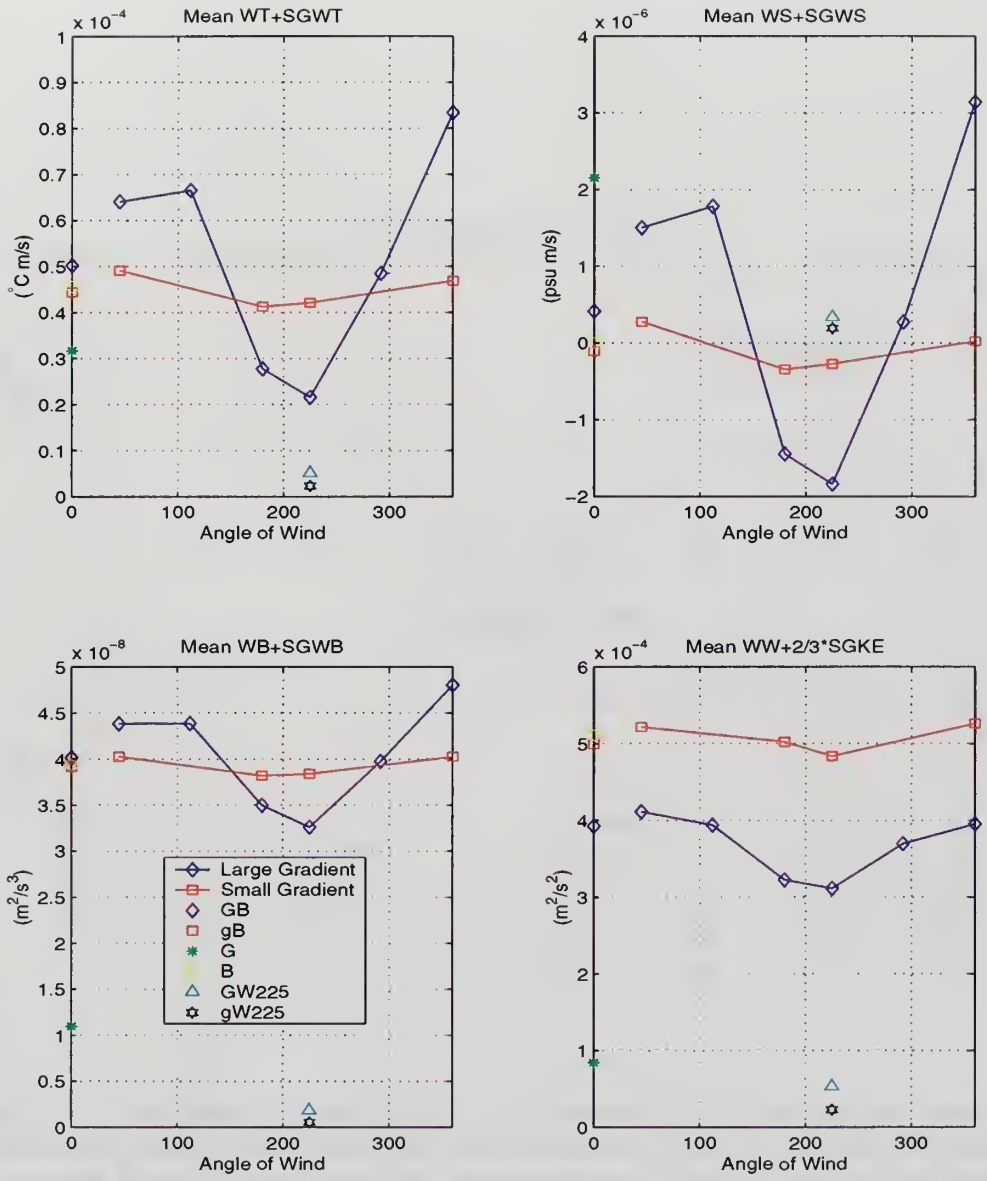

Figure 5.20. Bulk mean values of turbulent heat flux (top left), turbulent salinity flux (top right), buoyancy flux (bottom left) and TKE for all LES cases.

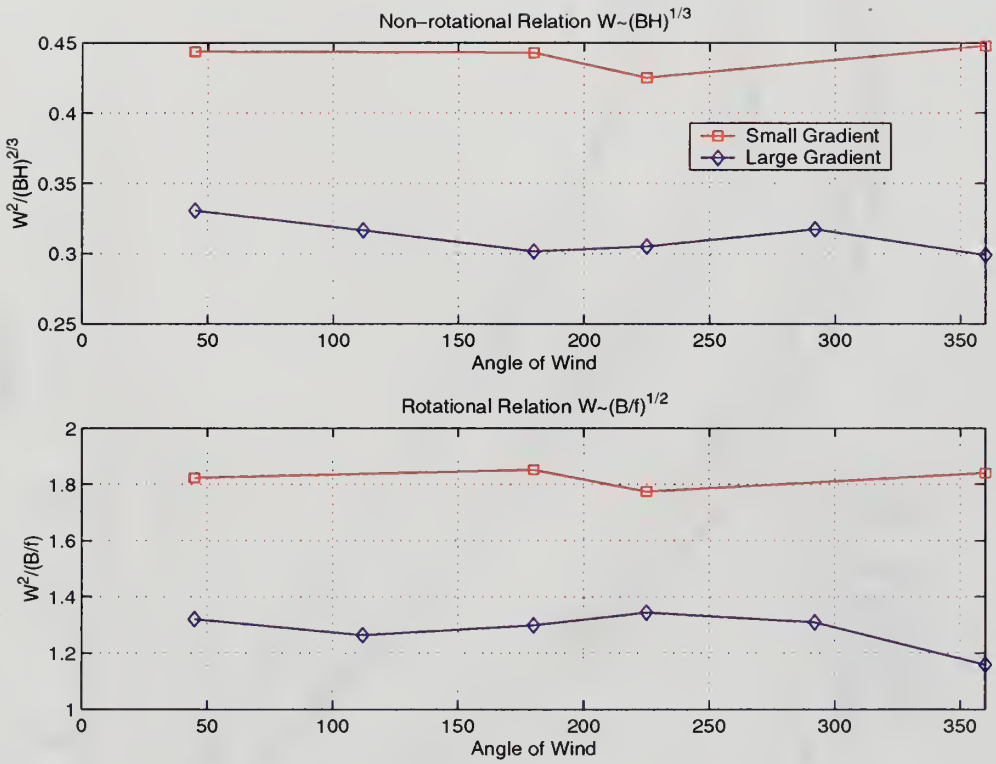

Figure 5.21. Comparison of the linearity of a relationship between vertical velocity and buoyancy flux for the strong and weak gradient cases varying in wind forcing direction using a depth limited relationship (top) and a depth independent relationship (bottom).

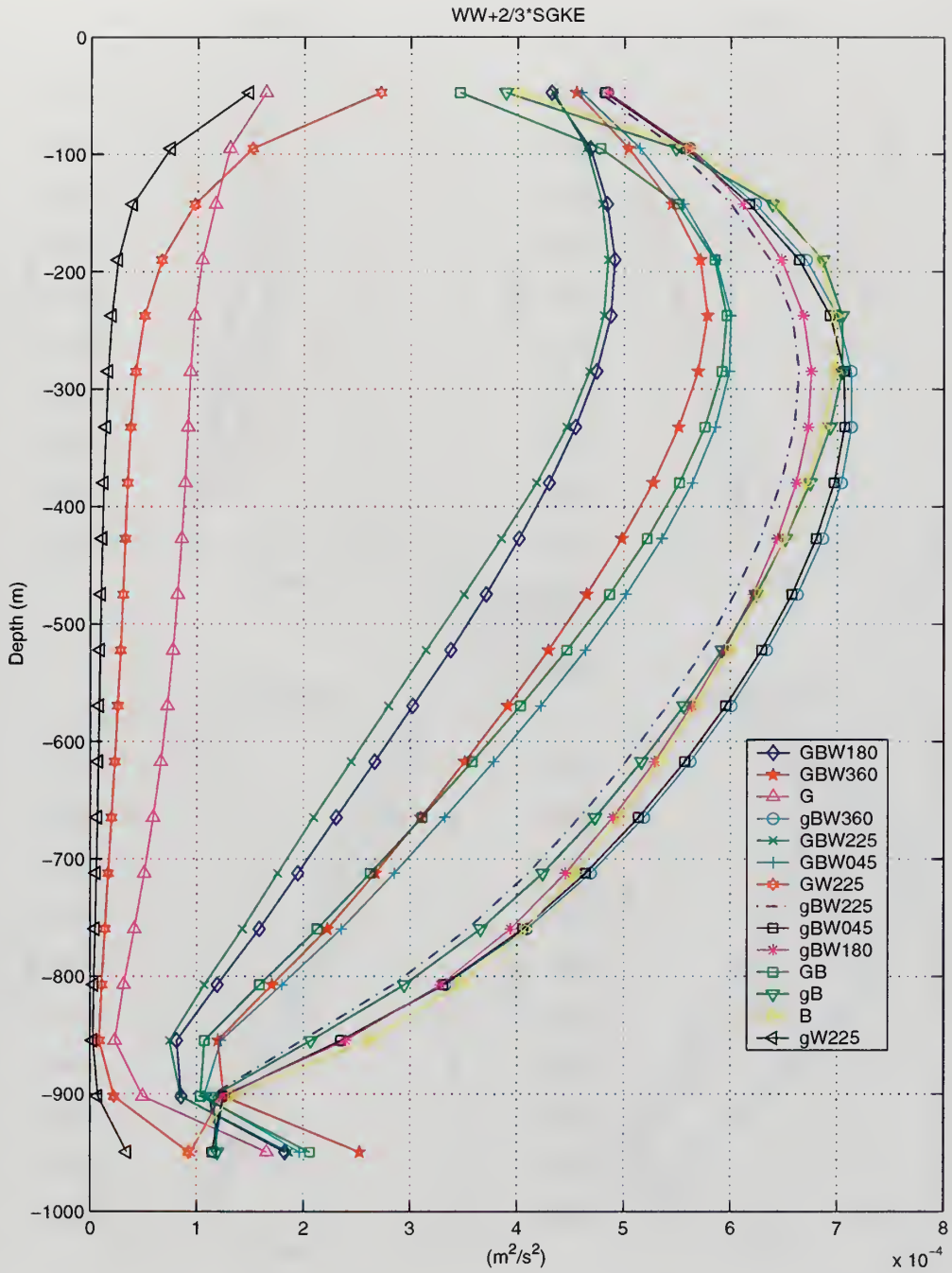

Figure 5.22. Vertical Total Kinetic Energy profiles for all LES cases.

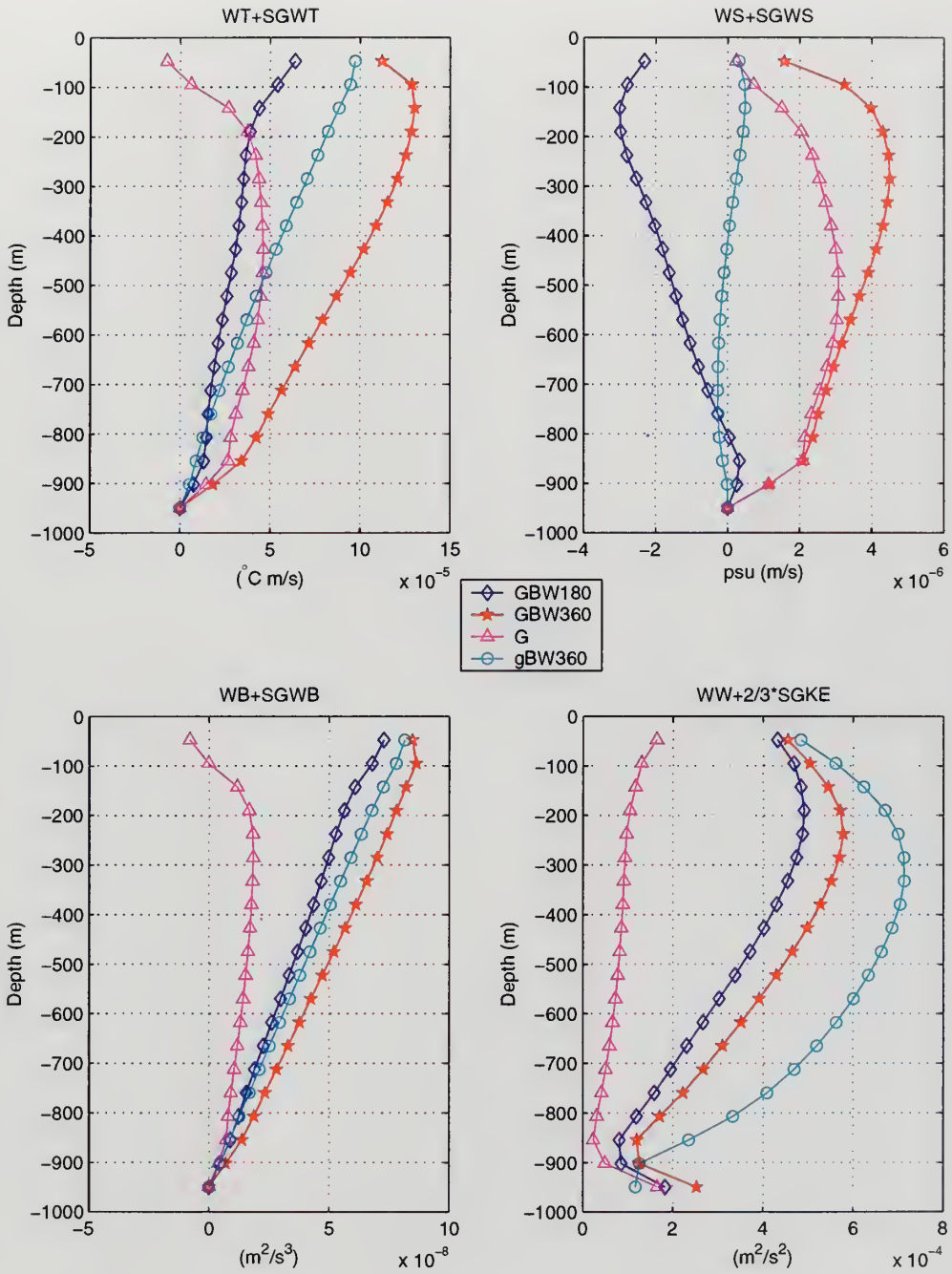

Figure 5.23. Select profiles from each of the VTKE bands of turbulent heat flux (top left), turbulent salinity flux (top right), and buoyancy flux (bottom left), and VTKE (bottom right).

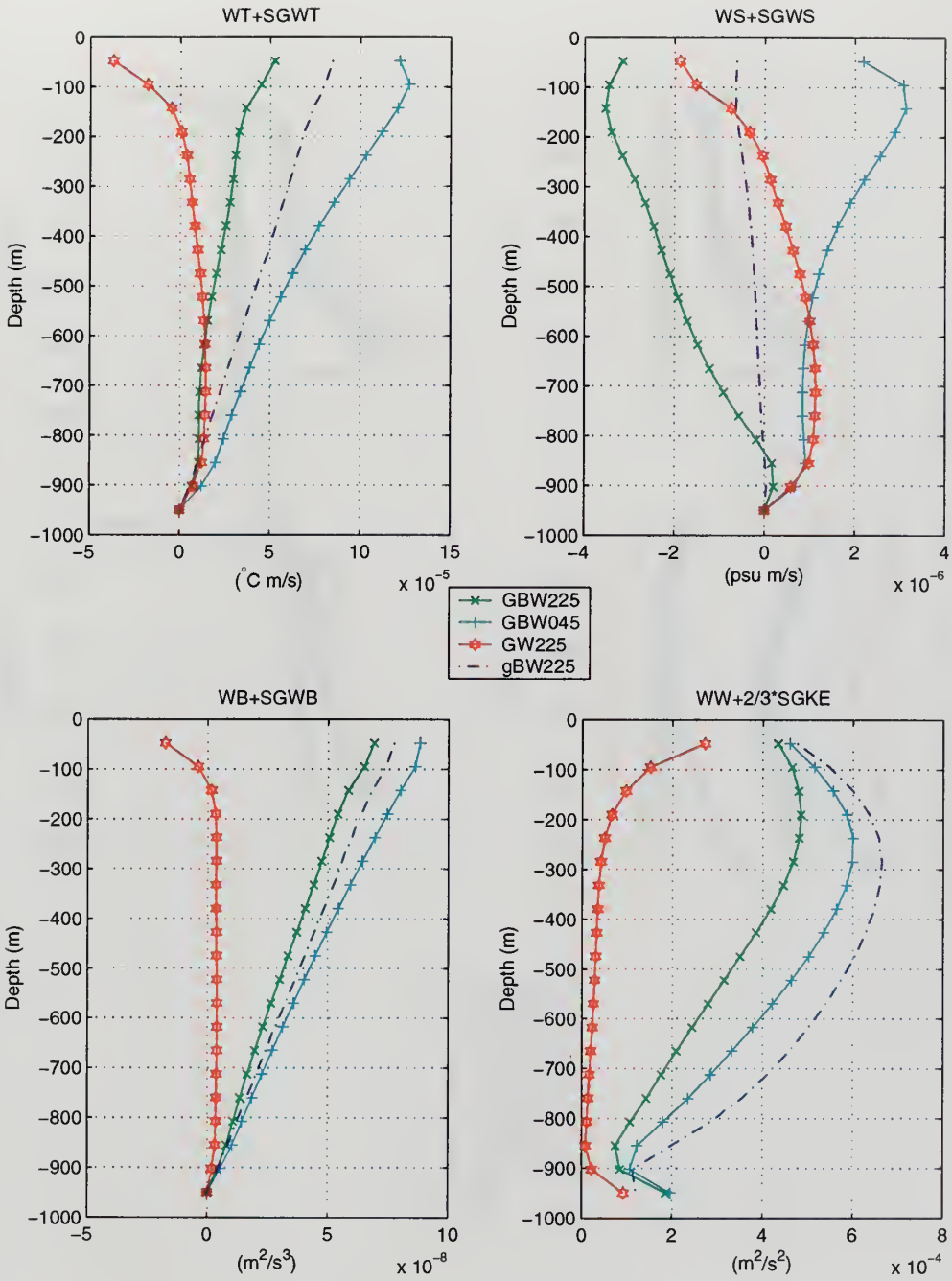

Figure 5.24. Select profiles from each of the VTKE bands of turbulent heat flux (top left), turbulent salinity flux (top right), and buoyancy flux (bottom left), and VTKE (bottom right).

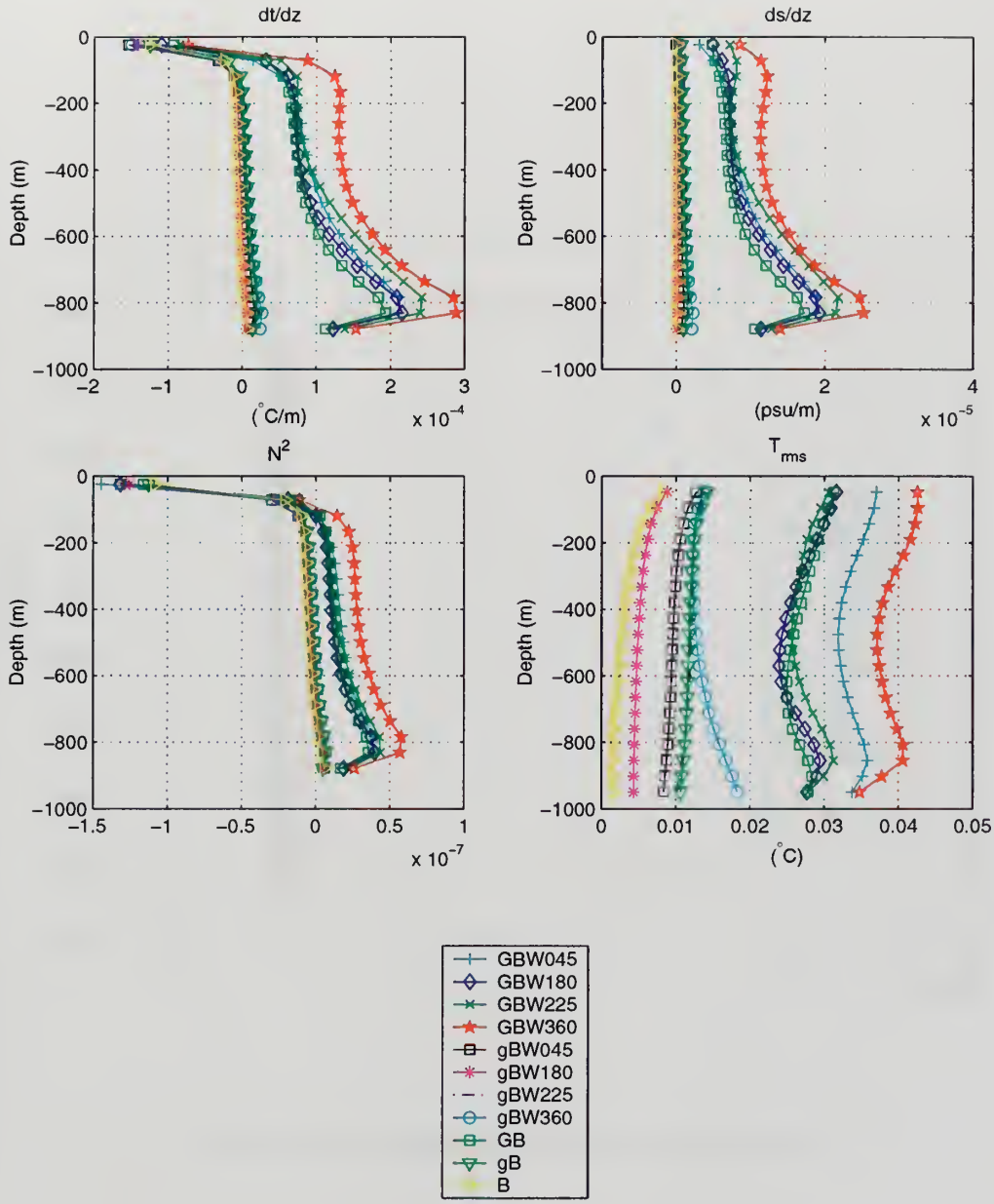

Figure 5.25. Profiles of vertical temperature (top left) and salinity (top right) gradients, stability(bottom left), and (rms) temperature fluctuation T_{rms} (bottom right) for all LES cases with cooling.

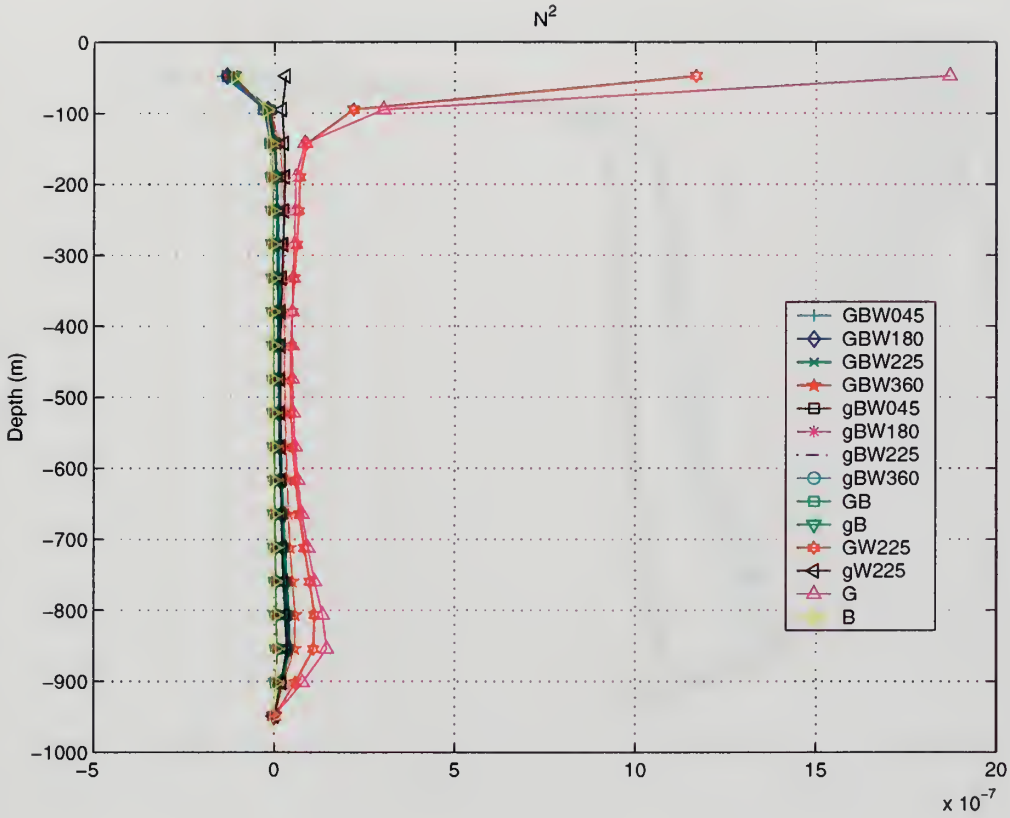

Figure 5.26. Stability profile for all LES cases.

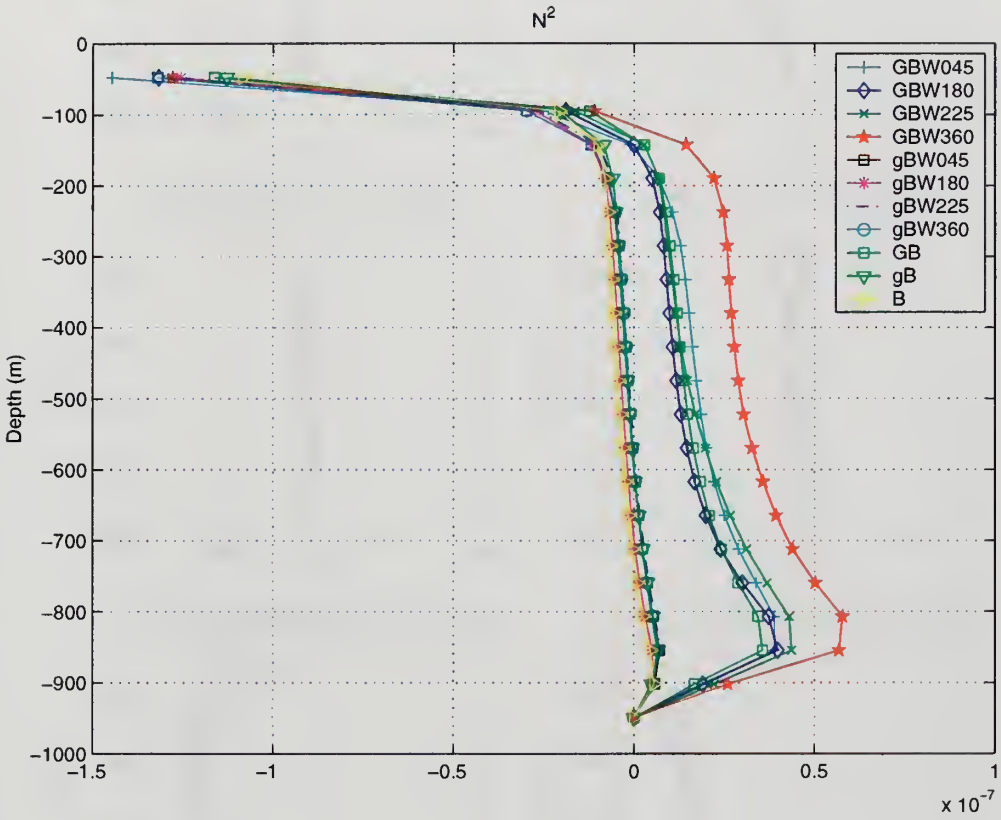

Figure 5.27. Stability profiles for all LES cases with cooling.

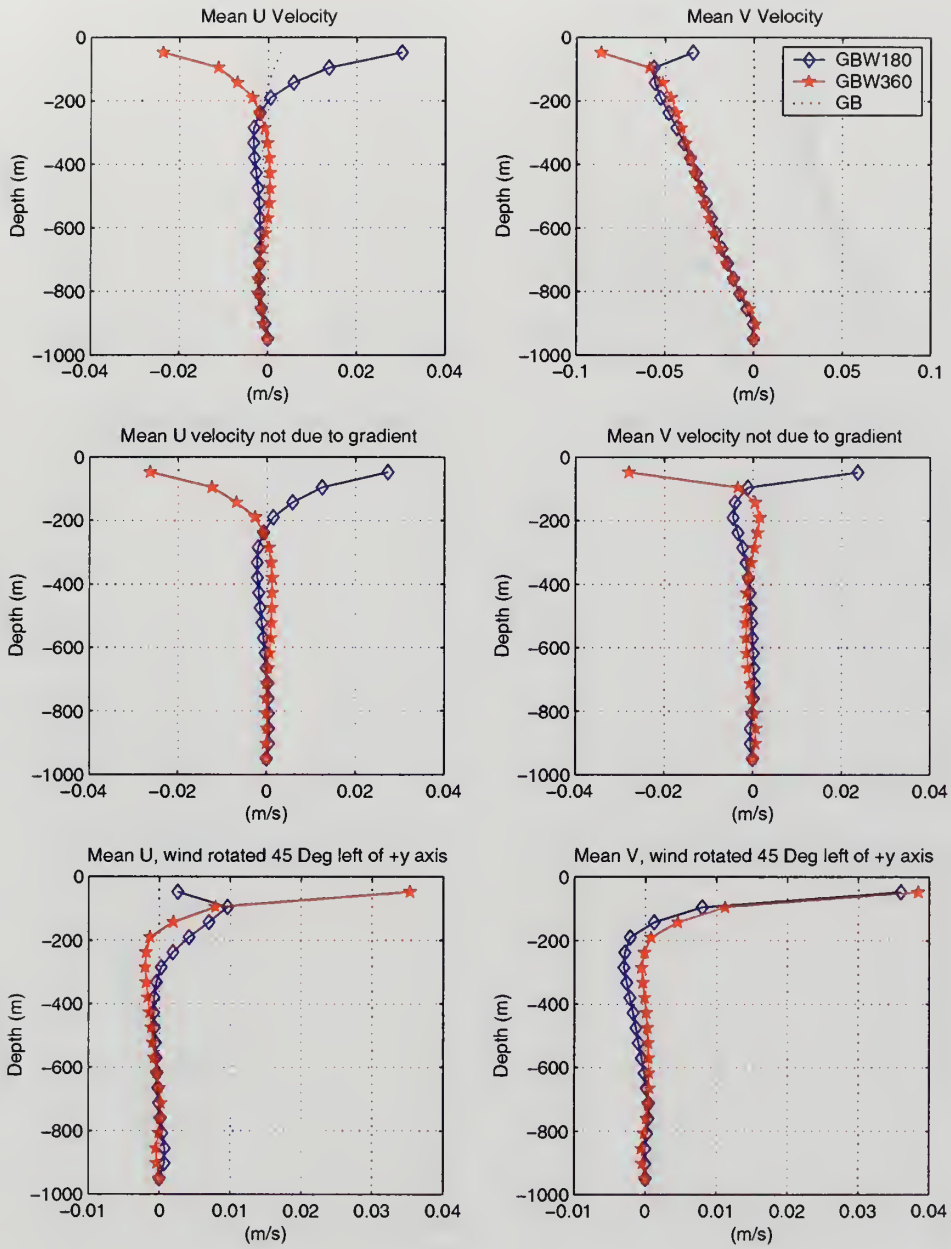

Figure 5.28. LES profiles of horizontal velocities produced by no wind, northerly, and southerly winds and a strong gradient (top). Profiles of horizontal velocities resulting from a strong gradient with northerly and southerly winds with the horizontal velocities resulting from the strong gradient only subtracted (middle). Profiles of wind induced horizontal velocities with the wind rotated to 45° left of the positive y axis (bottom).

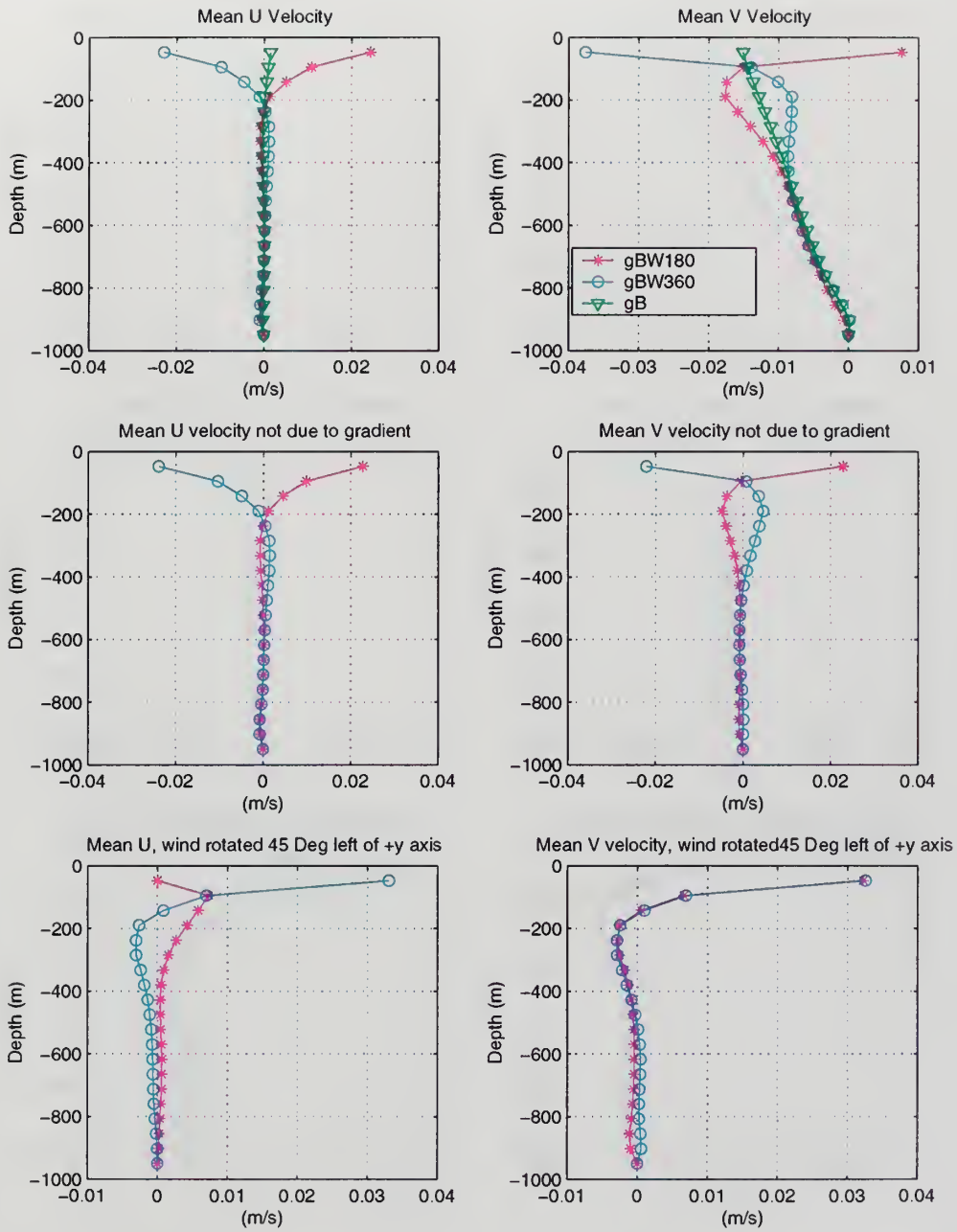

Figure 5.29. LES profiles of horizontal velocities produced by no wind, northerly, and southerly winds and a weak gradient (top). Profiles of horizontal velocities resulting from a weak gradient with northerly and southerly winds with the horizontal velocities resulting from the weak gradient only subtracted (middle). Profiles of wind induced horizontal velocities with the wind rotated to 45° left of the positive y axis (bottom).

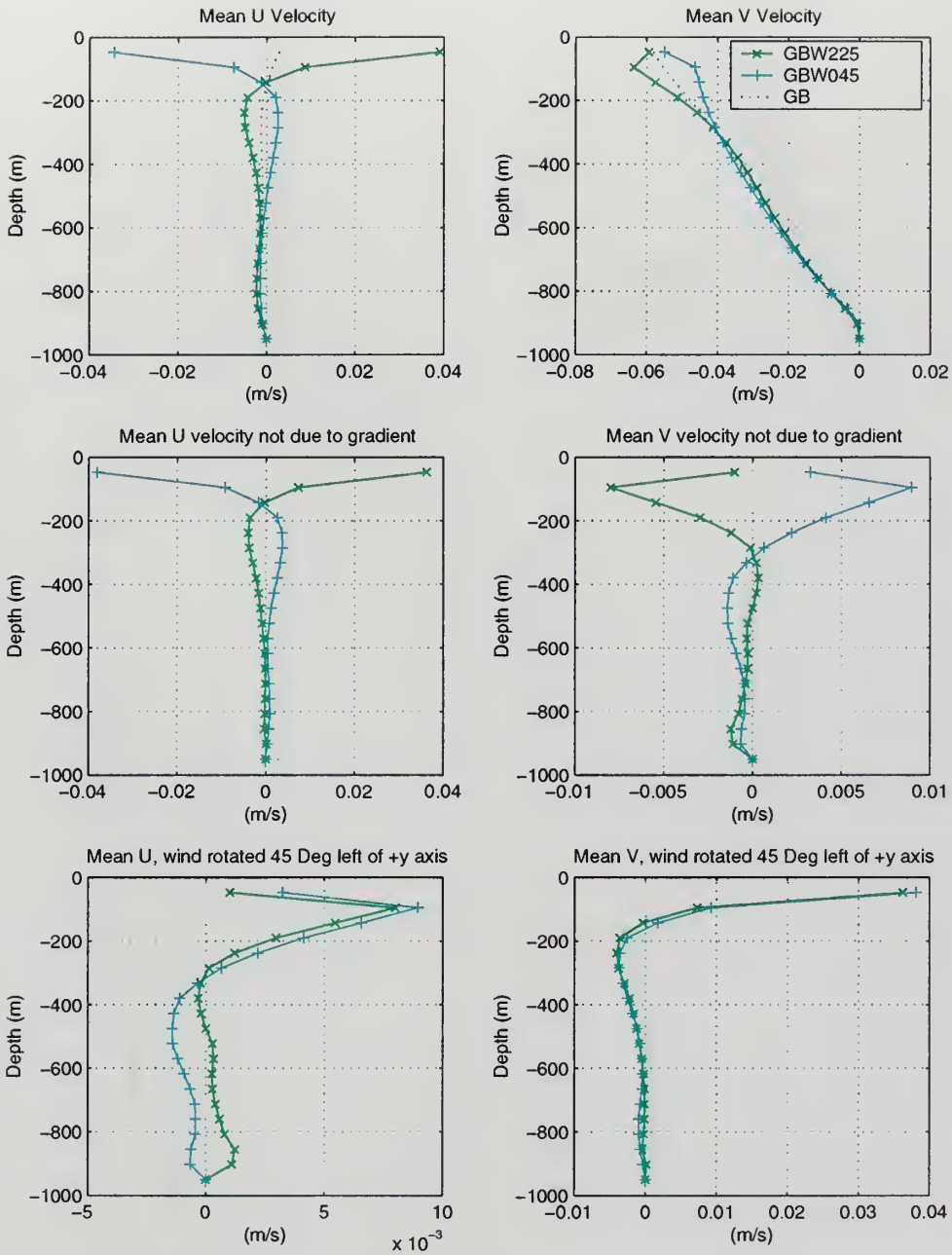

Figure 5.30. LES profiles of horizontal velocities produced by no wind, northeasterly, and southwesterly winds and a strong gradient (top). Profiles of horizontal velocities resulting from a strong gradient with northeasterly and southwesterly winds with the horizontal velocities resulting from the strong gradient only subtracted (middle). Profiles of wind induced horizontal velocities with the wind rotated to 45° left of the positive y axis (bottom).

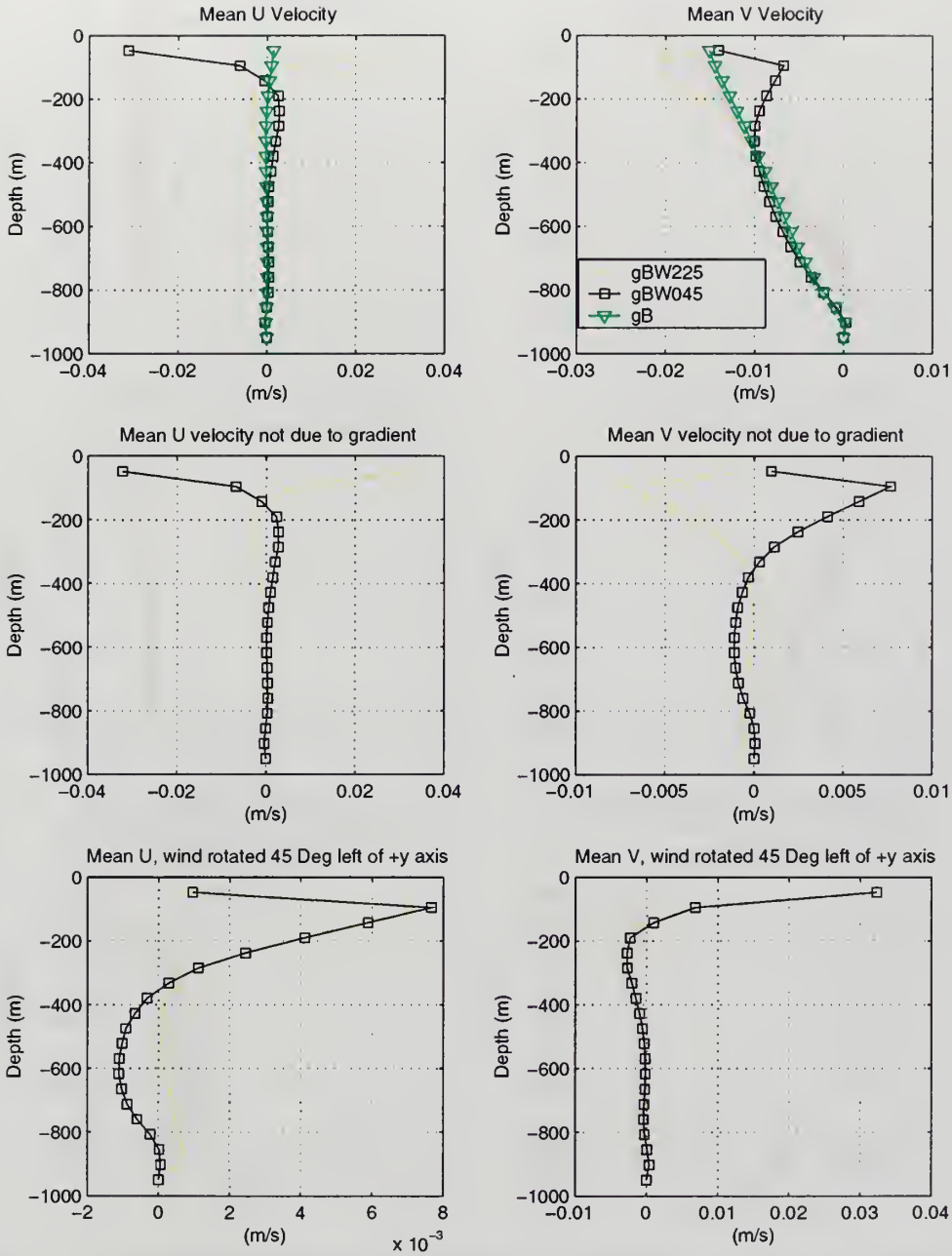

Figure 5.31. LES profiles of horizontal velocities produced by no wind, northeasterly, and southwesterly winds and a weak gradient (top). Profiles of horizontal velocities resulting from a weak gradient with northeasterly and southwesterly winds with the horizontal velocities resulting from the weak gradient only subtracted (middle). Profiles of wind induced horizontal velocities with the wind rotated to 45° left of the positive y axis (bottom).

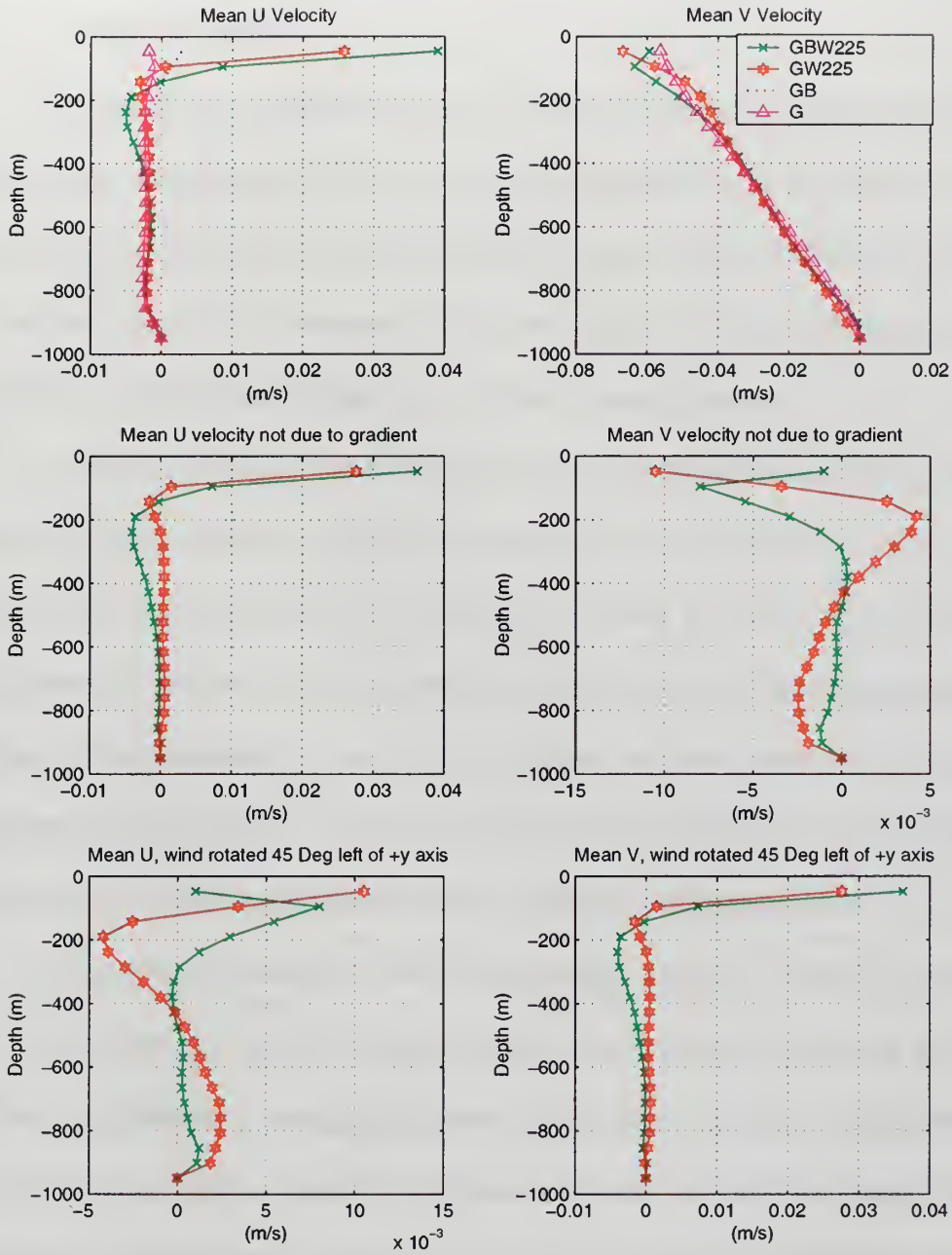

Figure 5.32. LES profiles of horizontal velocities produced by no wind with cooling, wind with cooling, southwesterly winds with cooling and southwesterly winds with no cooling all with a strong gradient (top). Profiles of horizontal velocities resulting from a strong gradient with southwesterly winds with cooling and without cooling with the horizontal velocities resulting from the strong gradient only with and without cooling subtracted accordingly (middle). Profiles of wind induced horizontal velocities with the wind rotated to 45° left of the positive y axis (bottom).

VI. CONCLUSIONS AND RECOMMENDATIONS

A. CONCLUSIONS

Results from an LES model show that both the strength of horizontal density gradients and wind direction relative to the gradient affect mixed layer scalar variances, turbulent vertical fluxes, and Vertical Turbulent Kinetic Energy (VTKE) during deep convection. These differences also affect water stability. Wind direction has the largest influence in combination with stronger horizontal density gradients.

A stronger horizontal gradient produces more temperature and salinity variance than does a smaller gradient regardless of wind direction. However, for a given horizontal density gradient, the TKE and scalar variances depend on wind direction. The same pattern of response to wind direction is found in both weak and strong gradient regimes. Winds producing westerly flow of denser, cold, fresh water over warm, salty water result in higher levels of temperature and salinity variance than do winds that cause easterly flow of warm, salty, lighter water over denser, cold, fresh water.

Wind direction relative to a horizontal gradient also has a significant impact on the turbulent heat, salinity, and buoyancy fluxes. Much greater changes are seen when different wind directions are applied to a strongly baroclinic ocean. Wind direction dominates over gradient strength in determining vertical flux profiles. Southerly or southwesterly wind acting on a strong gradient results in lower values of flux than the flux values all of the small gradient situations. Northerly or northeasterly winds acting on a strong gradient result in the highest flux values.

The relationship between TKE production from vertical buoyancy flux and the level of VTKE is different for strong and weak horizontal gradient regimes. Cases with weak or no horizontal density gradient have higher levels of TKE than strong gradient cases regardless of wind stress magnitude or direction. Wind direction dominates over gradient strength in determining vertical buoyancy flux, and gradient strength dominates over wind direction in determining VTKE profiles. This must be due to differences in shear production and dissipation of TKE resulting from the difference in gradient strength. Wind direction within the two gradient strength situations does alter the levels of VTKE. North and northeasterly wind have more VTKE and south and southwesterly wind have less VTKE in both gradient regimes following the trend in TKE production from buoyancy flux.

A horizontal density gradient is a stabilizing factor in an area of strong surface cooling and deep convection with stronger gradients increasing the stability. Mixing across the geostrophic current causes descending dense parcels to move westward and ascending lighter parcels to move eastward, promoting stability.

Cooling causes the Ekman depth, the depth to which the wind has an effect, to increase. Intense cooling reduces stability and causes vertical mixing. Cooling accentuates the transfer of momentum from the wind to lower levels. LES profiles indicate 400 W/m^2 of surface cooling more than doubles the Ekman depth.

B. RECOMMENDATIONS

Continuation of this work would be very beneficial to more completely understand the dynamics and reasons for variation due to gradient strength and wind forcing. There is more information in the LES output that can be analyzed here, and

more variations can be made to the parameters of surface heat loss, horizontal gradients, and surface wind stress.

1. Further Weak Gradient Cases

The weak gradient cases already studied should be integrated further in time to ensure a steady state has been achieved. Also, more weak gradient cases should be initiated with wind forcing in different directions for further comparisons. An even weaker gradient should be applied to learn if similar results are obtained, or if there is a limit to the strength of a gradient that can affect the various parameters. Applying different wind strengths and different cooling amounts would also aid in the understanding of the dynamics.

2. Lagrangian Drifters

Simulated drifters were included in all of the cases performed during this study. However, time constraints prevented this data from being fully analyzed. The drifter data from the LES model should also be analyzed. This data should be compared to actual Lagrangian drifter data collected during the Labrador Sea Deep Convection Experiments in 1997 and 1998.

3. Larger LES Domains

Stronger density gradient cases should be simulated in LES domains larger than the scale of the features that are present in these situations, to better resolve baroclinic eddies. Intermediate gradient strengths should also be considered.

THIS PAGE INTENTIONALLY LEFT BLANK

LIST OF REFERENCES

Brown, A. R., 1996. Large-eddy simulation and parameterization of the baroclinic boundary layer. *Q. J. R. Meteorol. Soc.*, 122,1779-1798.

Clarke, R. A., and J.-C. Gascard, 1983. The formation of Labrador Sea water, Part I: Large scale processes, *J. Phys. Oceanogr., 13, 1764-1778.*

Deardorff, J. W., 1973. The use of subgrid transport equations in a three-dimensional model of atmospheric turbulence, *J. Fluids Engineering*, 429-438.

Denbo, D. W., and E. D. Skyllingstad, 1996. An ocean large-eddy simulation model with application to deep convection in the Greenland Sea, *J. Geophys. Res.*, 101, 1095-1110.

Garwood R. W., Jr., S. M. Isakari, and P. C. Gallacher, 1994. Thermobaric Convection, in *The Polar Oceans and Their Role in Shaping the Global Environment*, O. Johannessen, R. Meunch, and J. Overland, Eds., Geophysical Monograph 85, 199-209.

Gascard J.-C., and R. A. Clarke, 1983. The formation of Labrador Sea water, part II: mesoscale and smaller scale processes, *J. Phys. Oceanogr.*, 13, 1779-1797.

Harcourt, R. R., 1999. Numerical simulation of deep convection and the response of drifters in the Labrador Sea. Ph. D. Dissertation, Univ. of Ca., Santa Cruz, Dept. of Physics.

Harcourt, R. R., and R. W. Garwood, Jr., 1994. Large eddy simulation of openocean deep convective plumes. *Trans. Am. Geophys. Union*, 75, 364-365.

Killworth, P. D., 1983. Deep convection in the world ocean, *Rev. Geophys. and Space Phys.*, 21, 1-26.

LAB SEA GROUP, 1998. The Labrador Sea deep convection experiment, *Bull. Amer. Meteorol. Soc.*, 79, 2033-2059.

Lazier, J. R. N., and D. G. Wright, 1993. Annual velocity variations in the Labrador Current, *J. Phys. Oceanogr.*, 23, 659-678.

Lazier, J. R. N., 1980. Oceanographic conditions at ocean weather ship Bravo 1964-1974, *Atmos. Ocean*, 18, 227-238.

Lilly, D. K., 1967. The representation of small-scale turbulence in numerical simulation experiments, In *Proceedings of IBM Scientific Symposium on Environmental Sciences,* IBM Form No. 320-1951, 195-210.

Lilly, J. M., P. B. Rhines, M. Visbeck, R. Davis, J. R. N. Lazier, F. Schott, and D. Farmer, 1999. Observing deep convection in the Labrador Sea during winter 1994/1995, *J. Phys. Oceanogr.*, 29, 2065-2098.

Marshall, J., and F. Schott, 1999. Open ocean convection: observations, theory, and models, *Rev. Geophys.*, 37, 1-64.

MEDOC Group, 1969. Observations of deep-water formaton in the northwetern Mediterranean Sea, *Nature*, 227, 1037-1040.

Moeng, C.-H., 1984. A large-eddy simulation model for the study of boundary-layer turbulence. *J. Atmos. Sci.*, 41, 2052-2062.

Pond, S., and G. L. Pickard, 1983. *Introductory Dynamical Oceanography 2nd Ed.*, Butterworth Heinemann, 329pp.

Smagorinsky E.D., T. Paluszkawics, D. W. Denbo, W. D. Smyth, 1996. Nonlinear vertical mixing processes in the ocean: modeling and parameterization. *Physica D*, 98, 574-593, Elsevier Science.

Stone, R. E., 1999. Entrainment, detrainment and large-scale horizontal gradients in oceanic deep convection. Ph. D. Dissertation, Naval Postgraduate School, Monterey, Ca., Dept. of Oceanography.

INITIAL DISTRIBUTION LIST

1. Defense Technical Information Center 2
   8725 John J. Kingman Road, Suite 0944
   Ft. Belvoir, VA 22060-6218

2. Dudley Knox Library 2
   Naval Postgraduate School
   411 Dyer Road
   Monterey, CA 93943-5101

3. Chairman (Code MR/Wx) 1
   Department of Meteorology
   Naval Postgraduate School
   Monterey, CA 93943-5101

4. Chairman (Code OC/Gd) 1
   Department of Oceanography
   Naval Postgraduate School
   Monterey, CA 93943-5101

5. Prof. Peter S. Guest (Code MR/Gs) 2
   Department of Meteorology
   Naval Postgraduate School
   Monterey, CA 93943-5101

6. Prof. Ramsey Harcourt (CodeOC/Ha) 2
   Department of Oceanography
   Naval Postgraduate School
   Monterey, CA 93943-5101

7. LCDR Denise M. Kruse 2
   115 Moreell Circle
   Monterey, CA 93940

60 290NPG TH 2349
6/02 22527-200 NLB

DUDLEY KNOX LIBRARY
3 2768 00403135 1